



**UNIVERSITY of the
WESTERN CAPE**

**RESERVOIR DISTRIBUTION AND CHARACTERIZATION OF LOWER CRETACEOUS
SANDS IN BLOCK 2A OF ORANGE BASIN, OFFSHORE, SOUTH AFRICA.**

A Thesis in Petroleum Geology

By



Nwabisa Gigi

UNIVERSITY of the

Supervisor: Dr Opuwari

**Submitted in Fulfilment of the Requirements for the Degree of Magister
Scientiae in the Department of Earth Sciences,
University of the Western Cape,
Bellville, South Africa.**

**Department of Earth Sciences, University of the Western Cape, Bellville,
South Africa.**

July, 2017

PLAGIARISM DECLARATION

I declare that **RESERVOIR DISTRIBUTION AND CHARACTERIZATION OF LOWER CRETACEOUS SANDS IN BLOCK 2A OF ORANGE BASIN, OFFSHORE, SOUTH AFRICA** is my own work, that it has not been submitted before for any degree or examination in any other university, and that all the sources I have used or quoted have been indicated and acknowledged as complete references.



Nwabisa Gigi

July 2017

Signed:

ABSTRACT

Orange Basin is a volcanic passive margin that forms part of the southwestern basins that were formed during the breakup of South America and Africa in Late Jurassic to Early Cretaceous. The basin comprises of numerous half grabens which are overlain by post rift fluvial deltaic sediments. This research study focuses on the distribution and characterization of the Albian deltaic sands across the Ibhubesi gas field. Geophysical and geological data such as 3D seismic data, wireline logs and core data from four wells (A-G 1, A-K 1, A-V1 and A-K 2) which tested the Albian reservoirs were integrated for a proper evaluation of the reservoirs.

From Seismic interpretation and well correlation it is apparent that the Albian sands in the Ibhubesi gas field were deposited in a fluvial-deltaic environment. Seismic attributes have shown that the wells covered by the 3D seismic data were drilled on sweet spots of the channel axis of a deltaic system. These channels seem to be diverted by incised valleys across the entire field. Better sands are expected to develop down dip of the current field as splays in a pro-delta setting.

Results obtained from petrography and petrophysical evaluations have revealed that quartz-overgrowths are the dominant cement across all the Albian reservoirs of the four wells. Quartz precipitation most likely resulted from the circulation of waters during sediment compaction. Although these Albian sands are highly cemented with silica, porosities in most reservoir intervals range between 18% and 23%. These fairly good porosity values are mostly primary porosities protected from quartz-overgrowth by chlorite rims. The formation of chlorite from volcanic fragments pre-dates the development of quartz-overgrowth; hence the preservation of primary porosities. Secondary porosity is also present in some of the reservoir intervals resulting from leaching of unstable minerals. Permeabilities are generally low due to chlorite rims, quartz overgrowth and other authigenic clays such as kaolinite and illite which blocked pore connectivity. Resistivity logs had generally low readings over most hydrocarbon bearing zones due to the presence of chlorite in the sands.

KEY WORDS

Orange Basin

Fluvial Deltaic Environment

Sandstone Reservoir Characterization

Reservoir Distribution

Porosity

Permeability

Chlorite

Quartz Overgrowth



DEDICATION

This research study is dedicated to my late grandparents:

Mr Zinkosi and Mrs Nophumzile Gigi.



ACKNOWLEDGEMENTS

I would like to thank everyone who have made this research study a success since it has benefited from generous contributions of many individuals. I would like to address my heartfelt thanks to Dr Opuwari whose guidance has shaped this study. His encouragement has been a source of strength throughout the course of the study.

Special thanks are addressed to the Petroleum Agency of South Africa for releasing their data that have served to document this study.

My gratitude extends to my parents, siblings, extended family and friends for their support. Most of all I am deeply grateful to the Almighty God for giving me strength to complete this research endeavour.



TABLE OF CONTENTS

| | |
|---|----------|
| PLAGIARISM DECLARATION | ii |
| ABSTRACT | iii |
| KEY WORDS | iv |
| DEDICATION | v |
| ACKNOWLEDGEMENTS | vi |
| TABLE OF CONTENTS | vii |
| LIST OF FIGURES | xii |
| LIST OF TABLES | xv |
| LIST OF APPENDICES | xv |
| LIST OF EQUATIONS | xvi |
| LIST OF ABBREVIATIONS | xvii |
| CHAPTER 1 | 1 |
| 1. THESIS LAYOUT | 1 |
| 1.1 Introduction | 3 |
| 1.2 Aims of the research study | 4 |
| 1.3 Objectives of the research study | 4 |
| 1.4 Location of the research study area | 5 |
| 1.5 General review of previous work | 7 |



| | |
|---|----|
| CHAPTER 2 | 9 |
| 2. GEOLOGY REVIEW | 9 |
| 2.1 Regional geology | 9 |
| 2.2 General sequence Stratigraphy | 10 |
| 2.3 Depositional Environments | 11 |
| 2.4 Tectonic Setting of the Orange Basin | 12 |
| 2.5 Petroleum systems of the Orange Basin | 13 |
| 2.5.1 Source rocks | 13 |
| 2.5.2 Reservoirs, Seals and Traps | 15 |
| CHAPTER 3 | 16 |
| 3. REVIEW OF TECHNIQUES | 16 |
| 3.1 Well logs | 16 |
| 3.1.1 Caliper logs | 17 |
| 3.1.2 Gamma ray logs | 18 |
| 3.1.3 Self potential logs | 19 |
| 3.1.4 Temperature logs | 19 |
| 3.1.5 Resistivity logs | 20 |
| 3.1.6 Sonic logs | 21 |
| 3.1.7 Density logs | 22 |
| 3.1.8 Neutron logs | 23 |
| 3.2 Petrophysical properties | 25 |
| 3.2.1 Porosity | 25 |

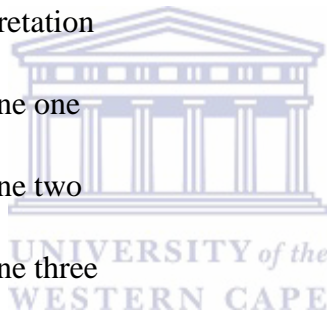


| | |
|---|----|
| 3.2.2 Permeability | 26 |
| 3.2.3 Water saturation | 27 |
| 3.2.4 Volume of shale | 28 |
| 3.3 Seismic interpretation and seismic attributes | 30 |
| 3.3.1 Amplitude seismic attributes | 31 |
| 3.3.2 Spectral decomposition | 31 |
| 3.3.3 Coherency attributes | 32 |
| 3.4 Sequence stratigraphy | 33 |
| 3.5 Core analysis and interpretation | 34 |
| 3.6 Lithostratigraphic well correlation | 35 |
| 3.7 Depositional environments, Diagenesis and Reservoir quality | 36 |
| CHAPTER 4 | 38 |
| 4. MATERIALS AND METHODOLOGY | 38 |
| 4.1 Desktop Study and Literature review | 40 |
| 4.2. Seismic data loading and interpretation | 40 |
| 4.3. Well data loading | 41 |
| 4. 4. Well correlation | 41 |
| 4. 5. Core logging | 42 |
| 4. 6. Petrophysical evaluation | 43 |
| 4.6.1 Porosity calculation | 43 |
| 4.6.2 Water saturation calculation | 44 |



| | |
|--|----|
| 4.6.3 Volume of shale calculation | 44 |
| 4.7. Petrography (Thin Sections) | 45 |
| CHAPTER 5 | 47 |
| 5. RESULTS AND INTERPRETATION OF WELL CORRELATION AND RESERVOIR DISTRIBUTION FROM SEISMIC INTERPRETATION | 47 |
| 5.1. Well correlation | 47 |
| 5.2. Seismic interpretation | 51 |
| 5.3. Reservoir distribution of the Albian reservoirs | 54 |
| CHAPTER 6 | 59 |
| 6. RESULTS AND INTERPRETATION OF RESERVOIR CHARACTERIZATION FROM CORE LOGS, PETROPHYSICAL EVALUATION FROM GEOPHYSICAL LOGS AND PETROGRAPHY | 59 |
| 6.1. Core logging results and interpretations | 59 |
| 6.1.1. Core description of AK1 (cores # 1 and 2) based on litho-facies classification | 60 |
| <i>6.1.1.1 A-K 1 Cross-plots from core analysis results</i> | 62 |
| 6.1.2. Core description of AG1 (core # 1) based on litho-facies classification | 69 |
| <i>6.1.2.1 A-G 1 Cross-plots from core analysis results</i> | 71 |
| 6.2. Results and interpretations of petrophysical evaluation from geophysical logs | 75 |
| 6.2.1. A-K 2 well results and interpretation | 75 |
| 6.2.1.1. A-K 2 Reservoir zone one | 76 |
| 6.2.1.2. A-K 2 Reservoir zone two | 76 |

| | |
|---|----|
| 6.2.1.3. A-K 2 Reservoir zone three | 76 |
| 6.2.1.4. A-K 2 Reservoir zone four | 77 |
| 6.2.1.5. A-K 2 Reservoir zone five | 77 |
| 6.2.2. A-K1 well results and interpretation | 80 |
| 6.2.2.1. A-K 1 Reservoir zone one | 81 |
| 6.2.2.2. A-K 1 Reservoir zone two | 81 |
| 6.2.2.3. A-K 1 Reservoir zone three | 81 |
| 6.2.2.4. A-K 1 Reservoir zone four | 83 |
| 6.2.3. A-V 1 well results and interpretation | 84 |
| 6.2.3.1. A-V 1 Reservoir zone one | 85 |
| 6.2.3.2. A-V 1 Reservoir zone two | 85 |
| 6.2.3.3. A-V 1 Reservoir zone three | 85 |
| 6.2.3.4. A-V 1 Reservoir zone four | 85 |
| 6.2.4. A-G 1 well results and interpretation | 87 |
| 6.2.4.1. A-G 1 Reservoir zone one | 88 |
| 6.2.4.2. A-G 1 Reservoir zone two | 88 |
| 6.2.4.3. A-G 1 Reservoir zone three | 88 |
| 6.2.4.4. A-G 1 Reservoir zone four | 88 |
| 6.2.4.4. A-G 1 Reservoir zone five | 89 |
| 6.2.5. Mineralogical predictions from well logs | 90 |
| 6.2.5.1 A-K 2 | 91 |
| 6.2.5.2. A-K 1 | 92 |



| | |
|--|-----|
| 6.2.5.3. A-V1 | 93 |
| 6.2.5.4. A-G 1 | 94 |
| 6.2.7. Results and interpretation of petrography | 95 |
| 6.2.6.1 A-K 1 | 95 |
| 6.2.6.2. A-G 1 | 98 |
| | |
| CHAPTER 7 | 102 |
| 7.1. Conclusion | 102 |
| 7.2. Recommendations | 104 |
| | |
| REFERENCES | 105 |
| | |
| APPENDICES | 113 |
| | |
| LIST OF FIGURES | |
| Figure: 1.0. Flow chart of the Thesis | 1 |
| Figure: 1.1. Location of the study area | 5 |
| Figure: 2.1. Regional geology of Orange Basin map | 9 |
| Figure: 2.2. Orange Basin Chronostratigraphic frame work | 11 |
| Figure: 2.3. Tectonic setting of Orange Basin map | 12 |
| Figure: 2.4. Schematic geological cross section of the pay zones within the Orange Basin | 14 |
| Figure: 3.1. Schematic of a calliper tool | 17 |
| Figure: 3.2. Schematic of a gamma ray tool | 18 |
| Figure: 3.3. Electrode distribution in wireline resistivity tools | 20 |
| Figure: 3.4. Schematic representation of wireline sonic tool | 21 |
| Figure: 3.5. Schematic representation of wireline density tool | 23 |
| Figure: 3.6. Schematic of wireline compensated neutron tool | 24 |
| Figure: 3.7. Example of a porous rock | 25 |



| | |
|---|----|
| Figure: 3.8. Schematic of core permeability measurement | 26 |
| Figure: 3.9. Nonlinear volume of shale chart | 30 |
| Figure: 3.10. Horizon slice of original seismic data and Colour-blend of three spectral decomposition components | 32 |
| Figure: 3.11. Normal 3D seismic slice with unclear faults and coherency attribute clear visible faults. | 32 |
| Figure: 3.12. Stratal surfaces and unconformities | 33 |
| Figure: 3.13. Core plug drilling press and typical core plugs | 35 |
| Figure: 3.14. Well correlation of the Buzzard field | 36 |
| Figure: 3.15. Diagram of diagenetic clay minerals associated with fluvial to hallow marine deposition environments | 37 |
| Figure: 4.1. Base map of block 2A with wells and 3D outline: | 38 |
| Figure: 4.2. Flow chart of the research methods | 39 |
| Figure: 4.3. Gamma ray responses to variation in grain size | 42 |
| Figure: 5.1 Block 2A base map | 48 |
| Figure: 5.2. Well correlation of the studied four wells in Ibhubesi gas field | 49 |
| Figure: 5.3. Well correlation of the studied four wells in Ibhubesi gas field (zoomed-in) | 50 |
| Figure: 5.4. NW-SE random line through the A-V 1, A-K 1 and A-K 2 | 52 |
| Figure: 5.5. Coherence cube over an interval of 50ms showing the main trapping fault of the field | 53 |
| Figure: 5.6. In-line section section through the Ibhubesi gas field | 54 |
| Figure: 5.7. Cross-line section through the Ibhubesi gas field | 55 |
| Figure: 5.8. Maximum Amplitude between top and base of reservoir unit | 56 |
| Figure: 5.9. Spectral decomposition between top and base of the reservoir. Blending 35 hz, 45 hz, and 50 hz showing the main sand bodies of the distributary channels in the Ibhubesi gas field | 57 |

| | |
|--|----|
| Figure: 5.10. Simple cartoon summarizing the fluvial deltaic depositional environment of the Ibhubesi gas field in Albian time | 58 |
| Figure: 6.1.1. Log strip of A-K 1, core one and two | 60 |
| Figure: 6.1.2. A-K 1 core 1 density vs depth plot | 63 |
| Figure: 6.1.3. A-K 1 core 2 density vs depth plot | 63 |
| Figure: 6.1.4. A-K 1 core 1 core porosity vs depth plot | 64 |
| Figure: 6.1.5. A-K 1 core 2 core porosity vs depth plot | 65 |
| Figure: 6.1.6. A-K 1 core 1 core permeability vs depth plot | 66 |
| Figure: 6.1.7. A-K 1 core 2 core permeability vs depth plot | 66 |
| Figure: 6.1.8. A-K 1 core 1 fluid saturation vs depth plot | 68 |
| Figure: 6.1.9. A-K 1 core 2 fluid saturation vs depth plot | 68 |
| Figure: 6.1.10. Log strip of A-G 1, core one | 69 |
| Figure: 6.1.11. A-G 1 core 1 density vs depth plot | 71 |
| Figure: 6.1.12. A-G 1 core 1 core porosity vs depth plot | 72 |
| Figure: 6.1.13. A-G 1 core 1 core permeability vs depth plot | 72 |
| Figure: 6.1.14. A-G 1 core 1 fluid saturation vs depth plot | 73 |
| Figure: 6.2.1. A-K 2 log template showing petrophysical parameters of zones one | 75 |
| Figure: 6.2.2. A-K 2 log template showing petrophysical parameters of zones two and three | 78 |
| Figure: 6.2.3. A-K 2 log template showing petrophysical parameters of zones four and five | 79 |
| Figure: 6.2.4. A-K 1 log template showing petrophysical parameters of zones one and two | 80 |
| Figure: 6.2.5. A-K 1 log template showing petrophysical parameters of zones three and four | 82 |
| Figure: 6.2.6. A-V 1 log template showing petrophysical parameters of zones one and two | 84 |
| Figure: 6.2.7. A-V 1 log template showing petrophysical parameters of zones three and four | 86 |

| | |
|--|--------|
| Figure: 6.2.8. A-G 1 log template showing petrophysical parameters of all five zones | 87 |
| Figure: 6.2.9. Neutron-density plot for mineralogy prediction for zones of A-K 2 well | 91 |
| Figure: 6.2.10. Neutron-density plot for mineralogy prediction for zones of A-K 1 well | 92 |
| Figure: 6.2.11. Neutron-density plot for mineralogy prediction for zones of A-V 1 well | 93 |
| Figure: 6.2.12. Neutron-density plot for mineralogy prediction for zones of A-G 1 well | 94 |
| Figure: 6.2.13. Thin section photographs of A-K 1 well | 96-97 |
| Figure: 6.2.14. Thin section photographs of A-G 1 well | 99-100 |

LIST OF TABLES

| | |
|--|----|
| Table 1.1: Location of the wells | 6 |
| Table 3.1: Classification of the common geophysical well log | 16 |
| Table 3.2: Grain densities of common clay minerals | 22 |
| Table 4.1: Interpreted wireline logs obtained from PASA | 41 |
| Table 6.1: Densities of common clay minerals | 62 |
| Table 6.2. Permeability classification scale | 67 |
| Table 6.3: Densities of common clay minerals | 90 |

LIST OF APPENDICES

| | |
|--|-----|
| Appendix A: Spectral decomposition Settings | 113 |
| Appendix B: Seismic attribute extractions between top and base of the reservoirs | 114 |
| Appendix C: Selected plates from A-G 1 and A-K 1 cores | 115 |
| Appendix D: Core analysis results of A-G 1 well core | 116 |
| Appendix E: Core analysis results of A-K 1 well core 1 | 117 |
| Appendix F: Core analysis results of A-K 1 well core 2 | 118 |

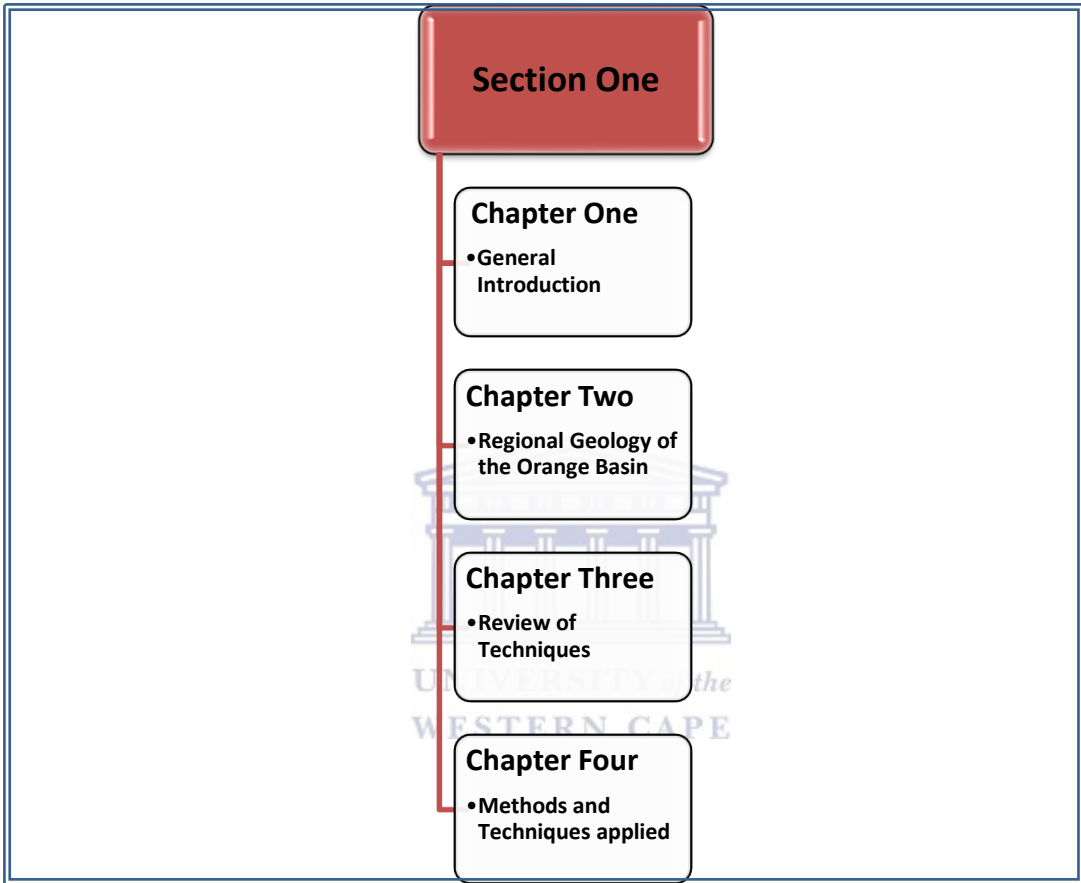
LIST OF EQUATIONS

| | | |
|--|--------|----|
| $\Phi = V_p/V_b$ | (3.1) | 25 |
| $K = Q \mu L / \Delta P A$ | (3.2) | 27 |
| $S_w^n = F.R_w / (R_t)$ | (3.3) | 27 |
| $F = a/\Phi^m$ | (3.4) | 27 |
| $1/R_t = [S_w^2/F*R_w(1-V_{sh})] + [(V_{sh}*S_w)/(R_{SH})]$ | (3.5) | 28 |
| $V_{sh} = (SP_{sh} - SP) / (SP_{sh} - SP_{cl})$ | (3.6) | 28 |
| $V_{sh} = (GR_{sh} - GR) / (GR_{sh} - GR_{cl})$ | (3.7) | 29 |
| Larionov (1969) for Tertiary rocks: $V_{sh} = 0.083 (2^{3.71 GR} - 1)$ | (3.8) | 29 |
| Steiber (1970) : $V_{sh} = (I_{GR}) / (3 - 2 * I_{GR})$ | (3.9) | 29 |
| Clavier (1971) : $V_{sh} = 1.7 [(3.38 - (I_{GR} + 0.7)^2)]^{1/2}$ | (3.10) | 29 |
| Larionov (1969) for older rock : $V_{sh} = 0.33 * (2^{2 I_{GR}} - 1)$ | (3.11) | 29 |
| Porosity (Φ_D) = $\frac{(\rho_{ma} - \rho_b)}{(\rho_{ma} - \rho_f)}$ | (4.1) | 43 |
| Porosity $\Phi_{Ncorr} = \Phi_{Nlog} - V_{sh} \times \Phi_{Nsh}$ | (4.2) | 43 |
| $1/R_t = [S_w^2/F*R_w(1-V_{sh})] + [(V_{sh}*S_w)/(R_{SH})]$ | (4.3) | 44 |
| Volume of Shale (V_{sh}) = $\frac{GR \text{ value (log)} - GR \text{ (min)}}{GR \text{ (max)} - GR \text{ (min)}}$ | (4.4) | 44 |
| Steiber (1970) : $V_{sh} = (I_{GR}) / (3 - 2 * I_{GR})$ | (4.4) | 45 |
| Clavier (1971) : $V_{sh} = 1.7 [(3.38 - (I_{GR} + 0.7)^2)]^{1/2}$ | (4.5) | 45 |

LIST OF ABBREVIATIONS

| | |
|-------------|----------------------------------|
| AVO | Amplitude Versus Offset |
| CALI | Caliper |
| CLAY | Volume Clay |
| DHI | Direct Hydrocarbon Indicators |
| GR | Gamma Ray |
| GWC | Gas Water Contact |
| HI | Hydrogen Index |
| ILD | Deep Resistivity |
| IP | Interactive Petrophysics |
| N/G | Net to Gross ratio |
| NPFI | Neutron |
| OBM | Oil Based Mud |
| PASA | Petroleum Agency of South Africa |
| PHIE | Effective Porosity |
| PSTM | Pre-stack Time Migration |
| RHOB | Bulk Density |
| VSH | Volume Shale |
| RMS | Root Mean Square |
| SFLU | Shallow Resistivity |
| SP | Self Potential |
| Spec Decomp | Spectral Decomposition |
| SW | Water Saturation |
| TOC | Total Organic Content |
| TWT | TWO Way Time |





CHAPTER ONE

1.0 THESIS LAYOUT

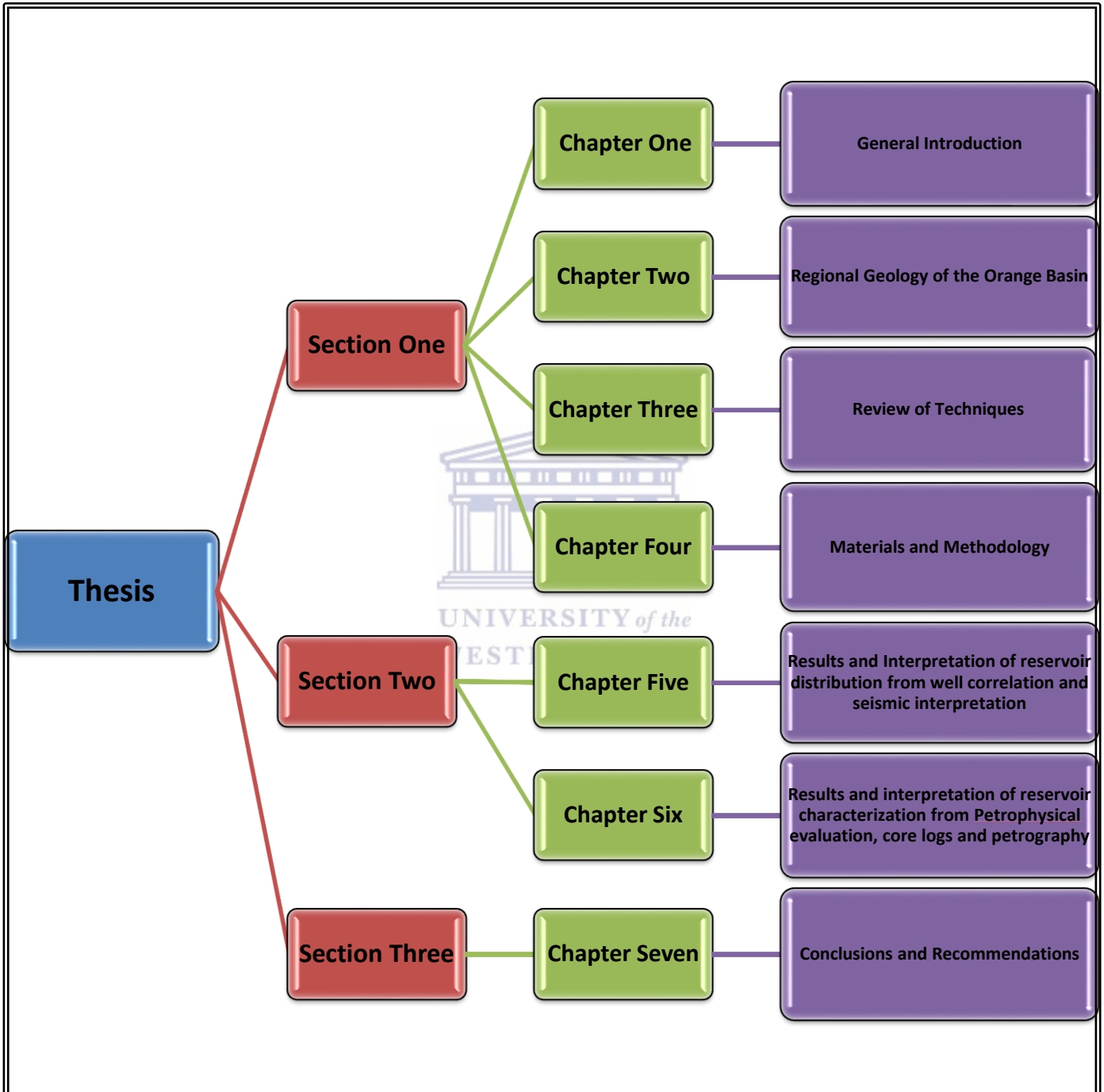


Fig.1.0. Flow chart of the thesis.

Figure 1.0 shows the flow of different sections of the thesis. Section One mainly focuses on the general introduction, geology of the study area and the techniques applied during the course of the study. This section is further subdivided into four chapters:

- Chapter one presents the introduction of the study; including the aims and objectives to be achieved at the end of the research and a brief introduction of the study location. The chapter ends with a brief review of the previous studies conducted in Orange Basin.
- In Chapter two, the regional geology, stratigraphy and tectonic setting of the entire Orange Basin are presented in detail.
- Chapter three mainly focuses on the description of techniques applied in the research study.
- Chapter four presents the methods and techniques used during the course of the study. These techniques include core logging, seismic interpretation, wireline logging, thin section studies e.t.c.

Section two presents results and interpretations of the study. This section is subdivided into chapters five and six.

- Chapter five presents the results and interpretation of reservoir distribution from seismic interpretation and well correlation.
- Chapter six focuses solely on the discussion of results of reservoir characterization of the studied well from wireline logs, core logs and petrography studies.

Section three which contains chapter seven presents the conclusion and recommendations of the study.

1.1 Introduction

South Africa is a rapidly growing country with high energy demands as the country is also the main energy supplier to other neighbouring countries in the continent. The exploration of hydrocarbons in the offshore and onshore basins is therefore of very high importance to the country and the continent. Exploration and drilling campaigns in the offshore basins of South Africa by both international and local companies has demonstrated large accumulations of movable hydrocarbons. Most exploration activities since exploration began offshore South Africa in 1967 have been in the Bredasdorp Basin (Roberts & Bally, 2012) where a number of gas and oil fields have been producing for decades. It is worth to mention that the Orange Basin is volumetrically the largest basin of South Africa's offshore basins (PASA, 2008); but it remains relatively under explored compared to the south coast basins as there was only one well drilled per 4000 square kilometres in 2008 (PASA, 2008). Exploration in the Orange Basin began around 1974 with the discovery of the Kudu gas field offshore Namibia (Brown et al., 1995). Some of the few wells that have been drilled in the South African side of the Orange Basin so far have encountered all the petroleum elements necessary for the accumulation of movable hydrocarbons. This validates the potential Orange Basin has for containing and generating both oil and gas. So, to enhance the economic viability of the basin a thorough evaluation of reservoir distribution and its petrophysical properties remains an essential key.

This study therefore serves as an attempt to characterize Lower Cretaceous reservoir intervals of selected wells in the Ibhubesi gas field in block 2A of Orange Basin and also to map the lateral extent of these reservoirs across the entire gas field.

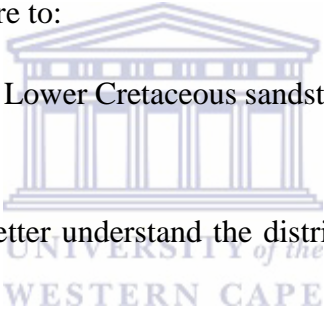
Petroleum reservoir characterization is an integration of all the available data from a basin or field with a purpose of analysing reservoir quality and performance. The quality and performance of reservoir rocks are primarily controlled by porosities and permeability which are in turn controlled by diagenetic processes. Understanding these main reservoir properties for any reservoir is crucial for reservoir characterization. In frontier areas with limited well data such as in the Orange Basin, reservoir characterization heavily relies on seismic interpretation. Using geophysical seismic attributes such as root mean square (RMS) for mapping the distribution of the proven Lower Cretaceous reservoir on a 3D seismic data volume and correlating these proven sands on wells may trigger new potential leads to be followed for further exploration.

1.2 Aims

The aims of the present study are to successfully map the regional distribution of the Albian sands within the Ibhubesi gas field of block 2A, Orange Basin and later characterize the reservoirs intersected by A-G 1, A-K 1, A-K 2 and A-V 1 wells. Mapping the extent of the Albian reservoirs that were intersected by the studied wells will help to better understand the distribution of the sands across the Ibhubesi field. Furthermore, this regional evaluation will trigger new prospectivity to be followed for future exploration/appraisal drilling campaigns. The characterization of the reservoirs will be achieved by integrating all the available data from seismic data, geophysical well logs, core logs and thin sections.

1.3 Objectives

The main objectives of this study are to:

- 
- ✚ Map the lateral extent of Lower Cretaceous sandstone reservoir on a 3D seismic data volume;
 - ✚ Correlate the wells to better understand the distribution of the reservoir across the field;
 - ✚ Identify new potential leads to be followed for further exploration;
 - ✚ Identify potential reservoir zones from the studied wells;
 - ✚ Calculate reservoir parameters (porosity, permeability, volume of shale and water saturation) from the identified reservoirs on wireline logs;
 - ✚ Determine the quality of the selected reservoir zones from the wells;
 - ✚ Determine the effect of clay minerals on the selected reservoir zones.

1.4 Location Of The Study Area

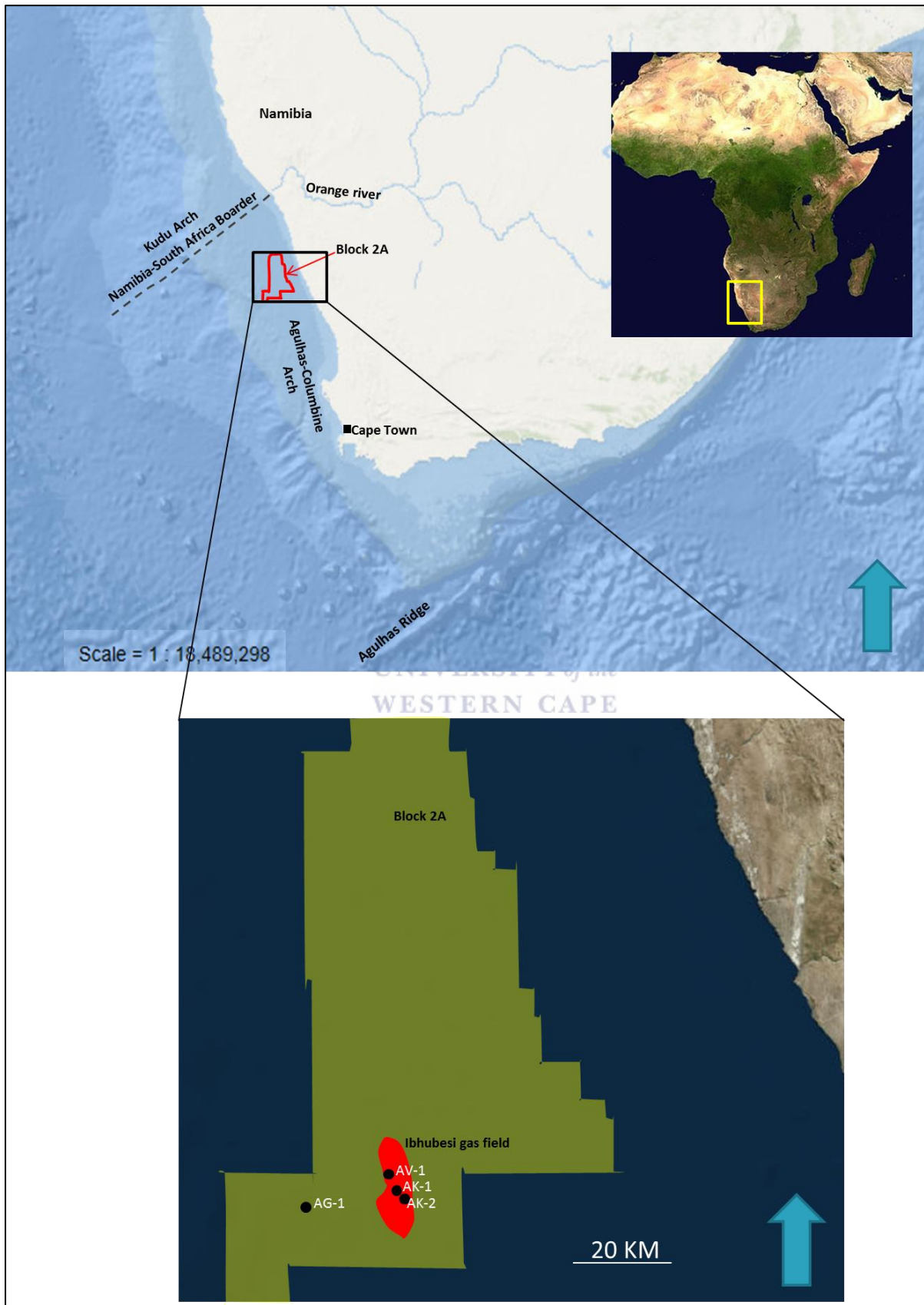


Fig.1.1. Location of the study area.

The central-southern part of the Orange Basin sits within the west coast of South Africa between 31° and 33.3° latitude (Adekole, 2010), and is enclosed on the northwest by the Kudu Arch of Namibia and to the south by the Agulhas Arch (Brown et al., 1995). The basin extends for about 500 km between the South African-Namibia boarder and Cape Town (Brown et al., 1995). The post rift basin which overlies numerous Early Cretaceous rift basins (Brown et al, 1995) sits within the 400 000 km² passive continental margin of South Africa’s west coastline (Adekola et al., 2009). Maximum water depth in the basin varies from 2000m in the north eastern parts of the basin to 4000m in the south western boundary (PASA, 2011). The four wells incorporated in this research study are all drilled in block 2A of the basin. The four studied wells are A-K 1, A-G 1, A-V 1 and A-K 2. Table 1.1 below shows the coordinates of the well locations, water depths and total depths for all four wells.

Table1.1: Location of A-G 1, A-K 1, A-K 2 and A-V 1 wells.

| Well | Longitude and Latitude | Water Depth in Meters | Total Depth in Meters |
|-------|---|-----------------------|-----------------------|
| A-G 1 | Long: 16° 23' 06.27"E Lat: 30° 54' 58.23"S | 264 m | 4100 m |
| A-K 1 | Long: 16°35'50.6900"E Lat: 30°51'30.6900"S | 245 m | 3681 m |
| A-K 2 | Long: 16°36'41.5200"E Lat: 30°52'24.1440"S | 246 m | 3430 m |
| A-V 1 | Long:16°34'49.3000"E Lat: 30°49'45.8820"S | 242 m | 3714 m |

1.5 General Review Of Previous Work On Orange Basin

Exploration for hydrocarbons in the South African sector of the Orange Basin commenced in the 1970s after the discovery of the Kudu gas field on the Namibian side of the basin. Exploration campaigns were led by Soekor now known as PetroSA. Since then, a number of papers have been published by both the industry and the academic institutions. Jungslager (1999) reviewed and evaluated the petroleum system distribution along the Atlantic margin of South Africa and also identified new possible areas for future exploration. The evaluation revealed three major source rock groups and exploration plays associated with them. The major three groups of plays were those sourced from Syn-rift to Neocomian lacustrine source rocks, the second group were those sourced from the Barremian-Lower Aptian marine source and finally those sourced from the Turonian-Cenomanian source rock. Jungslager (1999) further subdivided the aforementioned groups into individual petroleum systems based on individual source rocks, level of uncertainty, type of hydrocarbon and stratigraphic level of reservoir units and trapping mechanisms. The study revealed that the Aptian source was in the gas window within the depocentre of Orange Basin and possibly in the oil window outboard in deep water.

Muntingh and Brown (1993) carried out a study on the interpretation of viable siliciclastic low-stand petroleum plays and fairways within the post-lower Aptian of the Orange Basin using seismic and sequence stratigraphy concepts and methods. The study identified twenty three third-order, type-one depositional sequences and five composite third-order, type one sequences comprising twelve fourth-order sequences. The study further revealed that the sequences were composed of four third-order progradational and or aggradational sequences bounded by second order type one unconformities. The results of the study further revealed that the most favoured petroleum plays and fairways are restricted to low-stand systems tracts within highly progradational third-order sequence sets.

Stevenson and McMillan (2004) integrated seismic stratigraphy, lithological and biostratigraphic data derived from core and seabed samples to create a detailed geological model for the Upper Cretaceous succession of the proximal Orange Basin. The study focused in great detail on the paleo-environmental interpretations of incised valley fill sequences. Seismic interpretation revealed that the coast was dominated by an aggradational fluvial braided-plain in middle Albian to Lower Cenomanian interval. Furthermore, it was found that major incision of the coastal plain by rivers only took place in Turonian to Coniacian time.

Adekole (2010) used an integrated approach to unravel the reasons for variable sandstone reservoirs and source rock potential of the Orange Basin. The results showed a complicated diagenetic history of sandstone including compaction, cementation, dissolution, and quartz-overgrowth. Seismic interpretation of the post Hauterivian succession by Campher et al. (2009) indicates thickening of the sedimentary strata towards the west as the basin evolves from the early drift to complete drift phases. The results obtained from petroleum system modelling (in the same study) show that the Barremian- Early Aptian source rock is currently over mature and generates mainly gas in the shelf area, whereas the potential for oil is approximated to be present in deep water areas of the basin where Tertiary progradation led to renewed petroleum generation (Campher et al., 2009).



CHAPTER TWO

2. GEOLOGY REVIEW

2.1 Regional Geology of the Orange Basin



Fig.2.1. Regional geology of Orange Basin (modified after Schmidt, 2004).

The Orange Basin is the southernmost basin developed during the opening of Atlantic Ocean in Early Cretaceous. Regionally, the basin forms part of the four basins of the southwest African offshore region (Schmidt, 2004). The four basins from north to south are: Namibe, Walvis, Luderitz and Orange Basin (see Figure 2.1 above). Clemson et al.(1999) suggested that the opening of the Orange Basin occurred in a basement that was already extended and occurred spontaneously with the eruption of flood basalts of the Etendeka-Parana igneous province which has been dated at 132 Ma (Menzies et al., 2002). Rifting of the African plate during the development of the basin led to the formation of the synrift succession. The synrift succession comprises of isolated remnants of half grabens which were fed by major river systems (Orange

River in particular with minor input of Olifants and Berg River systems) with a delta resembling those rivers further to the north of Africa (PASA, 2008). The basin is characterized by siliciclastic sediments of Hauterivian to Jurassic ranging from continental in the east to deep marine in the west (Paton et al., 2007; PASA, 2008). The Tertiary sedimentary fill mainly comprises of calcareous oozes and chemical sediments. In some parts of the basin, seaward dipping flood basalts which were considered to have erupted rapidly close to the active rifting phase were recognised by PASA (2008). Fadipe (2009) reported that these basalts are coeval with and in parts interbedded with continental to shallow marine sediments of the Barremian transgressive succession. The western margin is therefore a divergent volcanic margin (PASA, 2008) which covers an area of approximately 145 000 km² (Broad et al., 2006). Moreover, the margin is segmented into a number of crustal segments with the southern part of the margin being of the rift margin type (PASA, 2008).

2.2 General Sequence Stratigraphy

The sequence stratigraphy of the Orange Basin is divided into two main depositional mega sequences; namely the syn-rift mega sequence and the post-rift mega sequence (De Vera et al., 2009). Syn-rift mega sequence comprises of late Jurassic to Hauterivian (160-127 Ma) of basin ward dipping sediments with fanning geometries that increase in dip with depth and thicken towards the basin where they are overlain by sediments of the present day slope of the margin (De Vera et al., 2009). These synrift sediments were unconformably deposited on the Precambrian basement.

Seaward dipping reflectors of the syn-rift mega-sequence are unconformably overlain by the post-rift mega-sequence which reflects deposition during the drift phase (De Vera et al., 2009). The unconformity separating the two mega sequences occurred in Late Hauterivian (127 Ma). The post rift mega sequence has been grouped by De Vera et al., (2009) into five depositional sequences which record deposition from Hauterivian to the present day. Depositional sequence one reflects Barremian to Upper Aptian age (127-115 Ma) sediments. This is a transgressive anoxic marine sequence that forms the main source rock along the south-western margin. Depositional sequence two is a regression sequence varying in age from Upper Aptian to Santonian. This sequence marks the deposition of the main Cretaceous reservoirs in the basin. During this time, the Orange Basin was under a lot of fluvial influence from the Orange and Olifants Rivers. The deposition of sands during this sequence is proven in the study area of this research project. Depositional sequence three is of Santonian to Campanian age (Paton et al.,

2007). The aforementioned sequence is unconformably overlain by sediments of Maastrichtian age (72-65.5 Ma). The final sequence records deposition of sediments from the Tertiary period to present day (De Vera et al., 2009). The following figure presents the Orange Basin chronostratigraphic frame work.

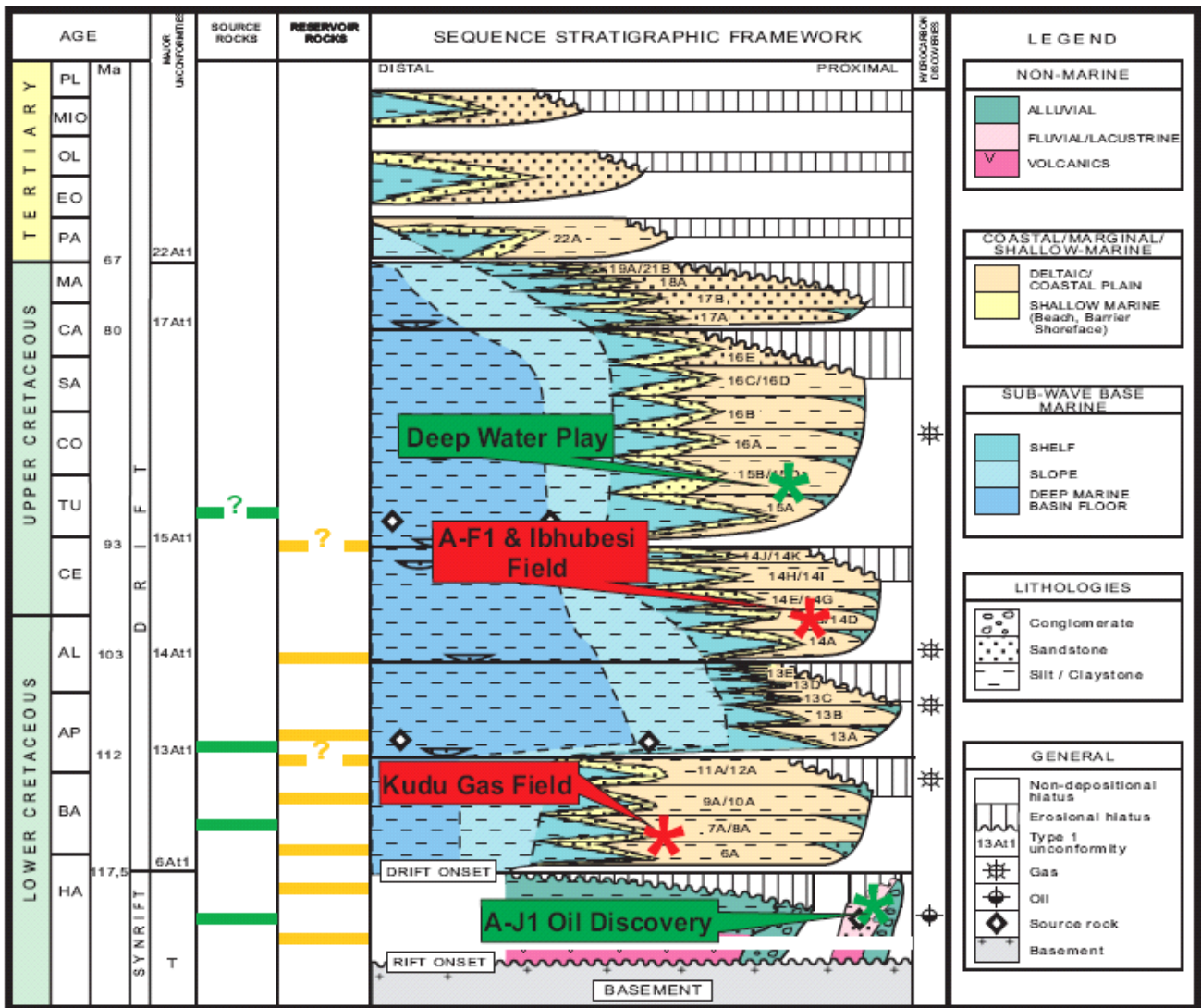


Fig.2.2. Orange Basin chronostratigraphic frame work, (PetroSA brochure, 2010).

2.3 Depositional Environments

The Orange Basin is a passive margin with sediments transported from the land by fluvial systems (Van der Spuy, 2003). The first sediments that entered the basin during the post rift (around Aptian) were mainly transported by the Olifants River. Around Albian time the basin was under the long term influence of the Orange River associated with a deltaic system and strike-fed coastal systems in the north-western part of the basin (Brown et al., 1995). The main depocenter of the basin evolved around the Albian due to the much higher influx of sediments

from the Orange River. The deltaic system associated with Orange fluvial system moved and prograded west-ward due to the sediment supply and changes in accommodation rate (Brown et al., 1995). Some of the sediments from the deltaic system were transported along strike by long-shore drift.

2.4 Tectonic Setting of the Orange Basin

The Orange Basin is a divergent plate margin underlain by syn-rift grabens and post rift section (Brown et al., 1995). The Orange Basin developed during the second stage of Gondwana-land rifting from Late Jurassic to Early Cretaceous which led to progressive opening of the Atlantic Ocean and the separation of the African plate from the South American plate (see Figure 2.3 below). This second stage of Gondwana-land rifting which succeeded the first stage of rifting occurred in a crust composed of granitic, metamorphic and ancient sedimentary rocks varying from Precambrian to Permian in age (Emery et al., 1975; Gerrard & Smith, 1983; Schmidt, 2004).

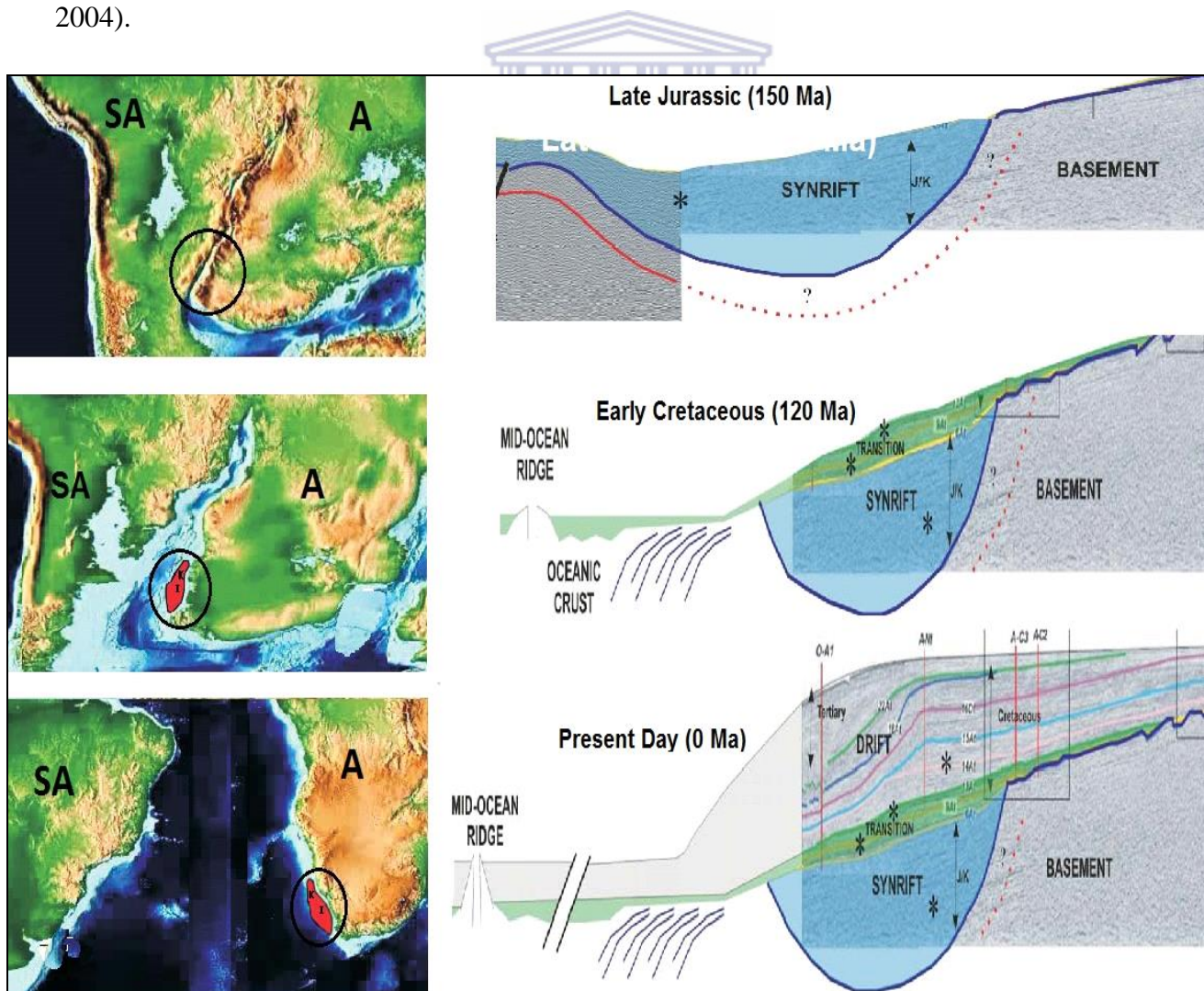


Fig.2.3. Tectonic setting of Orange Basin (modified after Paton et al., 2008).

The opening of the South Atlantic was diachronous, initiating from south to north and it was formed near to the Japetus suture; indicating that the second stage of Gondwana rifting developed along the old line of weakness (Schmidt, 2004). The syn-rift section of the basin comprises of a series of grabens and half grabens which run parallel to the present margin (Paton et al., 2007). The rifts are filled predominately with Lower Cretaceous continental clastic material, lacustrine rocks and widespread volcanic rocks (Brown et al., 1995). The syn-rift section sits unconformably on a pre-rift basement of Precambrian or Paleozoic age (Brown et al., 1995). Rifting was followed by post rift subsidence which resulted in basin flooding and deposition of source rocks in deep marine and subsequent progradation due to an influx of sands from fluvial systems (Light et al., 1993). Subsidence of the Orange Basin was presumably controlled by both thermal decay subsidence and depositional loading (Brown et al., 1995). The open marine conditions in Aptian mark the onset of the drift phase in the Orange Basin. Brown et al. (1995) recorded a total thickness of about 800 m of the drift sequence within the Orange Basin depocenter.



2.5 Petroleum Systems of Orange Basin

The geologic processes resulting in the formation and accumulation of hydrocarbons form a petroleum system (Magoon & Dow, 1994; Hartwig, 2014). A petroleum system is made up of an organic rich source rock, a reservoir rock, a seal or cap rock, a structural or stratigraphic trap, migration and timing. A number of wells drilled in the Orange Basin in both Namibia and South Africa have proven the existence of a working petroleum system in the basin.

2.5.1 Source Rocks

In the Orange Basin a total of three source rocks have been proven to exist within the Cretaceous-syn-rift and drift packages. An oil prone lacustrine shale source rock of Hauterivian age was encountered in the syn-rift package of A-J 1 well in block 2B of Orange Basin (Jungslager, 1999). This syn-rift source rock has a 60 m thick lacustrine shale with a TOC content of 10% and a Hydrogen Index (HI) of 600 mg HC/g TOC (Jungslager, 1999).

The main source rock in the entire basin is the Barremian to Early Albian aged black shales deposited in an anoxic marine environment (Van der Spuy, 2003). According to Hartwig (2014),

anoxic conditions occurred during the first marine incursion lasting from Barremian to Early Aptian times. This transition is marked by oil to gas prone organic rich marine shales. This source rock interval has been encountered in different parts of the basin such as in the Kudu gas field.

A younger potential source rock known in the Orange Basin is the Cenomanian/Turonian aged terrestrial organic matter rich oil-gas prone claystones with TOC content of approximately 2% (Hartwig, 2014). This source rock has also been encountered in other basins along South Atlantic margin. The following figure shows the schematic geological cross-section of the pay zones within the Orange Basin.

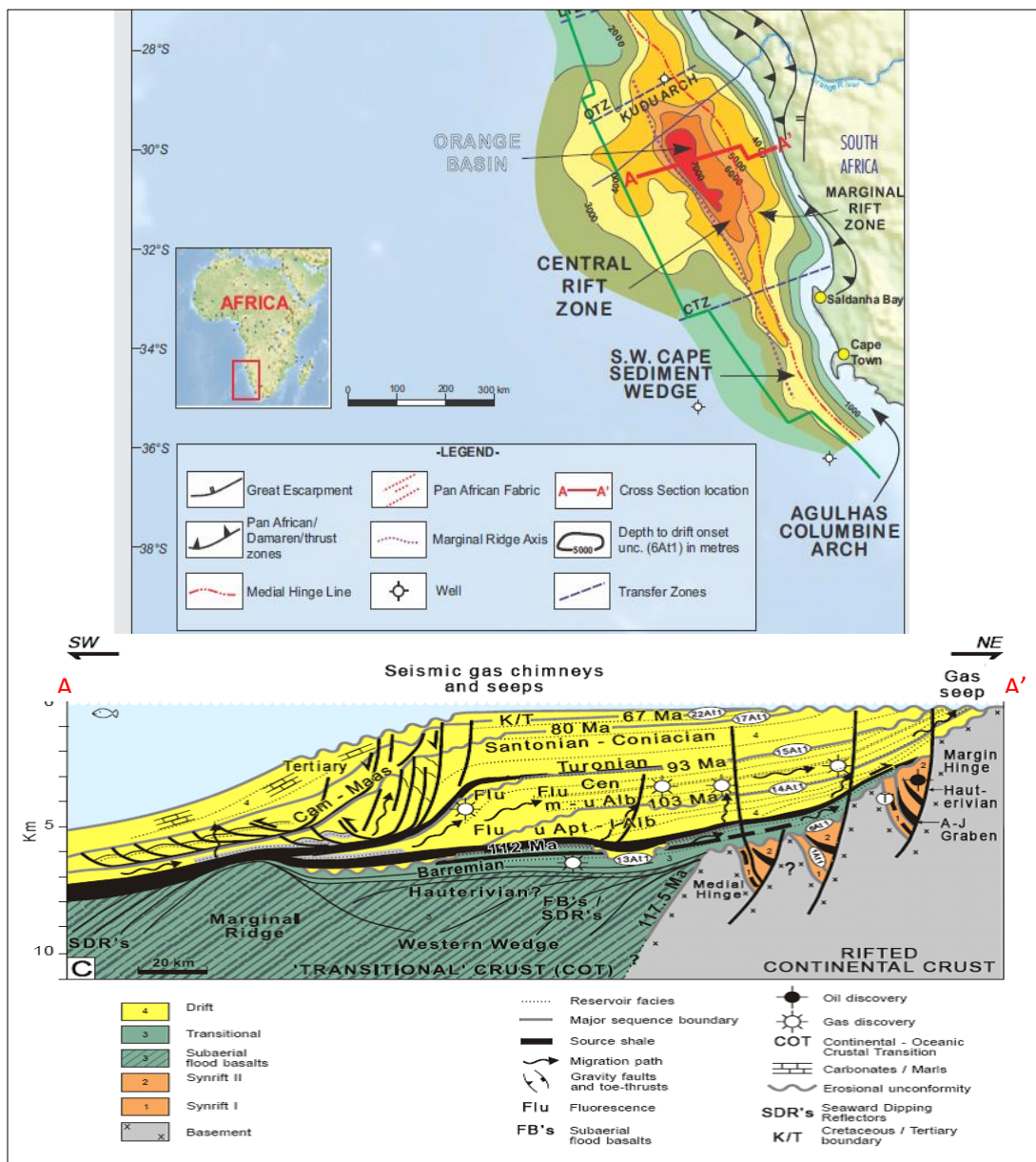


Fig.2.4. Schematic geological cross-section of the pay zones within the Orange Basin (PASA, 2008).

2.5.2 Reservoirs, Seals and Traps

The strongest petroleum system known to date in the Orange Basin is the natural gas produced from the Barremian aged aeolian sandstones of the Kudu gas field (PASA, 2008). These aeolian sands are expected to occur regionally in the northern Orange Basin (Van der Spuy, 2003). The reservoir zones are fluvial channel fill sandstones in the Ibhubesi gas field and permeable aeolian sandstones in Kudu gas field. Traps are mostly combination traps (stratigraphic and structural) while seals (top seals, seat seals, lateral seals and up-dip seals) are generally provided by the marine shales.



CHAPTER THREE

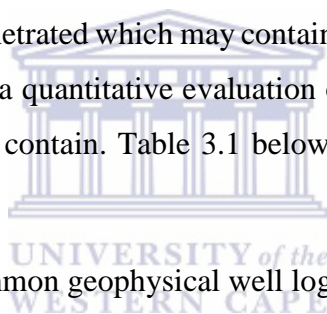
3. REVIEW OF TECHNIQUES

To achieve the main aims and objectives of this study various subsurface techniques from geophysics to geology and petrophysics have been integrated. In this chapter all the techniques incorporated in the study are reviewed and discussed in detail. Such techniques include wireline logs, petrophysical properties, seismic interpretation, core logging, well correlation, and petrography studies.

3.1 Well Logs

Geophysical well logging is the process of recording geophysical parameters along the borehole/well. The value of the recorded measurement is plotted continuously against depth in the well. Well logging enhances the ability to determine the types of formation intersected by the well and of those formations penetrated which may contain hydrocarbons. The measurements taken by the logging tools provide a quantitative evaluation of the formations encountered and the type and quantity of fluid they contain. Table 3.1 below shows common geophysical logs based on log measurements.

Table 3.1: Classification of the common geophysical well log (Rider & Kennedy, 2013).



| | Log type | Formation Parameter Measured |
|--------------------------|----------------------------|---|
| Mechanical measurements | Caliper | Hole diameter |
| Spontaneous measurements | Gamma ray | Natural radioactivity |
| | Self potential | Spontaneous electrical currents |
| | Temperature | Borehole temperature |
| Induced measurements | Resistivity | Electrical resistivity (direct measurement) |
| | Sonic | Velocity of waves |
| | Density | Response of higher energy gamma ray bombardment |
| | Neutron | Response to neutron bombardment |
| | Nuclear Magnetic Resonance | Induced proton electromagnetic field |

3.1.1 Caliper Logs

Caliper tools are used for measuring the size and shape of the well hole. The tools have 2, 4 or more extendable arms which can move in and out as the tool is withdrawn from the borehole (see Figure 3.1 below). Tools with more arms give a more detailed assessment of the borehole shape and size (Rider & Kennedy, 2013). The movement of the arms is converted into an electrical signal by a potentiometer. The caliper log is usually a dashed line plotted in track 1 along with the drill bit size log for comparison. The calliper log scale is mostly in inches of borehole diameter, which is standard for measuring bit size. The log can be used for various purposes such as:

- Calculation of mudcake thickness
- Measurement of borehole volume
- Measurement of required cement volume
- Assessment of the well hole quality
- Selection of consolidated formations for wireline pressure tests.

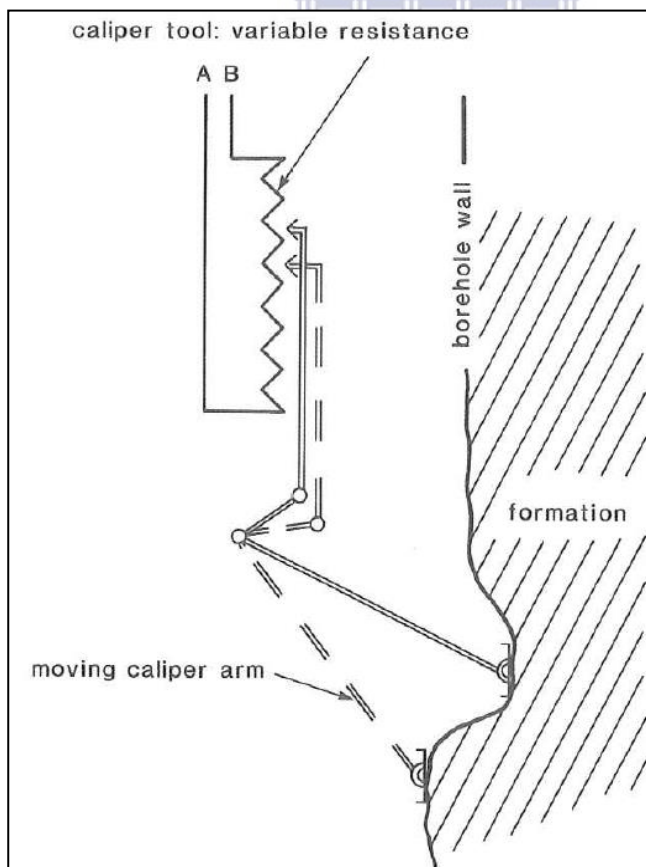


Fig.3.1. Caliper tool showing the conversion of a mechanical movement to an electrical signal (Rider & Kennedy, 2013).

3.1.2 Gamma Ray Logs

Gamma ray logs are used to measure the natural gamma ray emissions from radioactive formations. Gamma rays naturally occur from three sources. These are radioactive elements of the Uranium, Thorium and Potassium groups. The aforementioned elements are often concentrated in silts and shales but they can also be found in feldspathic sandstones. Since gamma rays can pass through steel casing, gamma ray logs can be run in both open and cased holes. Gamma ray tools consist of a gamma ray detector and the associated electronics for passing the gamma ray count rates to the surface (see Figure 3.2. below).

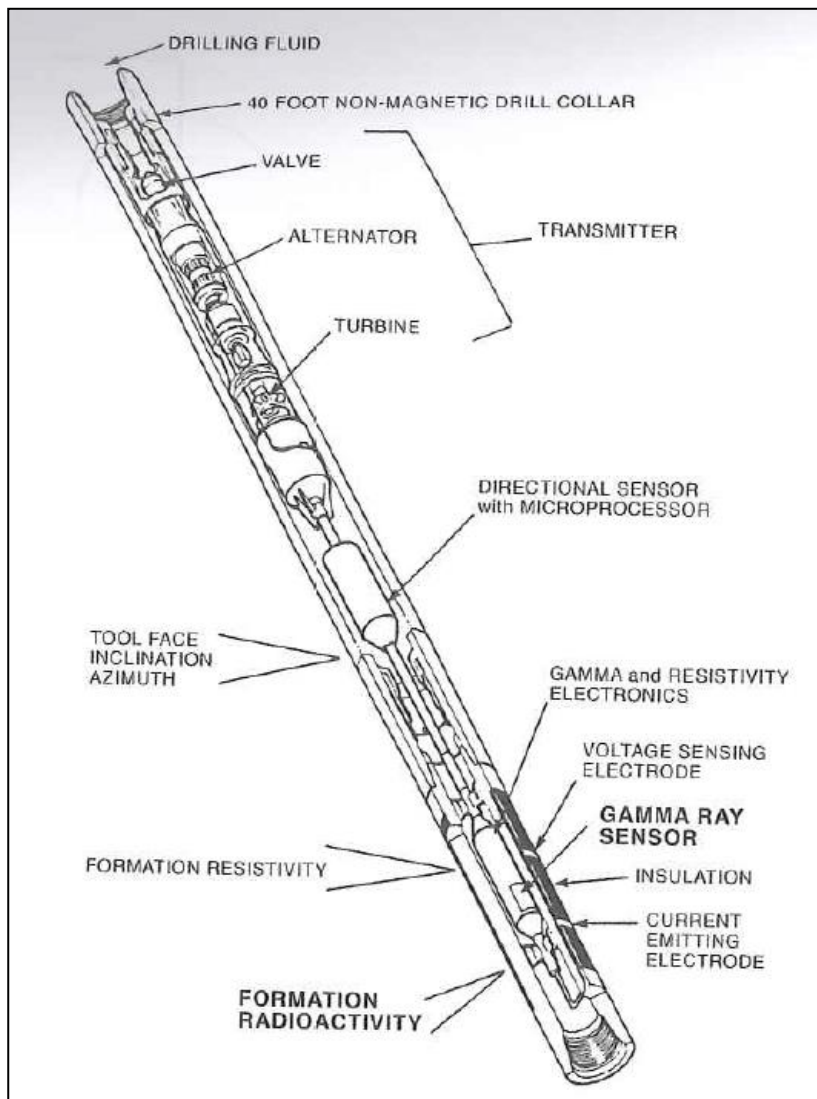
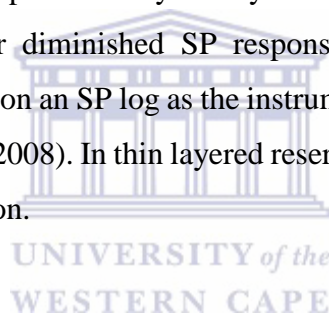


Fig.3.2. Gamma ray tool connected to drill collars as part of bottom hole assembly (Rider & Kennedy, 2013).

Gamma ray logs are measured in API (American Petroleum Institute) units. The log is usually represented in track two on a linear grid on a scale of 0-150 API. Clean non-feldspathic sands have low API causing the gamma ray log to be deflected to the left while shales have high gamma ray reading, deflecting the log to the right. Due to their potential to differentiate lithologies, gamma ray logs are often used for well correlation. They are also largely used for the evaluation of shale content of a formation and sometimes for mineralogy analysis.

3.1.3 Self Potential Logs

The SP log is a measurement of the natural potential differences or self potentials between an electrode in the borehole and a reference electrode at the surface (M. Rider & M Kennedy, 2013). The SP logs are mainly used to estimate shale volume (vsh), identify fresh water, indicate lithologies and also to measure permeability. They are also used for the detection of hydrocarbons through a muted or diminished SP response (Evenick, 2008). Thin layered lithologies are not easily detectable on an SP log as the instrument records bulk lithologies rather than separating the units (Evenick, 2008). In thin layered reservoirs gamma ray logs are probably the best to use for lithology detection.



3.1.4 Temperature Logs

In general, temperatures in subsurface formations increase with depth at a constant rate. This constant rate is known as geothermal gradient and it differs from basin to basin due to factors such as the tectonic history of a basin, overburden and sedimentation history. The temperature of a borehole is largely influenced by geothermal gradient and the drilling fluids. The temperature logging technique measures the temperature of the wellbore fluids and formations. The log detects changes in thermal conductivity of the rocks along the wellbore (Opuwari, 2010). Temperature logs can be used for various reasons. One of its well-known use is to assess the source rock potential to produce hydrocarbons.

3.1.5 Resistivity Logs

The electrical resistivity of a rock formation is its ability to impede the flow of electrical current. The resistivity log records the resistance to the flow of electricity through a subsurface formation in ohm/meter (Evenick, 2008). Most logged subsurface formations contain either water or hydrocarbons. Resistivity is sensitive to fluids and porosity. An electrical current will only flow through the rock formation if the formation water contains salt ions such as Na^+ and Cl^- ions. When electrically charged, these salt ions move through the formation carrying an electrical current. This results in salty water filled formations having lower resistivities than hydrocarbon filled formations. Hydrocarbons (oil and gas) are insulators and they do not conduct electricity; thus the resistivity of a gas/oil filled formation is high. Resistivity logs are the most powerful logs in differentiating formations fluids. While resistivity logs are most commonly used for differentiating fluids, they are also useful as lithology indicators. Shales usually have low resistivity readings while sandstone and limestone have high resistivity values. The three most common types of resistivity logs run during a logging programme include the shallow resistivity log, the medium resistivity log and the deep resistivity log. Shallow resistivity logs record the interface of the borehole and drilling fluid, the medium resistivity log records the zone between the interface and the un-invaded zone while the deep log records the un-invaded formation (Evenick, 2008).

UNIVERSITY of the
WESTERN CAPE

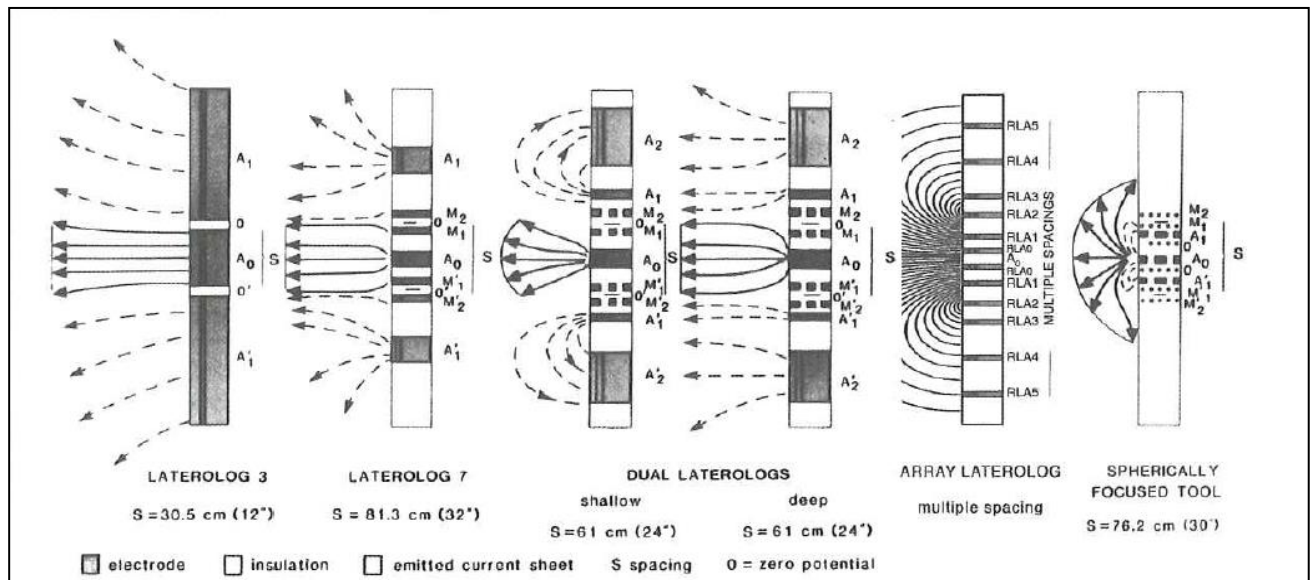


Fig.3.3. Electrode distribution in wireline resistivity tools, where A=electrode and M=monitoring electrode. (Rider and Kennedy, 2013).

3.1.6 Sonic Logs

A sonic log is the measure of the formations capacity to transmit sound waves in microseconds per foot. Sonic tools are designed to measure the acoustic characteristics of a formation. The logging tool measures the time that a pulse of sound travels through a formation over a known distance. The tool therefore comprises of a transmitter and one or more receivers placed at a measured distance apart. Sonic logs are good porosity indicators; hence they are called porosity logs because the speed at which the rock transmits sound waves is associated with the porosity of the formation. Sonic logs are also good formation fluid indicators (gas in particular). A formation section filled with gas usually gives an erratic sonic response because the gas has slower transmittal time (Evenick, 2008). Figure 3.4 below is a representation of a wireline sonic tool.

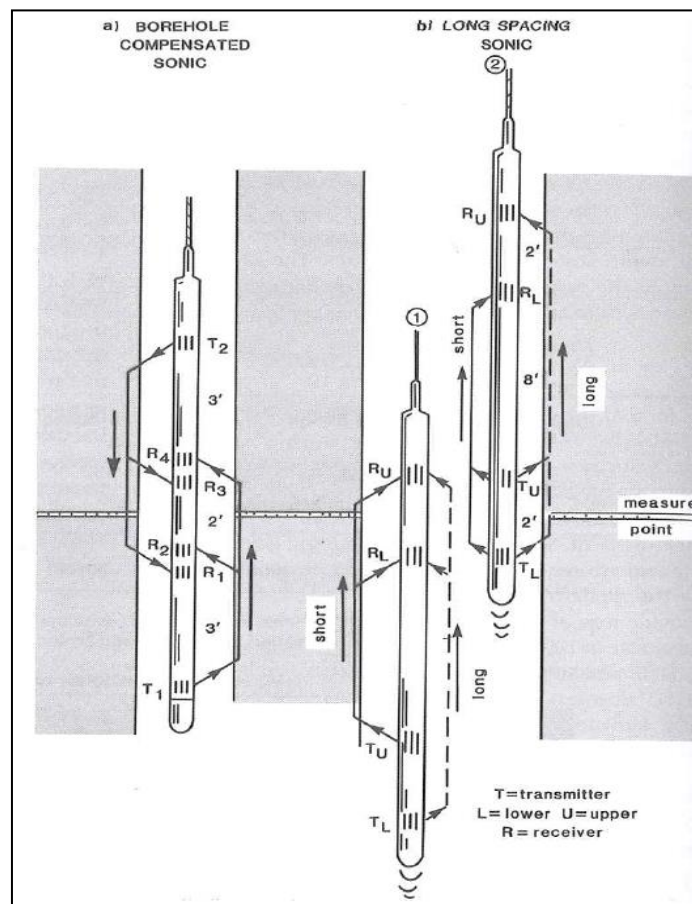


Fig.3.4. Schematic representation of a wireline sonic tool (Rider & Kennedy, 2013).

3.1.7 Density Logs

Density logs record the bulk density of a formation which is the sum of solid matrix density and fluid density enclosed in the pores of the formation (Horsfall et al., 2013). Table 3.2 below shows grain density values of common sedimentary rocks and fluids. Clastic sediments such as sandstone and shale often have low density values compared to carbonate rocks (Dolomite & limestone).

Table 3.2: Grain densities of common sedimentary rocks and fluids (Evenick, 2008).

| | |
|---------------------|---------------------------|
| Shale | 2.4-2.6 g/cm ³ |
| Sandstone | 2.65 g/cm ³ |
| Limestone | 2.71 g/cm ³ |
| Dolomite | 2.87 g/cm ³ |
| Salt | 2.03 g/cm ³ |
| Drilling Mud | 1-1.1 g/cm ³ |
| Water | 1.0 g/cm ³ |
| Crude Oil | 0.8-1.0 g/cm ³ |
| Natural Gas | 0.7 g/cm ³ |

During density logging, a radioactive source placed on the sides of a wellbore emits gamma rays into the formation. As these gamma rays travel into the formation, they collide with electrons within the formation. At each collision, the gamma rays lose some of their energy to the electrons and eventually run out of energy. The scattered gamma rays reaching the receivers are measured as formation density. Figure 3.5 is a representation of a wireline density tool. The fundamental use of a density log is to measure/calculate porosity of a formation straight from the log. Other uses could include detection of a gas reservoir when combined with a neutron log (gas effect), evaluation of shaly sands, identification of minerals in evaporate units, calculation of overburden pressure. The frequently used porosity calculation from a density log [(grain density-measured bulk density)/ (grain density-drilling fluid density)] tends to overestimate the porosity of a gas filled reservoir because the measured bulk density will be lowered (Evenick, 2008). This is what causes a gas effect when a neutron log in gas reservoir is cross plotted with a density log.

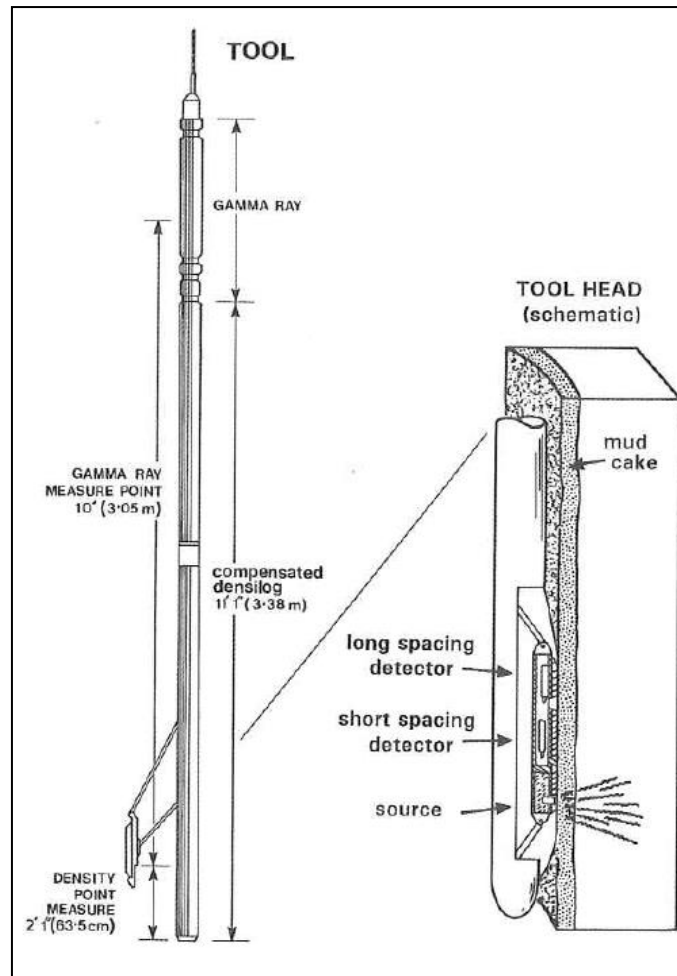


Fig.3.5. Schematic representation of a wireline density tool. (Rider & Kennedy, 2013).

3.1.8 Neutron Logs

Neutrons are electrically neutral particles each with a mass similar to that of a hydrogen atom. The neutron logging process involves three vital steps: neutron emission, neutron scattering and neutron absorption. During neutron emission, the tools operate by bombarding the formation with high energy neutrons from a radioactive source. The neutron sources used are often radium and beryllium. When these fast neutrons strike the formation, they undergo scattering losing energy and producing high energy gamma rays. The scattering process occurs most rapidly with hydrogen atoms. In formations with huge volumes of hydrogen atoms, neutrons are slowed down and absorbed rapidly. The count rate of the detected low energy neutrons is related to the amount of hydrogen atoms in the formation. Formations with high porosities have a low count rate and those with low porosities have a high count rate.

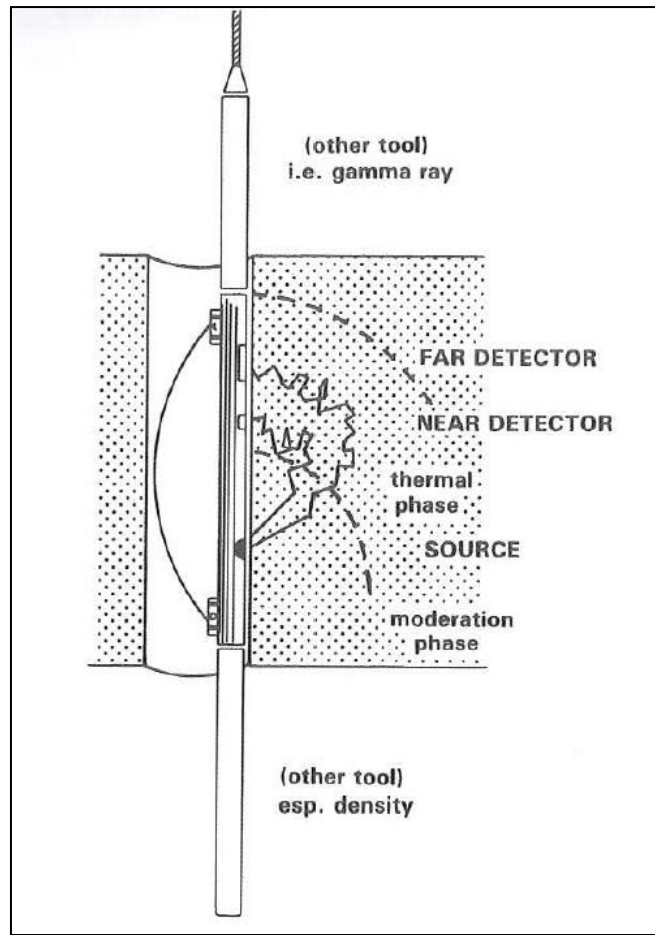


Fig.3.6. Schematic representation of wireline compensated neutron tool. The source and detectors are held pressed against the borehole wall by a bow-spring (Rider & Kennedy, 2013).

Neutron logging tools differ and the three common types are:

- Gamma ray/Neutron Tool (GNT)
- Sidewall Neutron Porosity Tool (SNP)
- Compensated Neutron Log (CNL)

Neutron log data are often recorded in either track 2 or track 3 with a density log. The units of the log depend on the type of a tool used. Data from the GNT tool is represented in API units while data from CNL and SNP is given in equivalent limestone porosity units. The main purpose of running a neutron log is to measure the porosity of a formation.

3.2 Petrophysical Properties

3.2.1 Porosity

Porosity is one of the most crucial rock properties. By definition it is the percentage of void space in a rock. It can also be expressed as the ratio of the volume of the pore space divided by the total volume (Zimmerle, 1995).

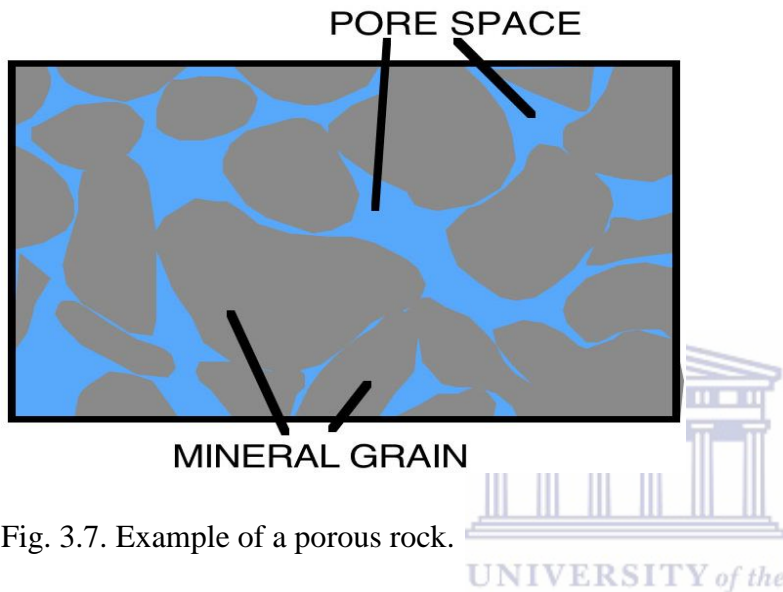


Fig. 3.7. Example of a porous rock.

Various types of porosities exist depending on the degree of connectivity or the time of pore development. The most common are total porosity and effective porosity. Total porosity is the ratio of the total pore space to the total bulk volume, as expressed in equation 3.1 below. Effective porosity on the other hand is the ratio of interconnected pore space to the bulk rock volume.

$$\phi = \frac{V_p}{V_b} \dots\dots\dots (3.1)$$

Where:

V_p =Pore Volume

V_b = Bulk Volume

Φ = Porosity

Porosity of a rock depends on many factors; including the rock type and the way the grains of a rock are arranged. During sediment deposition, primary porosity of a rock develops. Over time when sediments are buried secondary porosity may develop, resulting from diagenetic processes such as leaching, compaction, clay coating and sometimes bioturbation.

3.2.2 Permeability

Permeability is a measure of the ability of a rock to allow fluids to flow through it (Ulusay et al., 2016). It is therefore a crucial property in defining the flow capacity of a rock sample. The magnitude and/ or direction of permeability of a rock are controlled by numerous factors. Such factors include grain size distribution, sorting and packing of grains, type of clays present in a reservoir rock, type and amount of secondary porosity.

Formation permeability can be easily measured straight from the core samples taken at the reservoir zones or from well testing (Jahn et al., 2008). For measurements from the cores (see figure 3.8 below), the samples are mounted in a holder and gas is flowed through the core (Jahn et al., 2008). Pressure drop and gas flow rate across the core sample are then measured.

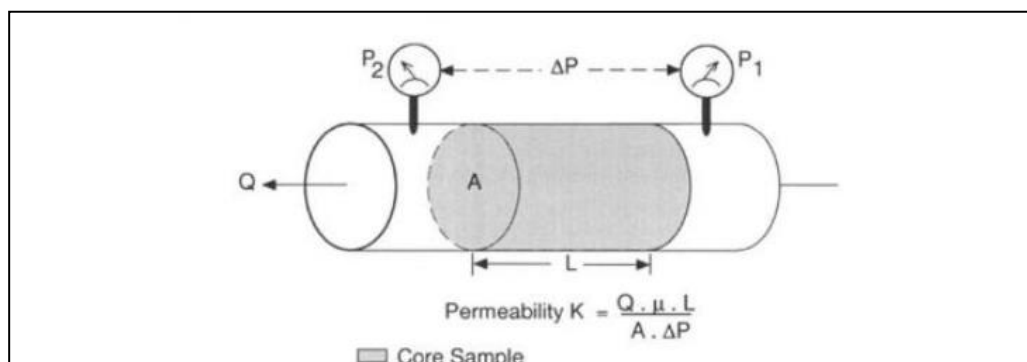


Fig.3.8. Core permeability measurement (Jahn et al., 2008).

Permeability is measured in Darcies, named after Henri Darcy who discovered the phenomenon. Mathematically, permeability is measured in terms of flow rate, area, length, pressure differential and fluid viscosity as expressed in the equation below:

$$K = Q \mu L / \Delta P A \dots\dots\dots (3.2)$$

Where:

- K = Permeability (darcy)
- Q = Flow per unit time (cm/s)
- μ = Viscosity of flowing medium (cp)
- A = Cross section of rock (cm²)
- L = Length of rock (cm)
- ΔP = Change in pressure (psi)

3.2.3 Water Saturation

Water saturation (S_w) is the fraction of the pore volume occupied by formation water. Water saturation is often derived from resistivity logs with knowledge of formation porosities, water resistivity and shale volume (Thompson & Woods, 1993). According to Archie's law, water saturation of clean formation water can be expressed as:

$$S_w^n = F.R_w / (R_t) \dots\dots\dots (3.3)$$

Where:

- S_w = Water saturation
- F = Formation resistivity factor
- R_w = Resistivity of formation water
- R_t = True formation resistivity
- n = Saturation exponent

The formation resistivity factor is the tortuosity of the conductivity paths in the formations (Thompson and Woods, 1993) and is expressed as:

$$F = a / \Phi^m \dots\dots\dots (3.4)$$

Where:

a and m are 0.81 and 2 for sediments respectively based on experiments.

Archie’s model for water saturation is only applicable for clean sands. For shaly formations Simandoux’s equation is used to account for the effect of shale conductivity in reservoirs (Thompson & Woods, 1993). The equation is expressed as:

$$1/R_t = [S_w^2 / F * R_w (1 - V_{sh})] + [(V_{sh} * S_w) / (R_{SH})] \dots \dots \dots (3.5)$$

Where:

S_w = Water Saturation

F = Formation resistivity factor

R_{SH} = Resistivity of shale

V_{sh} = Volume of shale

R_w = Resistivity of formation water

R_t = True formation resistivity

n = Saturation exponent



3.2.4 Volume of Shale

Volume of shale in a conventional reservoir rock is the volume fraction of shale in a formation (Kennedy, 2015). Volume of shale is best quantified by using logs that are sensitive to shales. Such logs include gamma ray logs and self potential (SP) logs. There are limitations and advantages associated with both logging measurements. Gamma ray logs are most useful in formations with minimal uranium while SP logs are useful where formation resistivities and mud filtrate contrast (Thompson & Woods, 1993). Estimation of shale volume from the SP log is often quick but it has limited vertical resolution and often overestimates shale volume in hydrocarbon bearing zones (Thompson & Woods, 1993). Volume of shale derived from an SP log is expressed as:

$$V_{sh} = (SP_{sh} - SP) / (SP_{sh} - SP_{cl}) \dots \dots \dots (3.6)$$

Where:

V_{sh} = Volume of shale

SP_{sh} = SP value of a shaly unit

SP = SP value at reservoir of interest

SP_{cl} = SP value of a clean reservoir

The gamma ray technique for calculating volume of shale in reservoirs is commonly used over the SP method. This method has a linear and a non-linear function. The linear method is frequently used but it often overestimates shale in reservoir formations (Thompson & Woods, 1993). The linear equation is expressed as:

$$V_{sh} = (GR_{sh} - GR) / (GR_{sh} - GR_{cl}) \dots \dots \dots (3.7)$$

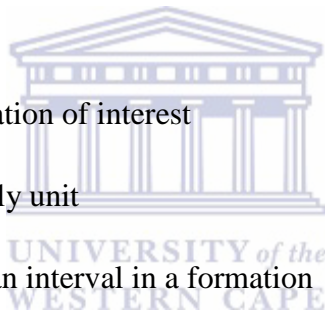
Where:

V_{sh} = Volume of shale

GR = Gamma ray value in the formation of interest

GR_{sh} = Gamma ray value over a shaly unit

GR_{cl} = Gamma ray value over a clean interval in a formation



Various non-linear equations for estimating volume of shale exist. This method firstly estimates V_{sh} from the linear equation then applies a correction to the aforementioned equation using figure 3.9 below. The nonlinear equations associated with figure 3.9 are:

- Larionov (1969) for Tertiary rocks: $V_{sh} = 0.083 (2^{3.71 GR} - 1) \dots \dots \dots (3.8)$

- Steiber (1970) : $V_{sh} = (I_{GR}) / (3 - 2 * I_{GR}) \dots \dots \dots (3.9)$

- Clavier (1971) : $V_{sh} = 1.7 [(3.38 - (I_{GR} + 0.7)^2)]^{1/2} \dots \dots \dots (3.10)$

- Larionov (1969) for older rock : $V_{sh} = 0.33 * (2^{2 I_{GR}} - 1) \dots \dots \dots (3.11)$

Where:

I_{GR} = Gamma ray index calculated from the linear equation.

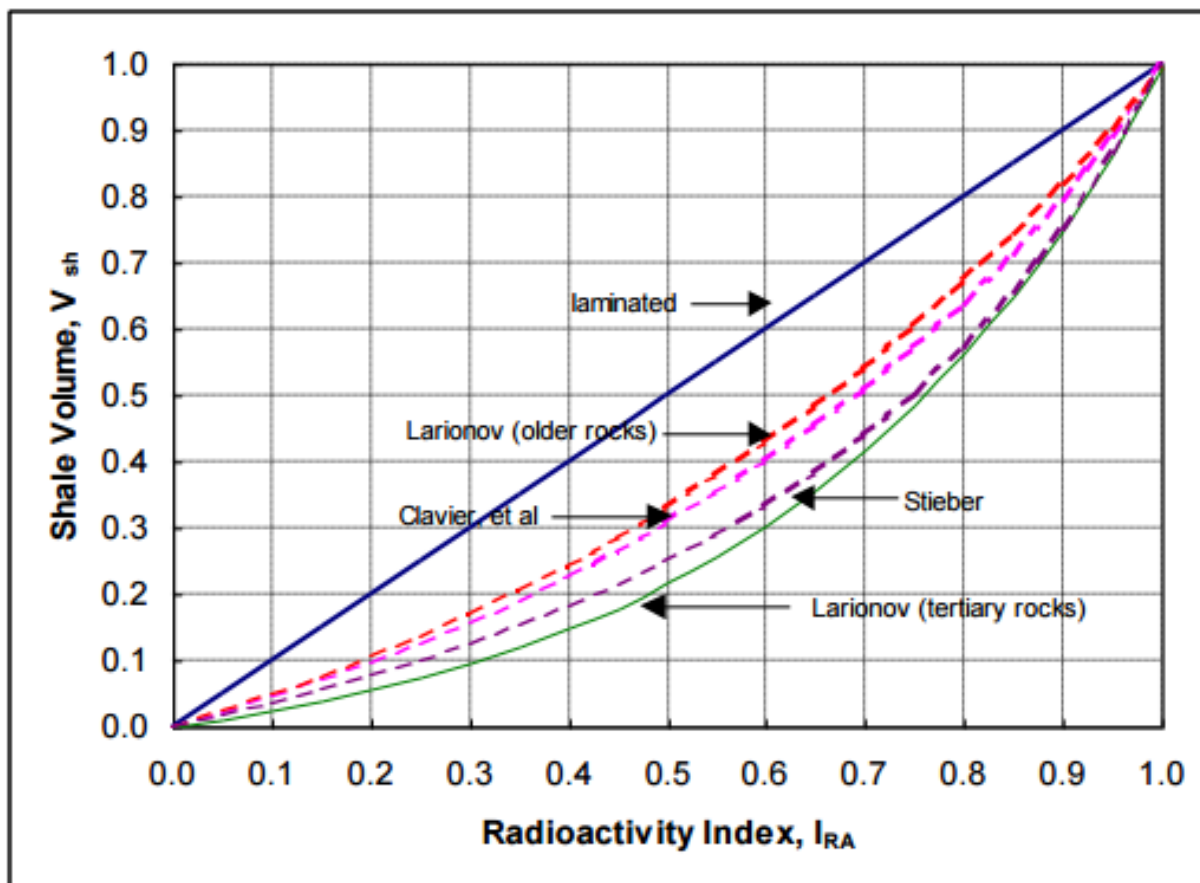
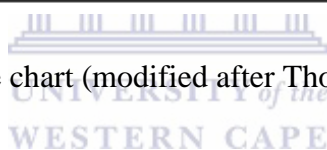


Fig.3.9. Non-linear volume of shale chart (modified after Thompson & Woods, 1993).



3.3 Seismic Interpretation And Seismic Attributes

Seismic interpretation is picking and tracking of seismic reflections for the purpose of mapping geologic structures, stratigraphy and reservoir architectures with an ultimate goal of detecting hydrocarbon accumulations (Chopra & Marfurt, 2005). A seismic reflection occurs when there is a contrast in acoustic impedance between layers in the subsurface. The change in properties between two rock layers results in an acoustic impedance boundary which in turn causes a seismic reflection. The fundamental objective of seismic interpretation is to determine the nature of the subsurface formations reflected on a seismic section and eventually the nature of fluids contained by the formations. Hence seismic interpretation is considered as one of the most crucial steps towards finding movable accumulations of hydrocarbons. Picking seismic events as they appear on seismic is the key step in seismic interpretation. Mapping of geologic features on seismic data is greatly influenced by the quality of the seismic data. Good quality seismic data

facilitates a more accurate interpretation. The quality of seismic data is dependent on the acquisition and processing of the data.

The geometry and distribution of geologic features are often identified from seismic data by employing seismic attributes. In a nutshell, seismic attributes are simply geophysical measurements based on seismic data. Seismic attributes may help to visually boost seismic interpretation from a regional depositional setting to a prospect scale. Good seismic attributes are sensitive to lithologies, geologic structures, reservoir properties (Chopra & Marfurt, 2007) and sometimes reservoir fluids. Seismic attributes used in this research study are amplitude attributes, the spectral decomposition attribute, and the coherency attribute.

3.3.1 Amplitude Seismic Attributes

Amplitudes are the result of acoustic impedance contrast and therefore they are sensitive to rock and fluid properties (Donald, 2011). Amplitude attributes include Root Mean Square (RMS), Mean Amplitude, Amplitude Versus Offset (AVO), average energy.

- RMS amplitude attribute is a post stack attribute that computes the root squares on the instantaneous trace over a given window. RMS attributes are good reservoir indicators (Schlumberger, 2015).
- Mean amplitude computes the arithmetic mean of the amplitudes of a trace over a certain window (Schlumberger, 2015).
- Maximum amplitude attribute measures maximum reflectivity over a given window. It usually detects positive direct hydrocarbon indicators (DHI) such as bright spots (Schlumberger, 2015).

3.3.2 Spectral Decomposition Attribute

Spectral decomposition attribute is a process by which a seismic cube is converted into selected frequency cubes using a mathematical algorithm (Das et al., 2013). The attribute is run mostly for delineating channels and fans within a seismic cube. This approach works because at some frequencies, certain seismic features are more visible due to the tuning effect (Das et al., 2013) as shown in the Figure 3.10 below.

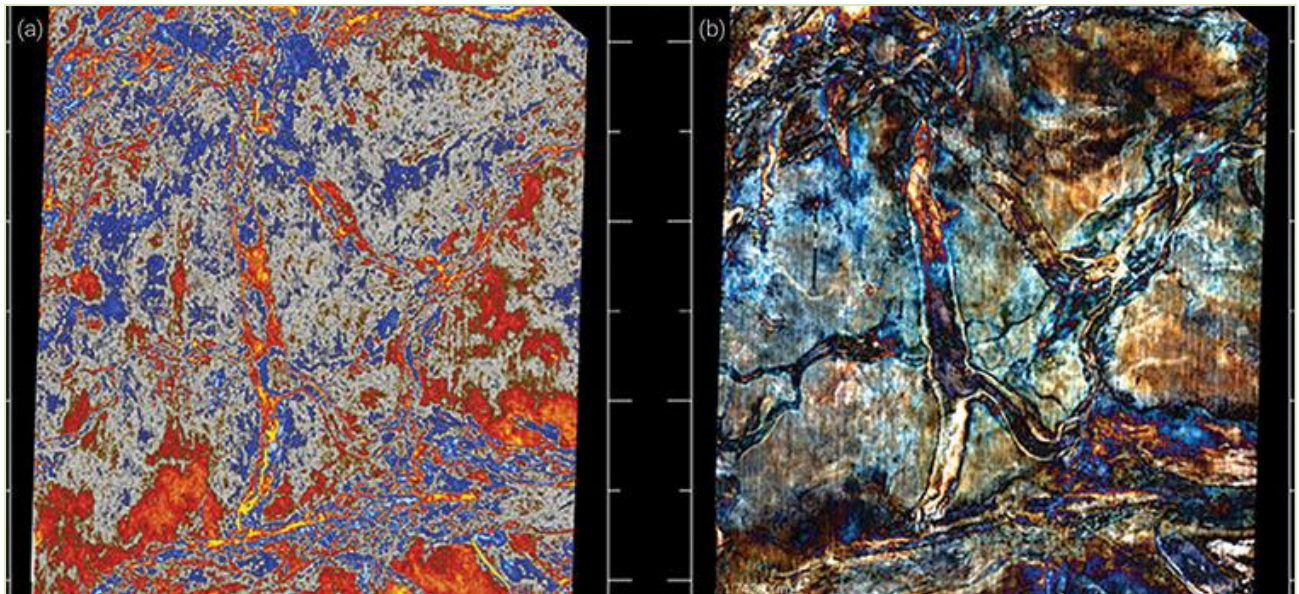


Fig.3.10. (a) Horizon slice of original seismic data (b) Colour-blend of three spectral decomposition components(<https://archives.aapg.org/explorer/2014/01jan/geocorner0114.cfm>).

3.3.3 Coherency Attribute

The coherency attribute is a 3D seismic attribute useful for mapping discontinuities such as faults, channels, salt domes and similar features on seismic data. The attribute measures the trace to trace similarity of the seismic waveform within a specified window (Donald, 2011) as indicated in the Figure 2.11 below.

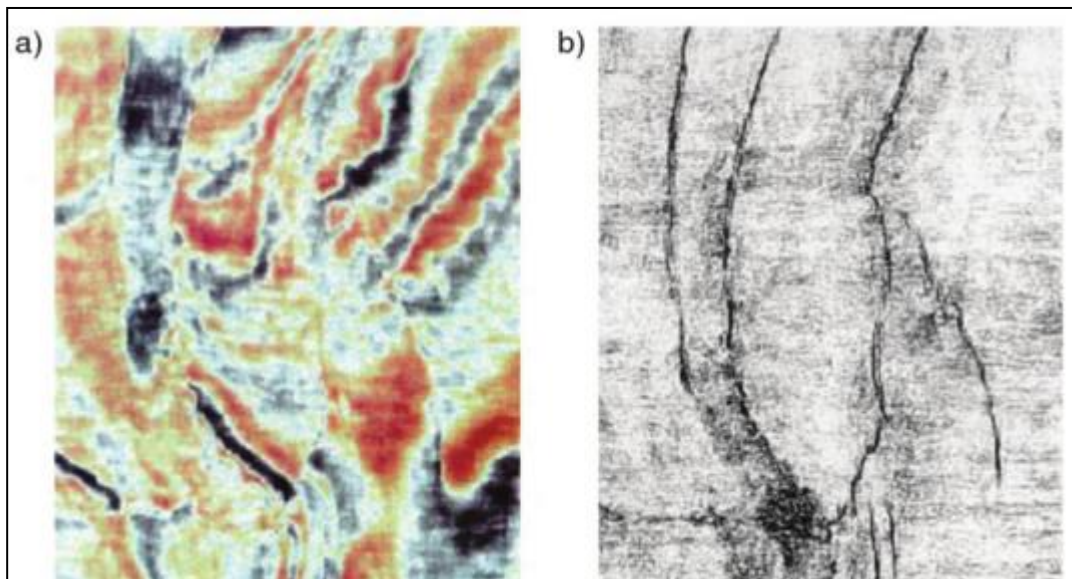


Fig.3.11. (a) Normal 3D seismic slice with unclear faults. (b) The same time slice but displayed in a coherency attribute shows clearly visible faults. (Bahorich & Farmer, 1995).

3.4 Sequence Stratigraphy

Sequence stratigraphy is a relatively new concept in the field of sedimentology and stratigraphy as it was only introduced in the 1970s by the research group of ExxonMobil. It is a very important aspect of reservoir characterization and distribution as it improves the understating of facies tracts, stratigraphic units and depositional setting in a sedimentary basin (Catuneanu, 2005). By definition, sequence stratigraphy is simply the subdivision of the stratigraphic record based on bounding discontinuities. A depositional sequence is deposited during one cycle of a sea level change and bounded by unconformities. On a basin scale these discontinuities/surfaces are best picked on seismic sections as seismic reflections often occur across discontinuities unless disrupted by structures such as faults and fold. The types of stratigraphic surfaces/discontinuities mapped on seismic in this study are unconformities (see Figure 3.12 below). Unconformities occur as a result of erosion of existing formations or due to non-deposition of sediments in geologic record. Angular unconformities are the most easily picked seismic reflectors because of an angularity between reflections (Telford et al., 2004). Although they are easily picked on seismic data, seismic character of unconformities usually changes across the studied basins/fields often due to facies changes. During the process of seismic interpretation, unconformities are useful for dividing the stratigraphy and facies of a studied basin/field into different depositional units. With seismic facies studies it is often possible to delineate the environment of deposition of a basin/field and its stratigraphy (Telford et al., 2004) as shown in Figure 3.12.

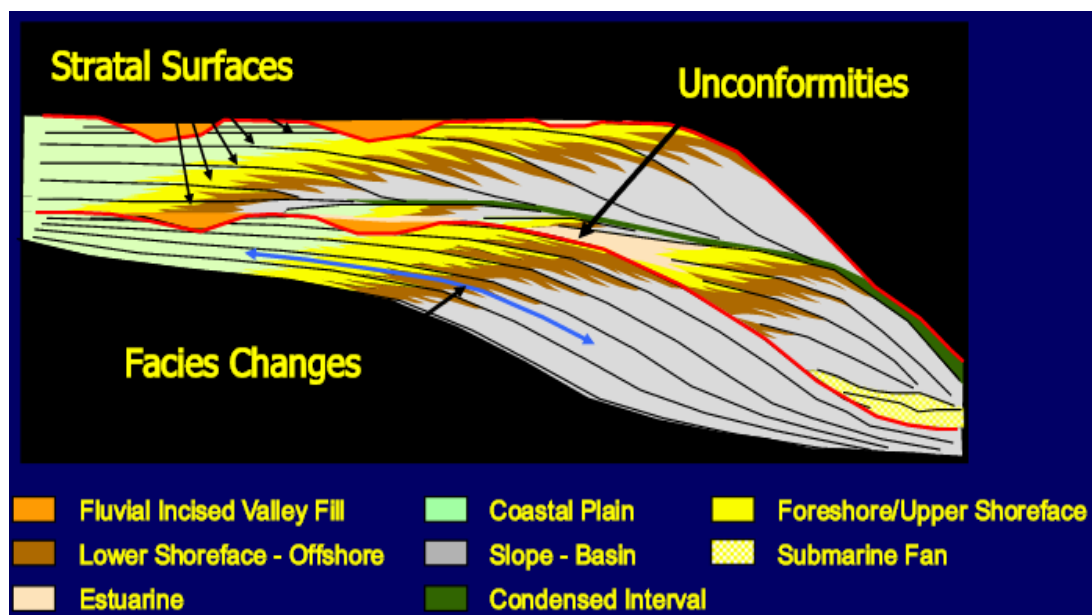


Fig.3.12. Stratal surfaces and unconformities (<http://slideplayer.com/slide/703732/>).

3.5 Core Analysis and Interpretation

Core data provide an accurate and comprehensive geological history of the formations/rocks drilled. The data measured from core logs are crucial as they are not available from either wireline log measurements or productivity tests (Ubani & Oriji, 2012). These data are also crucial for stratigraphic correlation and wireline log calibration purposes. Core analysis can make enormous contribution towards reservoir characterization and petrophysical evaluation of reservoir rocks as it is the only direct and quantitative measurement of the reservoir properties (McPhee et al., 2015). The core log analysis process may aim at determining several petrophysical properties such as effective porosity, permeability, capillary pressure, residual fluid saturation, flow rate of the reservoir and clay content in the reservoir (Konecki et al., 1963).

For accurate measurements of the reservoir properties, the core has to be in good condition and undamaged. Even the best petrophysical measurements might be meaningless if the core has been damaged or altered before conducting the tests on it (McPhee et al., 2015). Core damage or alteration can be caused by a number of things such as the type of coring fluid used, handling of the core at the wellsite, drying of the core samples in the laboratory. The aforementioned risks can be avoided if the core is handled well. Selection of coring fluids often depends on the requirements of core analysis (McPhee et al., 2015). Water based muds (WBS) are recommended for residual oil saturation determination and oil based muds (OBM) for residual water saturation (McPhee et al., 2015).

In the laboratory core analysis is often carried out on core plugs cut from the main core with a cylindrical rotary core bit attached on a drill press (see Figure 3.13 below). The plugs are cylinder shaped with a diameter of 38 millimetres and length varying between 25 millimetres and 76 millimetres (McPhee et al., 2015). Once the plug has been cut, it is then prepared for analysis by first cleaning and drying it to remove mud-filtrate and other solvents (McPhee et al., 2015). According to (Worthington, 1991) the preferred method of analysis is to measure fluid saturations on core plugs using the Dean Stark method, porosity and grain density using Boyle's law gas expansion method and lastly permeability measured using Hassler method.



Fig.3.13. Core plug drilling press and typical core plugs (McPhee et al., 2015).

3.6 Lithostratigraphic Well Correlation

Well log correlation can be defined as the demonstration of the continuity and equivalence of geologic features in time, age or even stratigraphic position. The technique involves the mapping of the lateral extent and variation of lithologies across a field or basin. It is a crucial process in basin and reservoir analysis as it often aims at determining the subsurface position and thickness of marker beds, facies thickness (Zimmerle, 1995). Figure 3.14 on the following page is an example of well log correlation of deep marine turbidites in the North Sea.

Usually well logs such as the gamma ray logs, SP logs, sonic logs, density logs, resistivity logs and dipmeter logs are the only type of data used for well correlation (Jahn et al., 2008). SP and short spacing resistivity logs are often used for regional correlations (Zimmerle, 1995). The lateral extent of lithofacies is best studied by combining gamma-ray logs, density logs and an SP log. Depositional environments also greatly influence the type of well logs to use for correlation. In carbonate environments, best well correlations are achieved by combining gamma-ray logs, resistivity logs and density logs (Zimmerle, 1995). In evaporites, a combination of gamma-ray logs, sonic logs and density logs often give good results due to their notable segregation (Zimmerle, 1995). Other depositional environments such as fluvial and deltaics are not easily

correlated on a regional scale. Correlation in these environments is usually achieved if there are marker beds such as coals, shales and volcanic ashes.

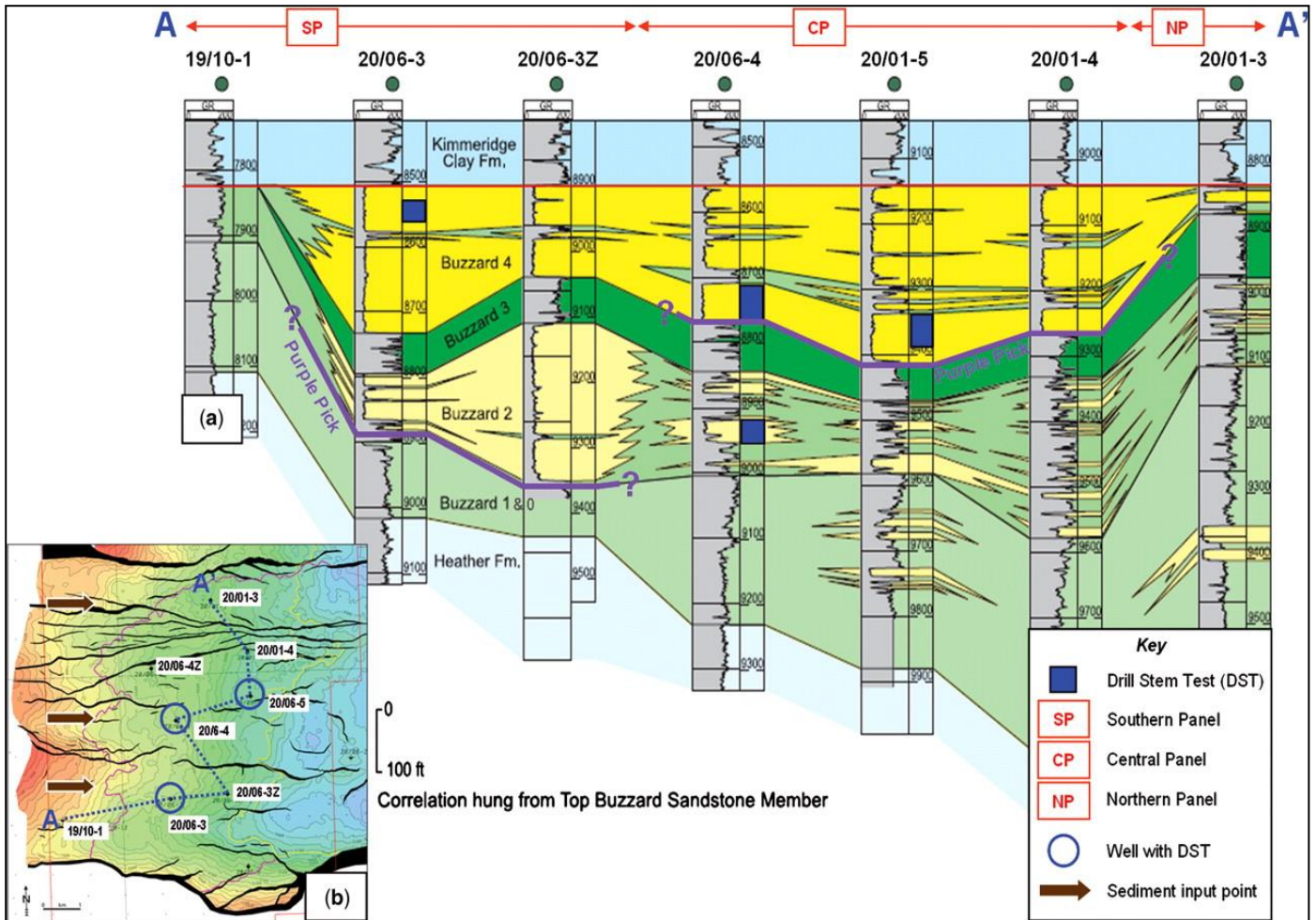


Fig.3.14. Well correlation of the Buzzard field, North Sea (Ray et al, 2010).

3.7 Depositional Environments, Diagenesis and Reservoir Quality

The quality and performance of a hydrocarbon reservoir is strongly influenced by its depositional environment and later by diagenesis. By definition, diagenesis is a process involving all the physical, chemical and biological changes that occur when sediments are transformed into a sedimentary rock. These processes vary for all depositional environments and they heavily influence reservoir parameters such as porosity, permeability, volume of shale, water saturation and types of authigenic minerals formed. The effects of diagenesis on clastic reservoirs include

destruction either by cementation and/or compaction and the enhancement of porosity by solution (Selly & Sonnenberg, 2014).

Therefore, the amount of recoverable hydrocarbons a reservoir can produce is largely controlled by the environment of reservoir deposition. Figure 3.15 below shows the diagenetic clay minerals associated with various depositional environments. In this figure, kaolinite occurs in a non-marine to shore-face environment with higher concentrations towards the unconformities where fluvial sands are exposed to meteoric water flushing (Catuneanu, 2005). Water flushing promotes the formation of kaolinite from dissolution of unstable minerals such as feldspar (Catuneanu, 2005). Smectites often occur in a non-marine to shoreface environment. Under shallow marine conditions, glauconites are most abundant towards unconformities (Catuneanu, 2005).

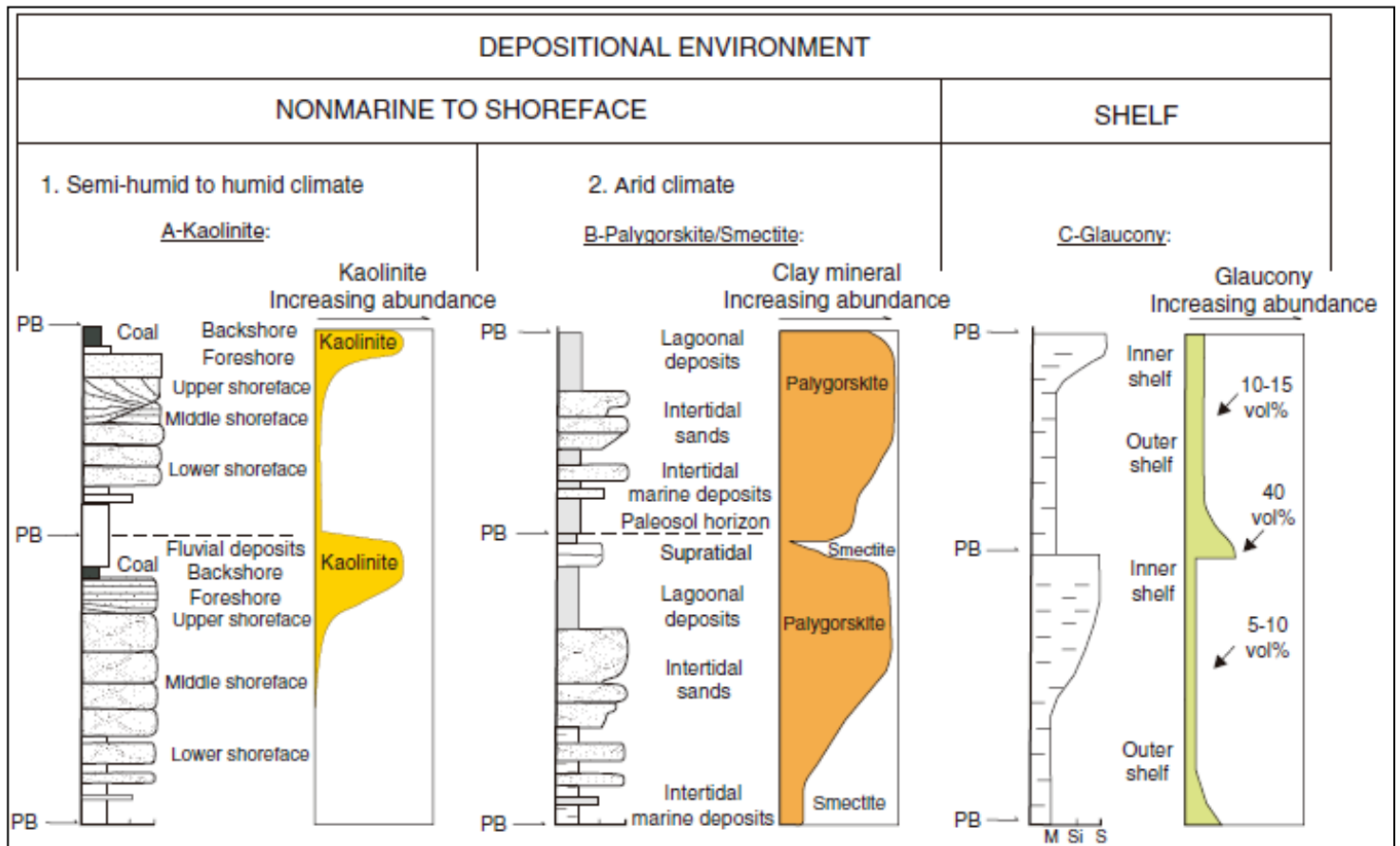


Fig.3.15. Predictive distribution of diagenetic clay minerals associated with fluvial to shallow marine depositional environment (Catuneanu, 2005).

CHAPTER FOUR

4. MATERIALS AND METHODOLOGY

This chapter discusses the methods and materials used during the course of this research study. The study commenced in February 2015 by reviewing previous work done on the Orange Basin and it concluded in November 2016 by submitting the final report. Petrel 2014 version and Interactive Petrophysics version 4.3 were used for the interpretation of seismic and log data. Figure 4.2 summarises the methods applied to carry out the study. The materials used for the research study were obtained from the Petroleum Agency of South Africa (PASA). The dataset consists of:

- ✓ Digital wireline logs
- ✓ 3D Seismic data
- ✓ Well tops
- ✓ Well reports
- ✓ Conventional core log data
- ✓ Sidewall cores of selected depths

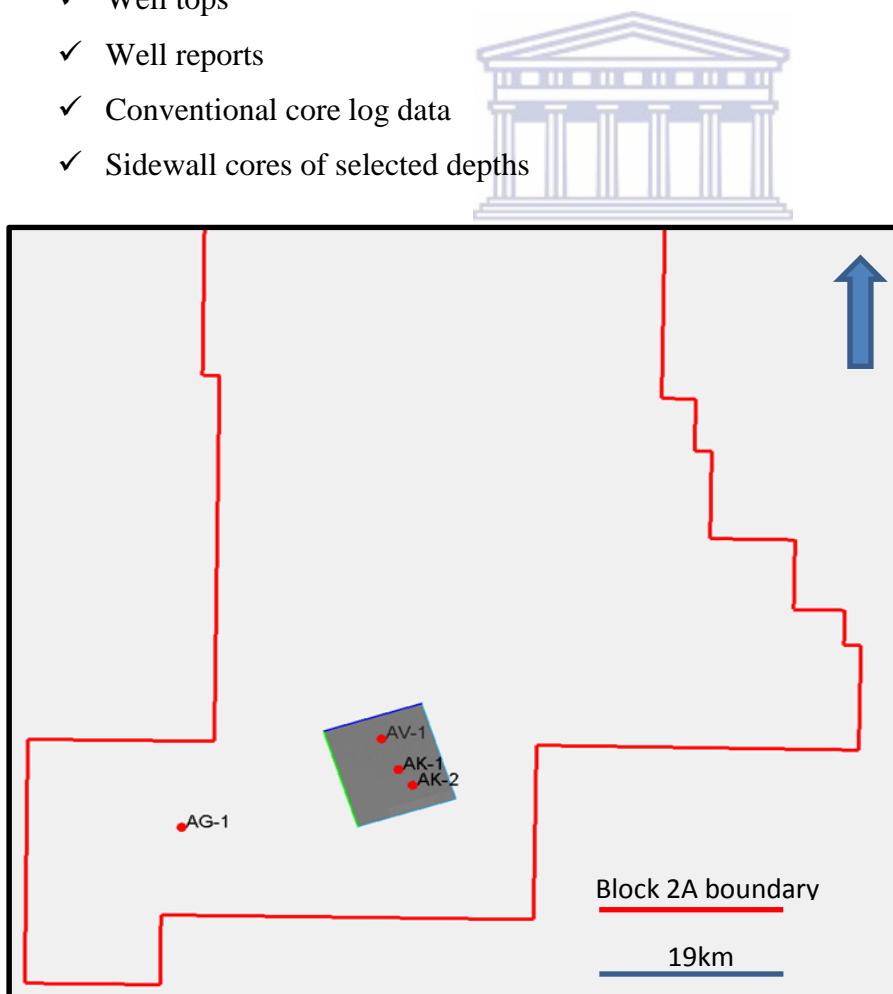


Fig.4.1. Base map of block 2A with wells and 3D outline.

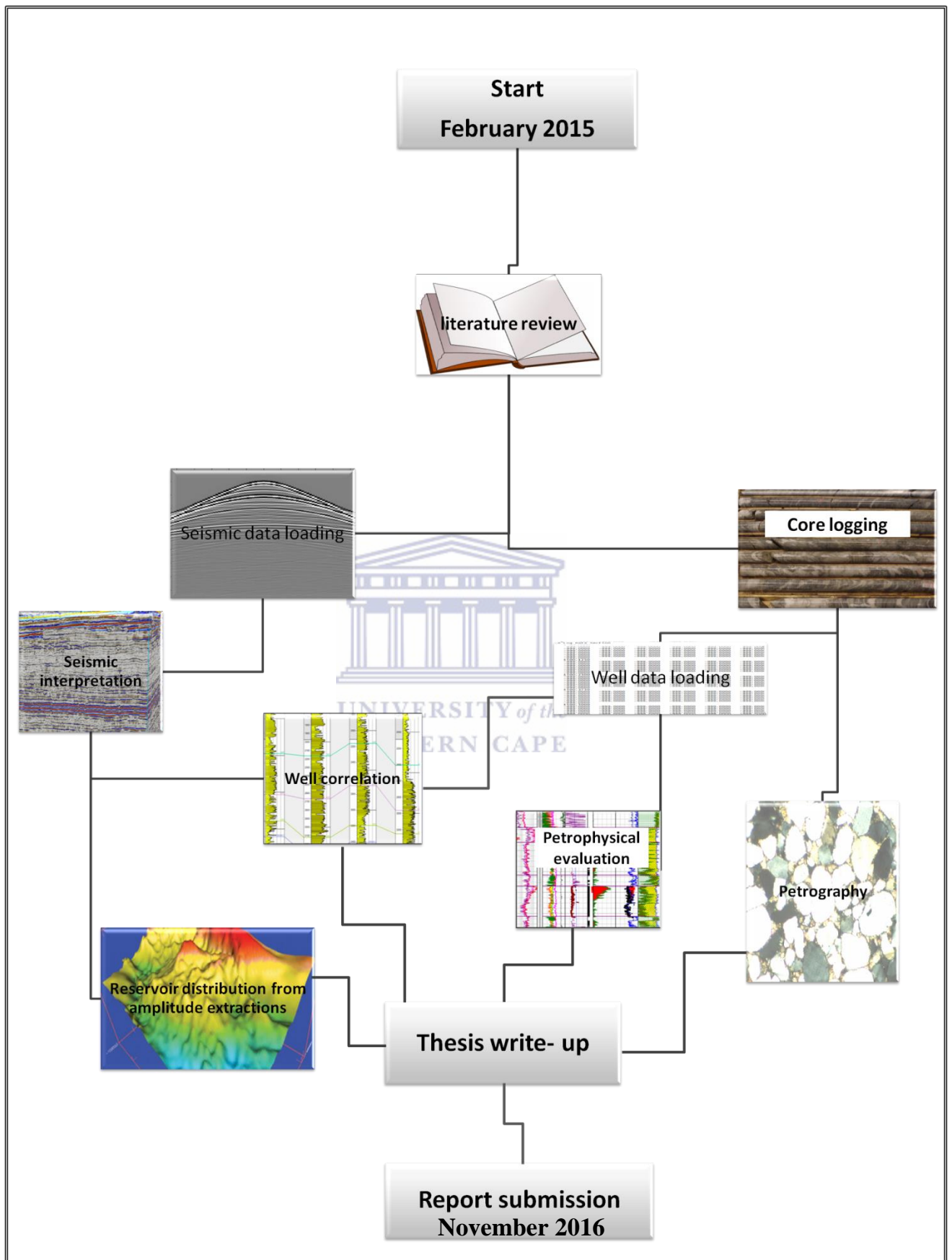


Fig. 4.2. Flow chart of the research methods.

4.1. Desktop Study and Literature Review

Journals, published books and papers were used prior to the collection of data to give an idea on what other researchers have established about the geology, tectonic setting, stratigraphy and the petroleum system of the Orange Basin and its potential to preserve and produce hydrocarbons.

4.2. Seismic Data Loading and Interpretation

A 3D PSTM final full stack 1999 vintage covering an area of 104 square kilometres with a maximum travel two way time (TWT) of 6 seconds was obtained from the Petroleum Agency of South Africa and loaded on a Petrel 2014 project created for the research study. The seismic volume was loaded in a ZGY format. Horizons identified from well tops were mapped on seismic sections displayed on interpretation windows. Two horizons (top reservoir-M2KI and base reservoir-14At-1) were carefully mapped across the cross-lines and in-lines. Upon finishing horizon picking, grids were generated from the mapped horizons. Different seismic attributes were extracted on the grids to help identify and enhance the interpretation of lateral distribution of the Albian reservoirs intersected by the studied wells. The attributes used for sand distribution were spectral decomposition, RMS amplitudes, coherency and maximum amplitude.

For the spectral decomposition attribute, 30Hz, 45Hz and 50Hz frequency cubes were generated from the final full stack volume. Ricker wavelet was chosen for the filter (see Appendix A).

After all three frequency cubes were generated, a horizon probe was inserted into the M2K1 grid which is the top of the reservoirs to create a geobody extraction. The three frequency cubes were blended in the probe and red, green and blue (RGB) colour blending were used for the display (see Appendix A).

A coherency cube was created from the seismic volume to better pick structural features such as faults. This was done by picking structural methods from volume attributes and a variance edge method under the attribute tab.

Faults were also mapped using the fault stick pick method. Fault polygons were generated based on the trend of the faults.

4.3. Well Data Loading

Geophysical well log data for AG-1, AK-1, AK-2 and AV-1 wells were obtained from the Petroleum Agency in excel format. These were later loaded in both Petrel 2014 and Interactive Petrophysic softwares in Ascii and LAS formats respectively. Different curves including gamma ray, sonic, depth, caliper, resistivity, neutron, and density were displayed on different tracks. Environmental corrections, spike eliminations, smoothing and depth shifting were performed where necessary. Table 4.1 presents the interpreted wireline logs obtained from PASA.

Table 4.1: Interpreted wireline logs obtained from PASA.

| LOG | Explanation |
|-------|-----------------------|
| DEPTH | Measured Depth/TVD |
| GR | Gamma Ray |
| CALI | Caliper |
| SP | Spontaneous Potential |
| ILD | Deep Resistivity |
| SFLU | Shallow Resistivity |
| MSFL | Rxo resistivity |
| NPHI | Neutron Porosity |
| DT | Sonic |
| RHOB | Bulk Density |

4.4. Well Correlation

The wells were correlated based on the gamma ray responses and lithology descriptions from core logs. The gamma ray trends in Figure 4.3 below which are associated with grain size were used as the guide during well correlation. Well tops extracted from geological well reports were used as markers and they helped to correlate all four wells.

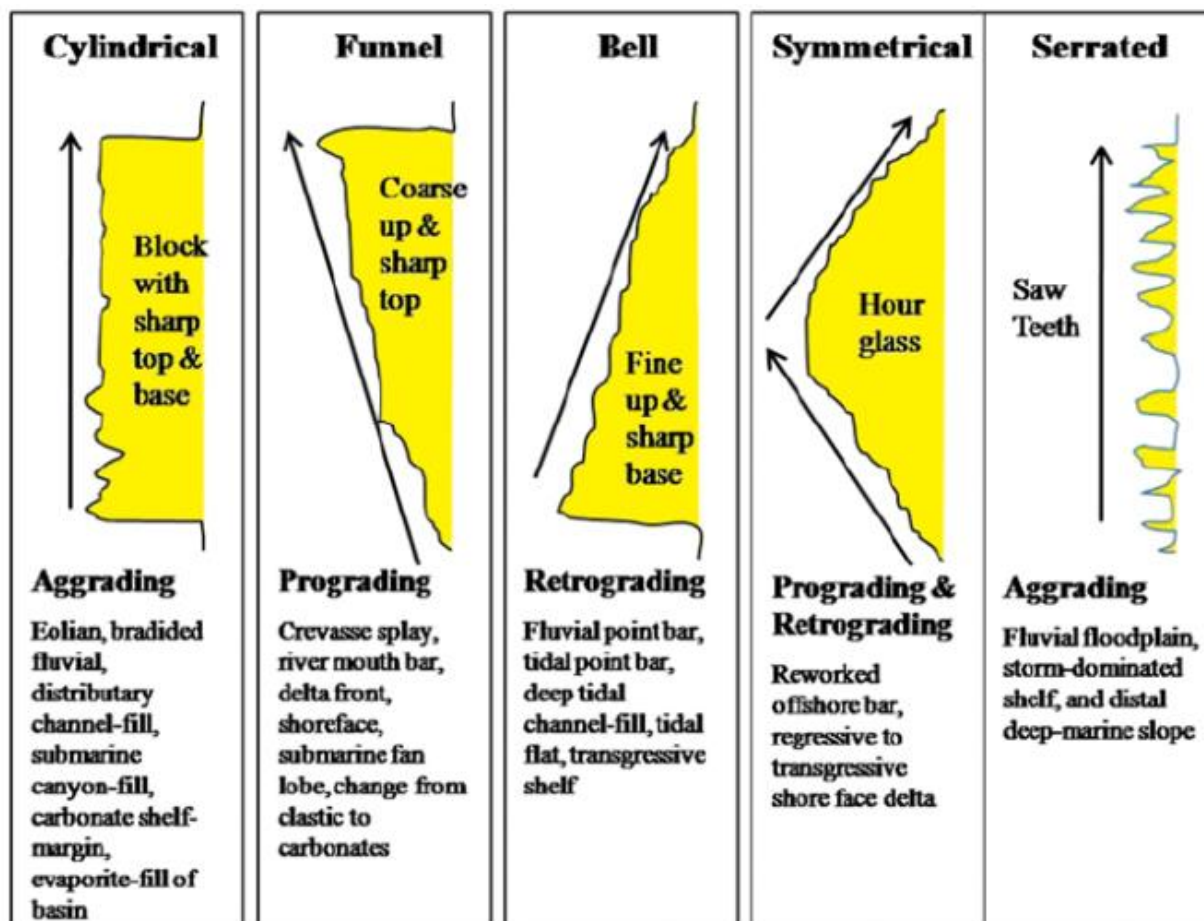


Fig.4.3. Gamma ray responses to variation in grain size (Emery & Myers, 1996).

4.5. Core Logging

Only two of the studied four wells had core data. The two wells are AG-1 and AK-1. AK-1 had two cores. Core one of A-K 1 (see Figure 6.1.1) was cut from 3236m to 3249m in Albian and core two (see Figure 6.1.1) was cut from 3283m to 3296m also in the Albian section. Both cores were examined and interpreted in detail. The AG-1 core was cut from 3370m to 3383 m of the Albian section. The cores were laid on 1.5 meter trays. Each tray was marked with a start and end depth of the cores within it. Each core of the selected wells was described from its end depth towards the top. The following materials were used during logging:

- ✓ Tap water
- ✓ Camera
- ✓ Log sheet and pencil
- ✓ Clipboard
- ✓ Grain size chart

- ✓ Magnifying Lens
- ✓ Tape measure

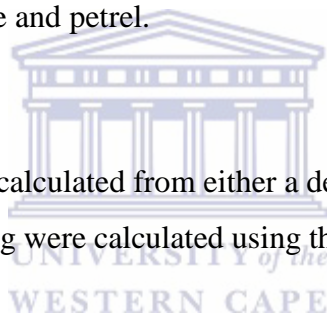
During the interpretation and analysis, each core was classified into different lithofacies based on lithology, grain size/pattern and depositional environment. Magnifying lens were useful for closely examining the grain sizes and sorting. This was also enhanced by wetting the logs to easily observe the grain sizes and most importantly sedimentary structures. Depositional environments from all the units were deduced based on the observed sedimentary structures. The observations were recorded on a log sheet.

4. 6. Petrophysical Evaluation

For petrophysical evaluation, a number of reservoir parameters were calculated. These include porosity, water saturation, volume of clay and permeability. The calculations were performed on interactive petrophysics software and petrel.

4.6.1 Porosity calculations

Porosities from all four wells were calculated from either a density log or from a neutron log. Porosities derived from a density log were calculated using the following formula:



$$- \text{ Porosity } (\Phi_D) = \frac{(\rho_{ma} - \rho_b)}{(\rho_{ma} - \rho_f)} \dots\dots\dots (4.1)$$

Where:

ρ_{ma} =Matrix (or grain) density= 2.67g/cc from core

ρ_b = Bulk density as measured by the tool

ρ_f = Fluid density (derived from pressure test). Field water density of 1.02 g/cc and gas density of 0.2 g/cc

Porosities from a Neutron log were calculated using the following formula:

$$- \text{ Porosity } \Phi_{Ncorr} = \Phi_{Nlog} - V_{sh} \times \Phi_{Nsh} \dots\dots\dots(4.2)$$

Where:

Φ_{Ncorr} =Corrected neutron porosity

Φ_{Nlog} = Neutron log reading of the interval

V_{sh} = Volume of shale

ΦN_{sh} = Neutron log of the adjacent shale formation

4.6.2 Water Saturation Calculations

Water saturation for all the wells was calculated on Interactive Petrophysics software using the Simandoux equation below:

$$1/R_t = [S_w^2/F * R_w (1-V_{sh})] + [(V_{sh} * S_w)/(R_{SH})] \dots \dots \dots (4.3)$$

Where:

S_w = Water Saturation

F = Formation resistivity factor

R_{SH} = Resistivity of shale

V_{sh} = Volume of shale

R_w = Resistivity of formation water

R_t = True formation resistivity

n = Saturation exponent



4.6.3 Volume of Shale Calculations

Volume of shale was estimated from the linear equation by calculating the Gamma ray index which is equivalent to volume of shale.

- Gamma ray Index = Volume of shale = $\frac{GR \text{ value (log)} - GR \text{ (min)}}{GR \text{ (max)} - GR \text{ (min)}} \dots \dots \dots (4.4)$

Where:

GR value (log) = GR log value reading of formation to be evaluated

GR (min) = Clean formation

GR (max) = GR value of maximum shale reading in the formation

The gamma ray index derived from the linear equation was used in clavier and Steiber equations to correct for overestimation of shales in reservoirs.

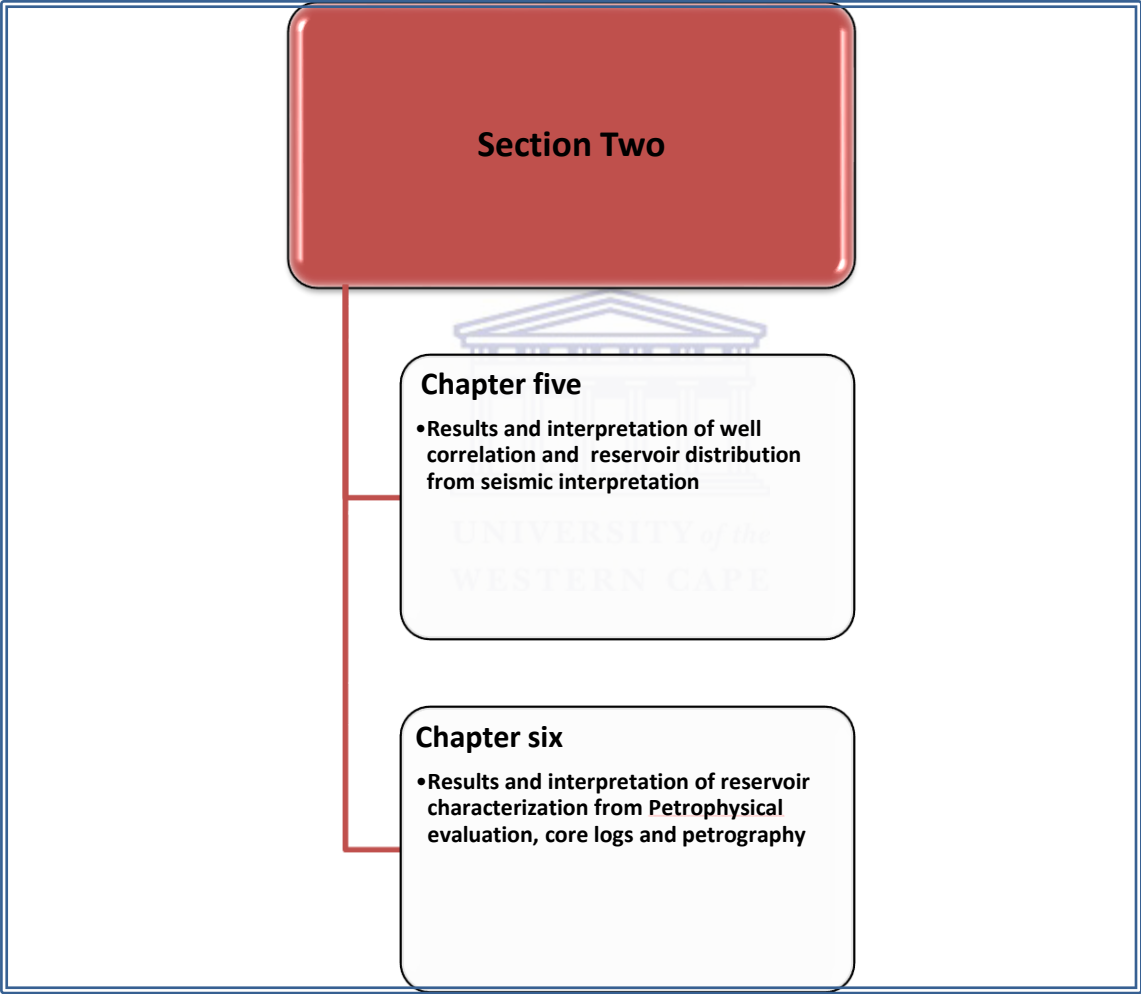
- Steiber (1970) : $V_{sh} = (I_{GR}) / (3-2 * I_{GR}) \dots \dots \dots (4.4)$

- Clavier (1971) :
$$V_{sh} = 1.7 [(3.38 - (I_{GR} + 0.7)^2)]^{1/2} \dots\dots\dots(4.5)$$

4.7 Petrography (Thin Sections)

Thin sections for A-G1, and A-K1 were prepared cutting a 10 millimetre slice from a rock sample using a saw. These thin sections were examined under-microscope with polarized light. Different minerals were identified by their distinguishable characteristics under polarized light. After proper examination of the thin sections, photographs were captured with a digital camera.





CHAPTER FIVE

5. RESULTS AND INTERPRETATION OF WELL CORRELATION AND RESERVOIR DISTRIBUTION FROM SEISMIC INTERPRETATION

5.1. Well Correlation

The four wells studied in this research have been correlated for over 28 km in block 2A of Orange Basin to help better understand the stratigraphy and also the distribution of the investigated Lower Cretaceous sands in the Orange Basin. Stratigraphic tops for all four studied wells were obtained from the Petroleum Agency of South Africa (PASA) in excel format. The tops were picked on all the wells on Petrel software and carefully mapped across the cross-section. Reservoir zones were then correlated using the unconformities as time makers. Figure 5.1 on the following page shows the location of the correlated wells while Figure 5.2 and Figure 5.3 are the cross-sections of the correlated four wells.

The most prominent time markers that were easily followed across all four wells are the 14At 1, M2KI, 14Ht 1, 14Jt 1 and 15Bt1. 14At 1 is an unconformity marked by a low acoustic impedance. Above this marker a series of gas sand bodies interpreted to be channel/deltaic sands at the proximal wells (A-K1, A-K2 and A-V1) and inner shelf sands at the distal A-G1 well were observed on logs and seismic attributes. These sands between the 14At 1 and M2KI unconformities are the main reservoirs of the Ibhubesi gas field and appear to have a blocky aggrading gamma ray response across the four correlated wells. Learnings from core examinations and wireline logs indicate that these reservoirs are distributary deposits of a deltaic system. Their thickness appears to be uniform across the four drilled wells in the field. It is worth mentioning that these Albian sands across all the studied wells are not in communication as they are fed from separate distributary channels. Overlaying the Lower Albian fluvial/deltaic sand bodies is the M2KI unconformity. This event marks a period of erosion in the Albian. It's possible that meteoric waters may have been flushed into the reservoirs through this unconformity to enhance silica precipitation resulting in the dominant quartz cement observed on thin sections of A-G1 and A-K1 wells. Above this unconformity are good quality sands with a general upward fining gamma ray log response. This type of a gamma ray response shows that the basin was experiencing a gradual rise in sea level. All four wells also had a number of good quality sands in the Upper Cretaceous. The aforementioned reservoirs are water wet, probably due to lack of conduit for vertical migration of hydrocarbons from the deeper source rocks.

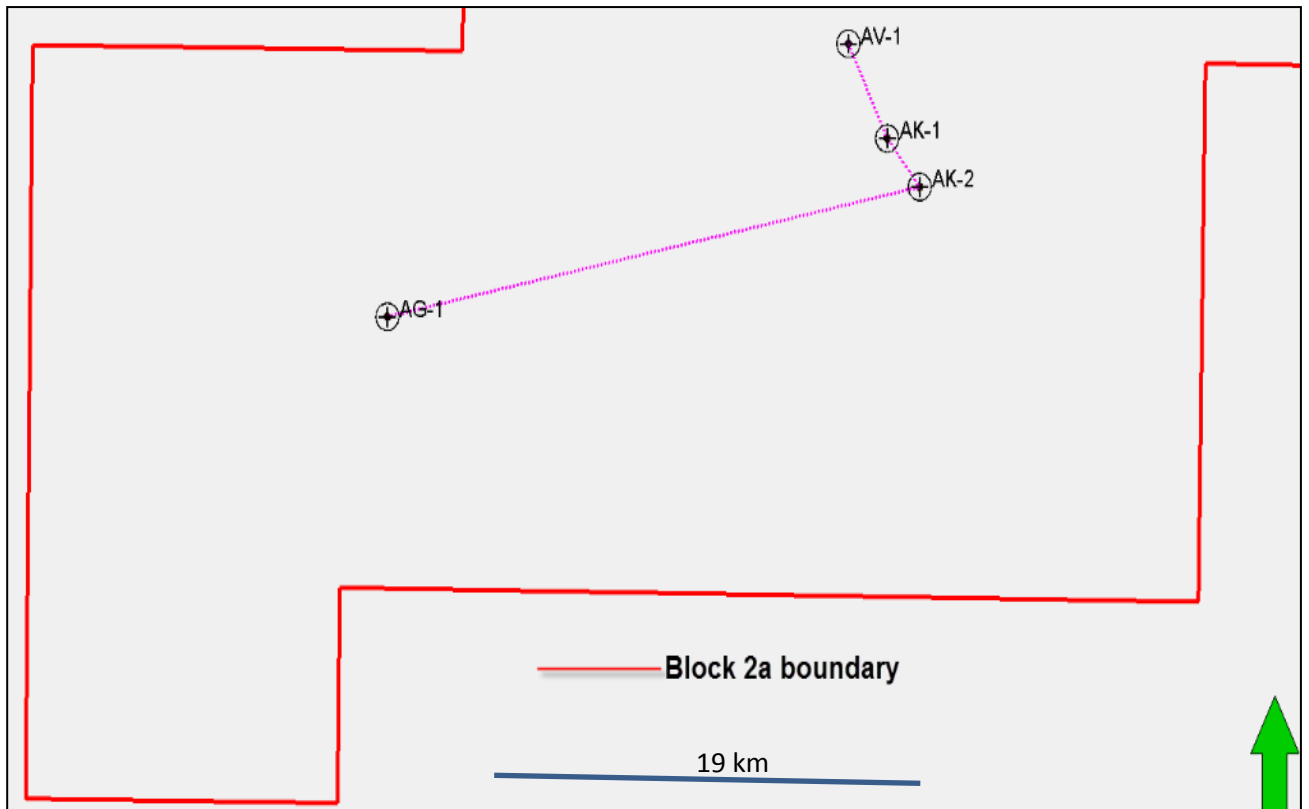


Fig.5.1. Block 2A base map.



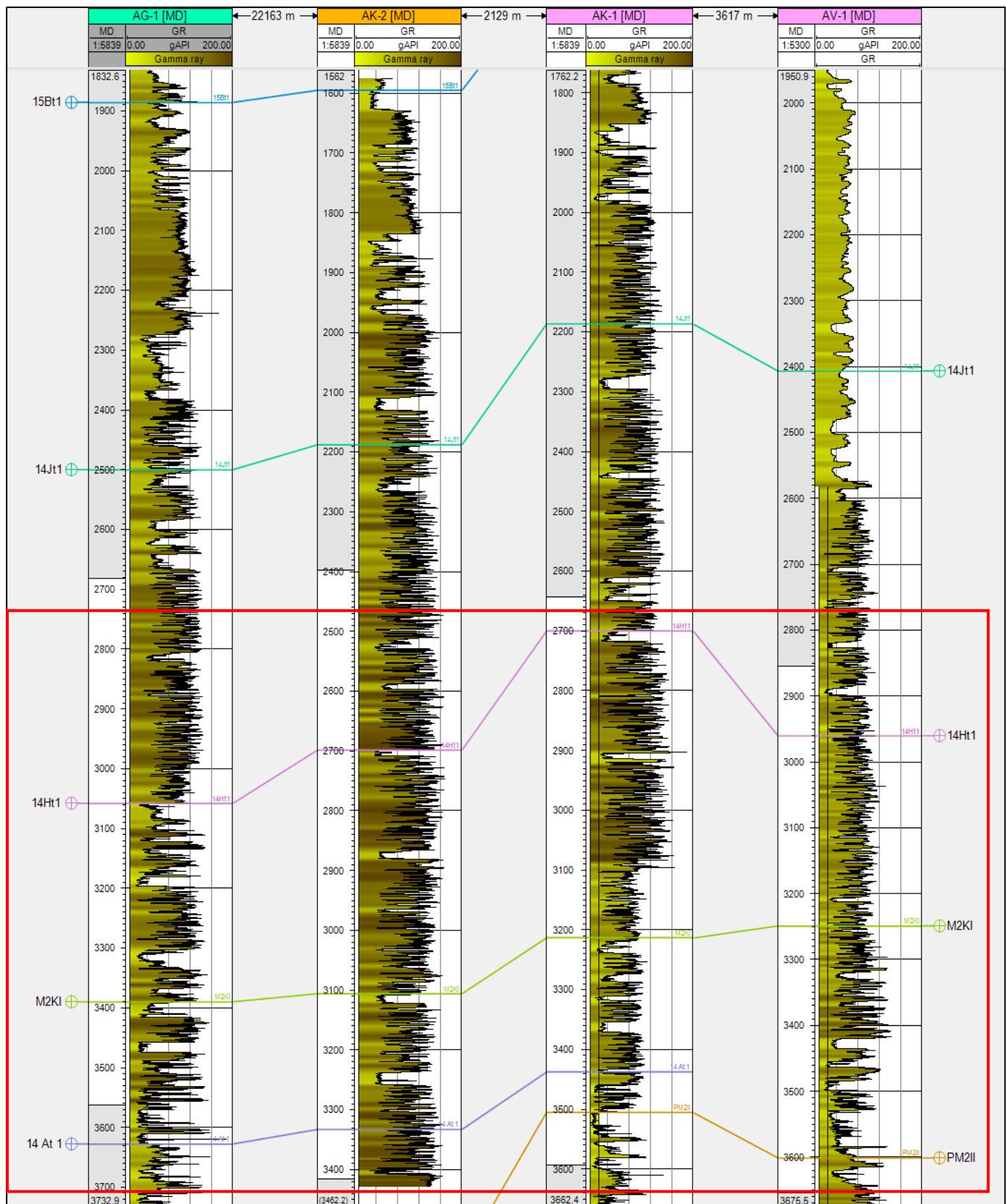


Fig.5.2. Well correlation of the studied four wells in Ihubesi gas field (the red rectangle is the displayed section in figure 5.10.).

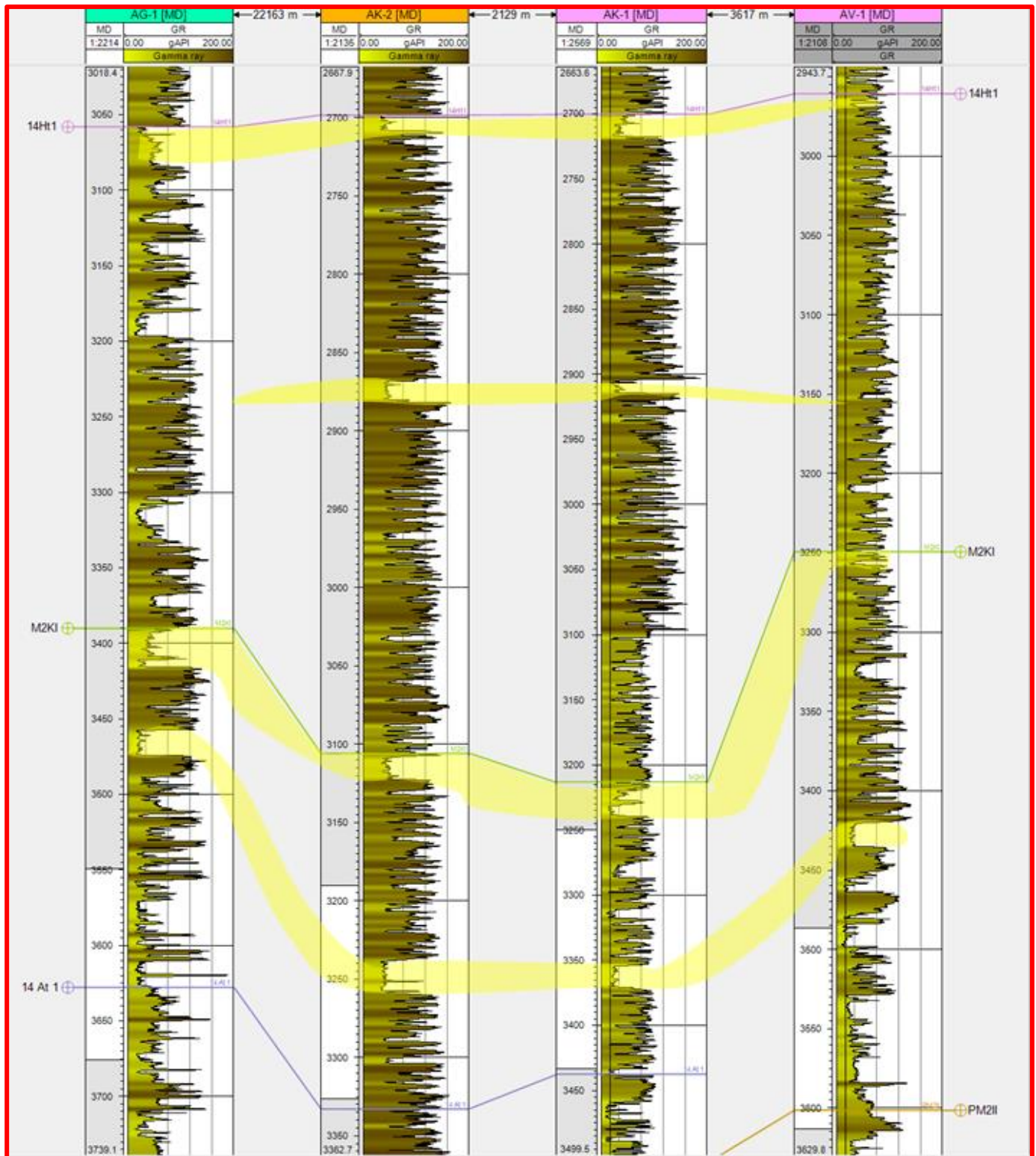


Fig.5.3. Well correlation of the studied four wells in Iubhesi gas field (zoomed-in section of figure 5.9).

5.2 Seismic Interpretation

The process of seismic interpretation is one of the first crucial steps towards finding hydrocarbon deposits before any wells can be drilled. Techniques of seismic interpretation have evolved over the past years from manual 2D interpretation on paper to sophisticated 3D interpretation on workstations. The distribution of reservoirs can be mapped on a 3D seismic volume by using seismic attributes such as spectral decomposition, maximum amplitude and RMS. In this research study a 3D PSTM final full stack volume (1999 vintage) covering an area of 104 square kilometres with a maximum travel two way time (TWT) of 6 seconds was used for mapping the distribution of Lower Cretaceous sands of Orange Basin in block 2A.

The gas bearing Albian reservoir sandstones in block 2A of Orange Basin is situated between horizon M2KI and 14At1. In two way time this interval is between 2390 ms and 2467 ms. In this research study, the M2KI event is mapped as a regional top reservoir marker across the field. The M2KI appears to have a low acoustic impedance response, which is interpreted to be a soft event. Throughout this report, decrease in acoustic impedance responses are displayed as blue (trough) and peaks which are an increase in acoustic impedance responses are the red events.

The M2KI event is an unconformity and it seems to have a strong seismic response at all three well locations (A-V 1, A-K 1 and A-K 2 locations). In between the wells the amplitude response appears less bright which is probably due to both lithology and reservoir fluid change. Below this unconformity, the Albian interval comprises of numerous gas sands represented by the bright seismic amplitudes in Figure 5.4. The three wells (A-K 1, A-K 2, and A-V 1) covered by the 3D survey targeted these Albian sandstone reservoirs. On a strike section the seismic anomalies drilled by the aforementioned wells appear to be distributary channels of a deltaic system. Brighter anomalies above the M2KI unconformity are interpreted to be channel sands with minor gas accumulations. Reservoirs below the 14At1 unconformity which were the main target at the first exploration well in the field (A-K 1) are tight impermeable sandstones that form non-

commercial reservoirs. Fig.5.4. is a composite time section through the A-V 1, A-K 1 and A-K 2

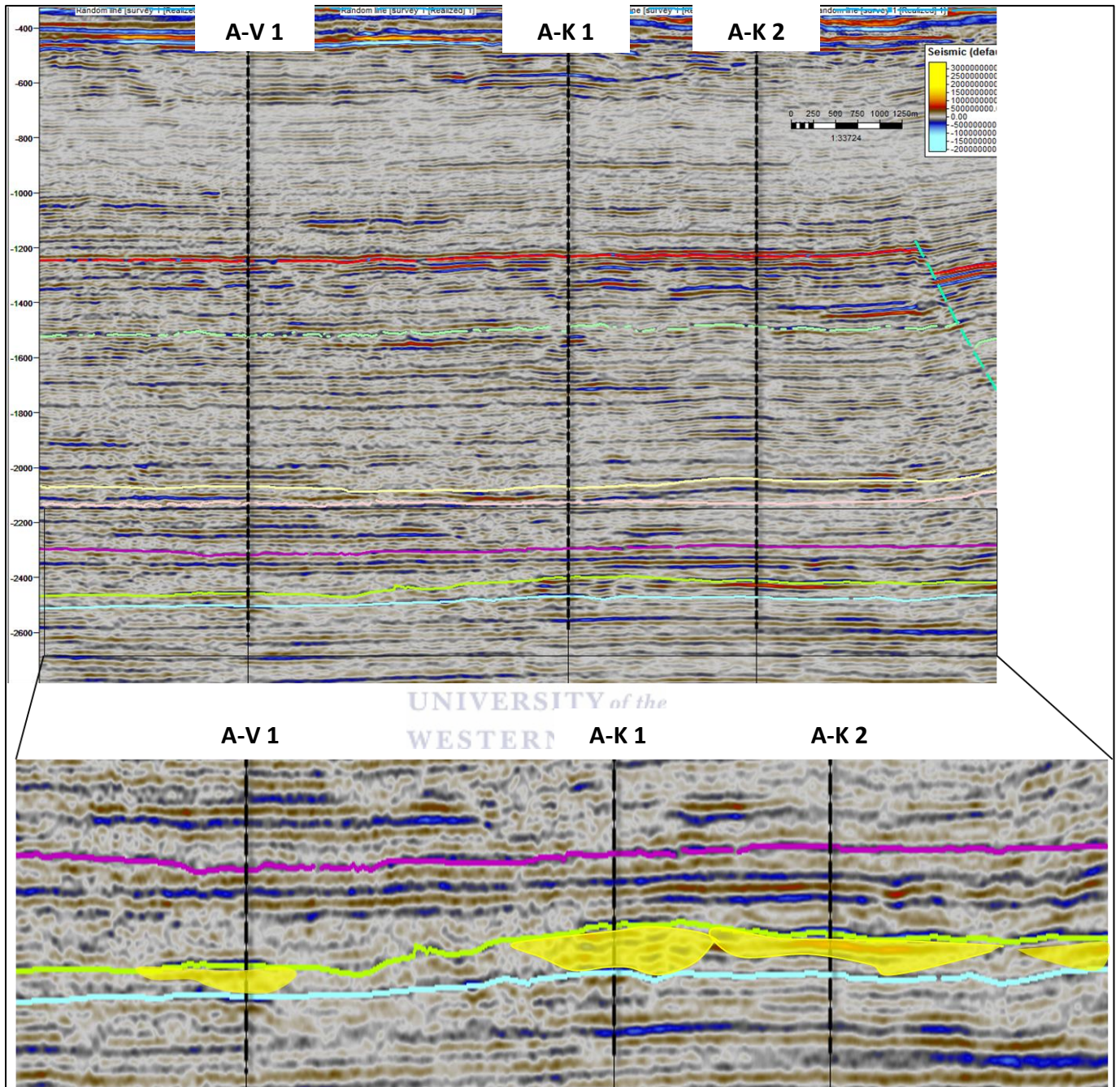
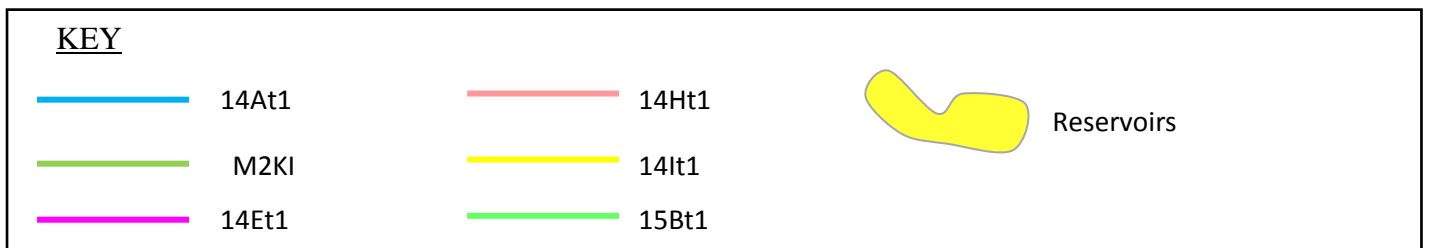


Fig.5.4. NW-SE random line through the A-V 1, A-K 1 and A-K 2.



These fluvial-deltaic sands form structural traps against a fault. The structural component of these traps was first proven by the A-K 1 well. On 2D seismic data, the A-K 1 structure was thought to be a small trap (Jungslager, 1999). The A-V 1 and A-K 2 drilling campaigns on 3D were aimed at delineating the lateral extent of the AK-1 closure against the fault. A coherency slice was generated over an interval of 50ms to clearly demonstrate the extent and the trend of the main trapping fault. This fault extends across the mapped 3D survey in a northwest - southeast direction. Any potential leads of this play type along this margin would potentially need a structural component for hydrocarbons to be trapped or rely on sands to shale-out up dip. The latter scenario is unlikely as the sands seem to continue up-dip along the channels. Fig.5.5 shows the coherence cube over an interval of 50 ms showing the main trapping fault of the field

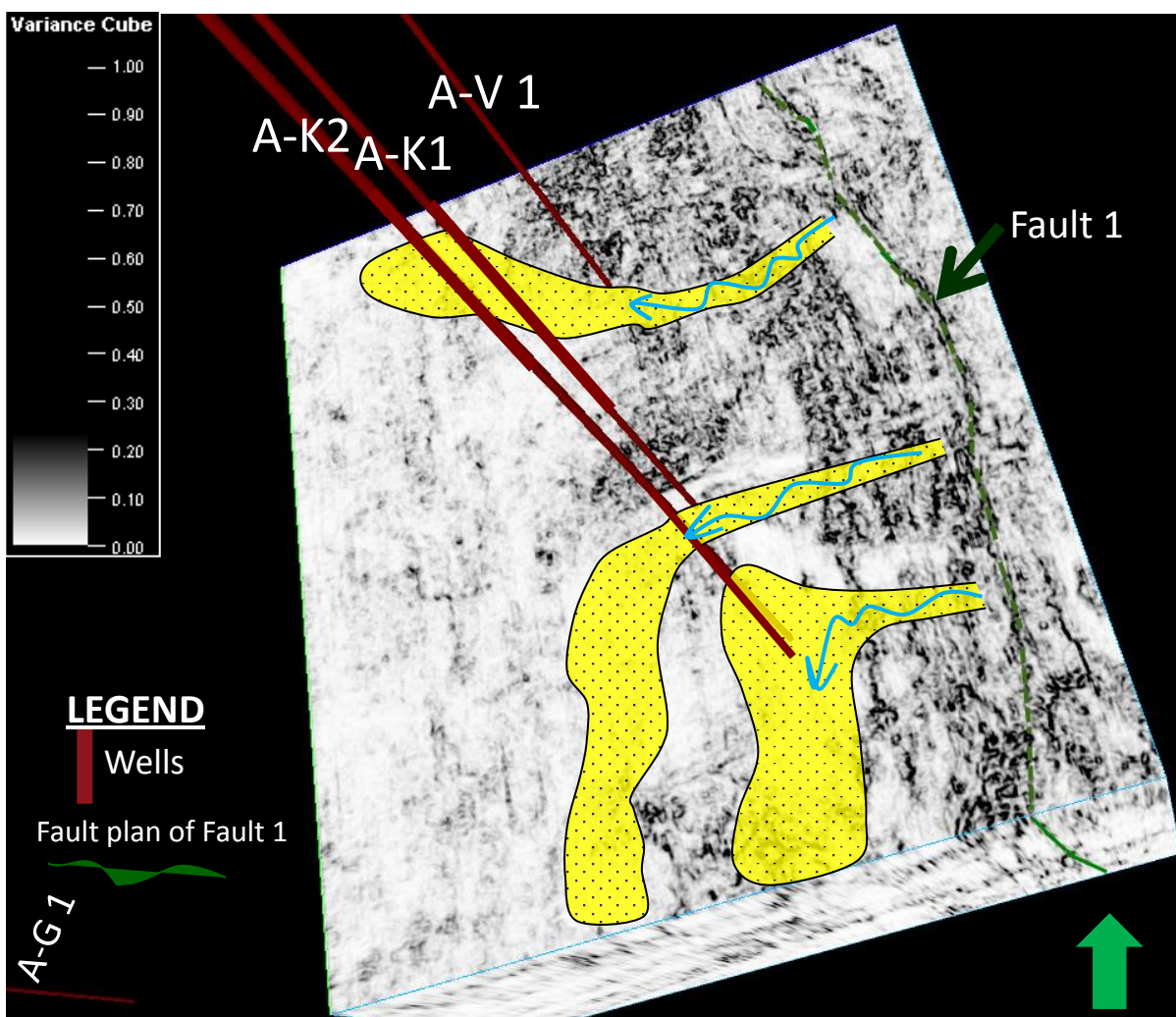


Fig.5.5. Coherence cube over an interval of 50 ms showing the main trapping fault of the field.

5.3 Reservoir Distribution of the Albian Reservoirs

In the synrift section, a series of faults interpreted to be associated with the opening of the South Atlantic during the Gondwana breakup were mapped. These faults form a series of horst blocks across the entire margin. Situated between A-K 1 and A-V 1, bounded by a northwest to southeast trending half grabens is one of these horst blocks (see Figure 5.6 and Figure 5.7 below). The grabens on either sides of the structural high formed accommodation space for sediment accumulation. Although these grabens and horst blocks were formed during the opening of the basin in Late Jurassic to Early Cretaceous, it seems as though they continued controlling the distribution of the sediments and accommodation space in the Cretaceous drift section. Figure 5.6 is a time section and it does not show the structural high clearly. On a depth section this high should stand out. Seismic amplitude extractions and spectral decomposition show sand bodies wrappings around these highs following the trend of the grabens. An alternative interpretation for the distribution of these sand bodies would be that these sands were deposited in incised valleys which are following the trends of the underlying grabens. The latter scenario has also been suggested by Jungslager (1999). These scenarios remain unproven until a well is drilled down dip of the existing wells along these seismic anomalies.

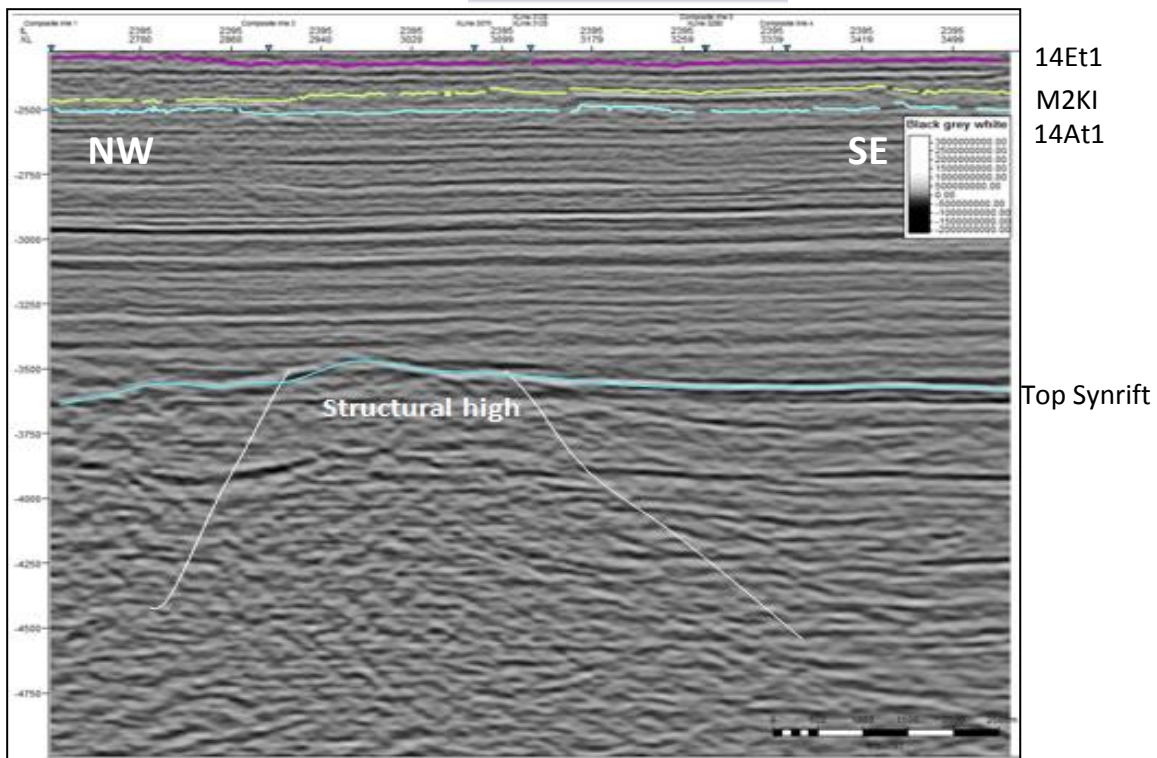


Fig.5.6. In-line section through the Ibhubesi gas field.

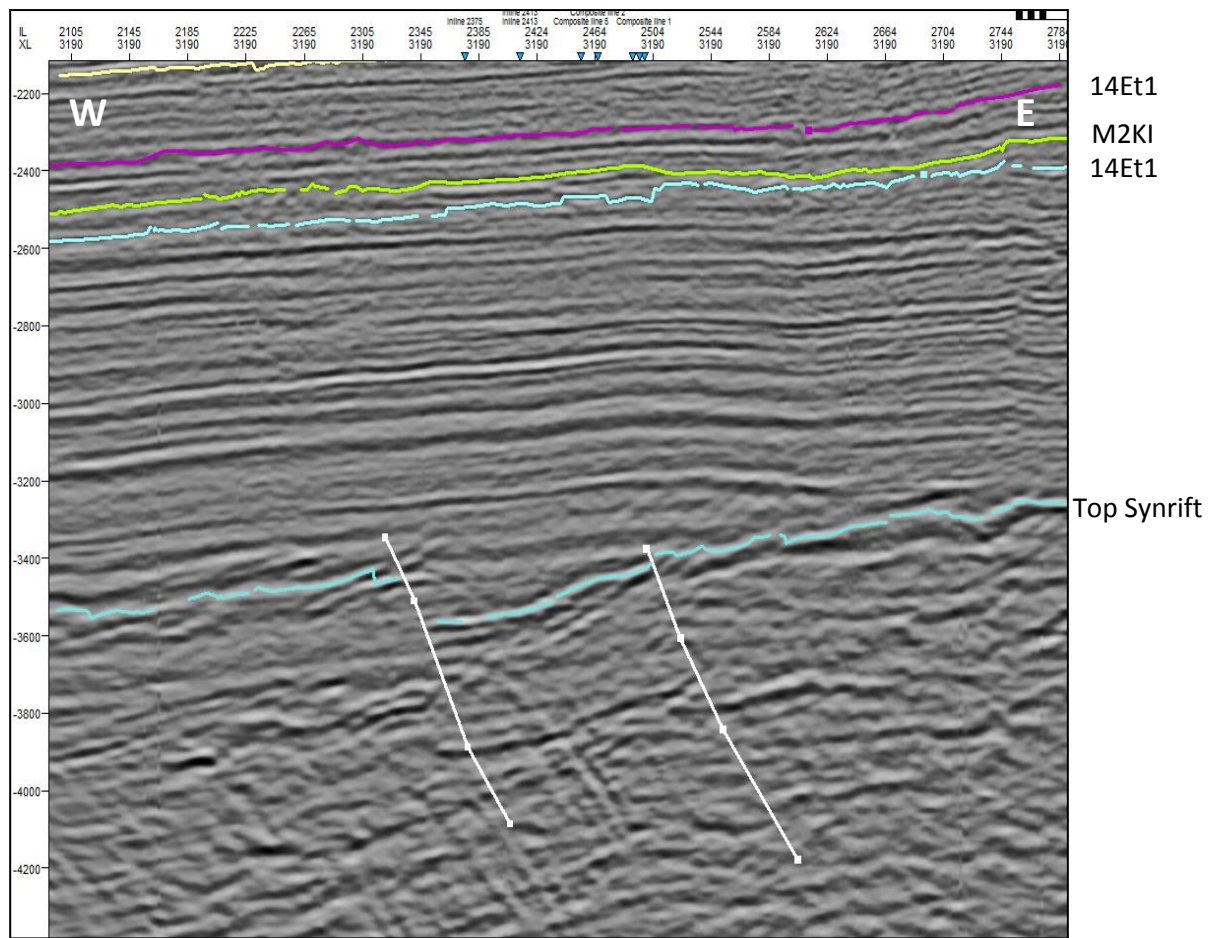


Fig.5.7. Cross-line section through the Ithubesi gas field.

Surface attributes such as spectral decomposition, coherence, maximum amplitude and RMS were generated between the 14At 1 and M2KI interval' to help demonstrate the distribution of the studied Albian sands. From these seismic attributes it is clear that during the Lower Albian time the basin was under a lot of fluvial/deltaic influence. Around this time sea-level was in the process of regression (De Vera et al., 2009) due to high influx of sediments from the Orange River system. According to Brown et al. (1995) the deltaic system associated with the main Orange River system shifted and prograded towards the west due to high sediment supply and accommodation rate.

The Albian reservoirs were mainly sourced from the east onshore and transported into the basin by the Orange River which is still active today. However, some of the sediments from the deltaic system were transported along strike by long-shore drift. These fluvial deltaic sandstone reservoirs were encountered at all the studied four wells.

All the three wells covered by the 3D seismic data appear to have been drilled on distributary channels of the delta system. The main channels passing through the A-K 1 and A-K 2 wells seem to be controlled by incised valleys associated with syn-rift troughs which diverted the direction of these systems towards southwest (see Figures 5.8, 5.9 and 5.10). Therefore, thicker sands can be expected to be ponded against these valleys down-dip of the A-K 1 and A-K 2 wells. The A-G 1 well is more distal and it is not covered by the 3D seismic data incorporated in this research study. Based on the analysis of well logs and core data of A-G 1, the sands encountered in Albian appear to be inner shelf sands rather than mainly fluvial/deltaic.

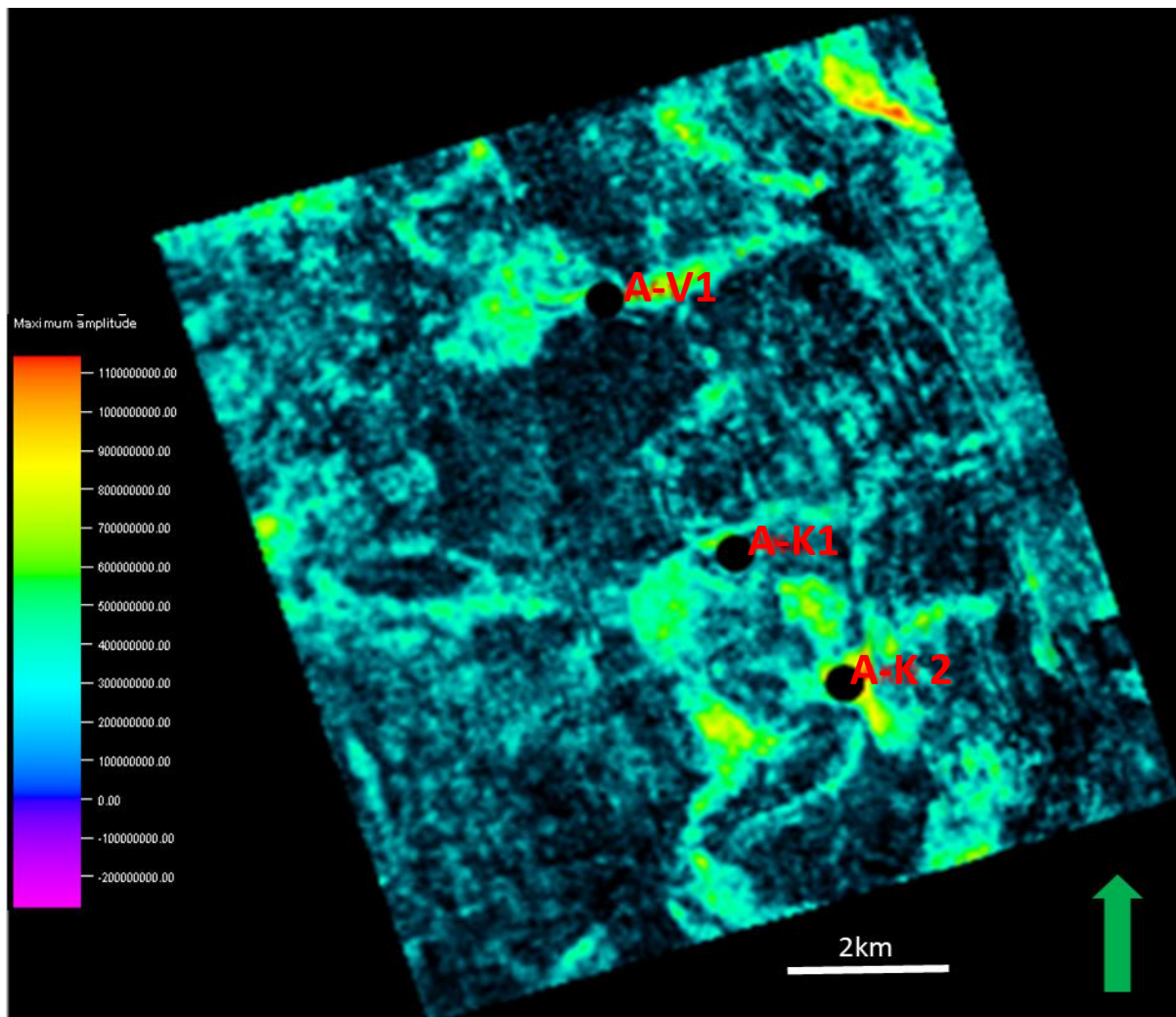


Fig.5.8. Maximum amplitude extraction between top and base of the reservoirs.

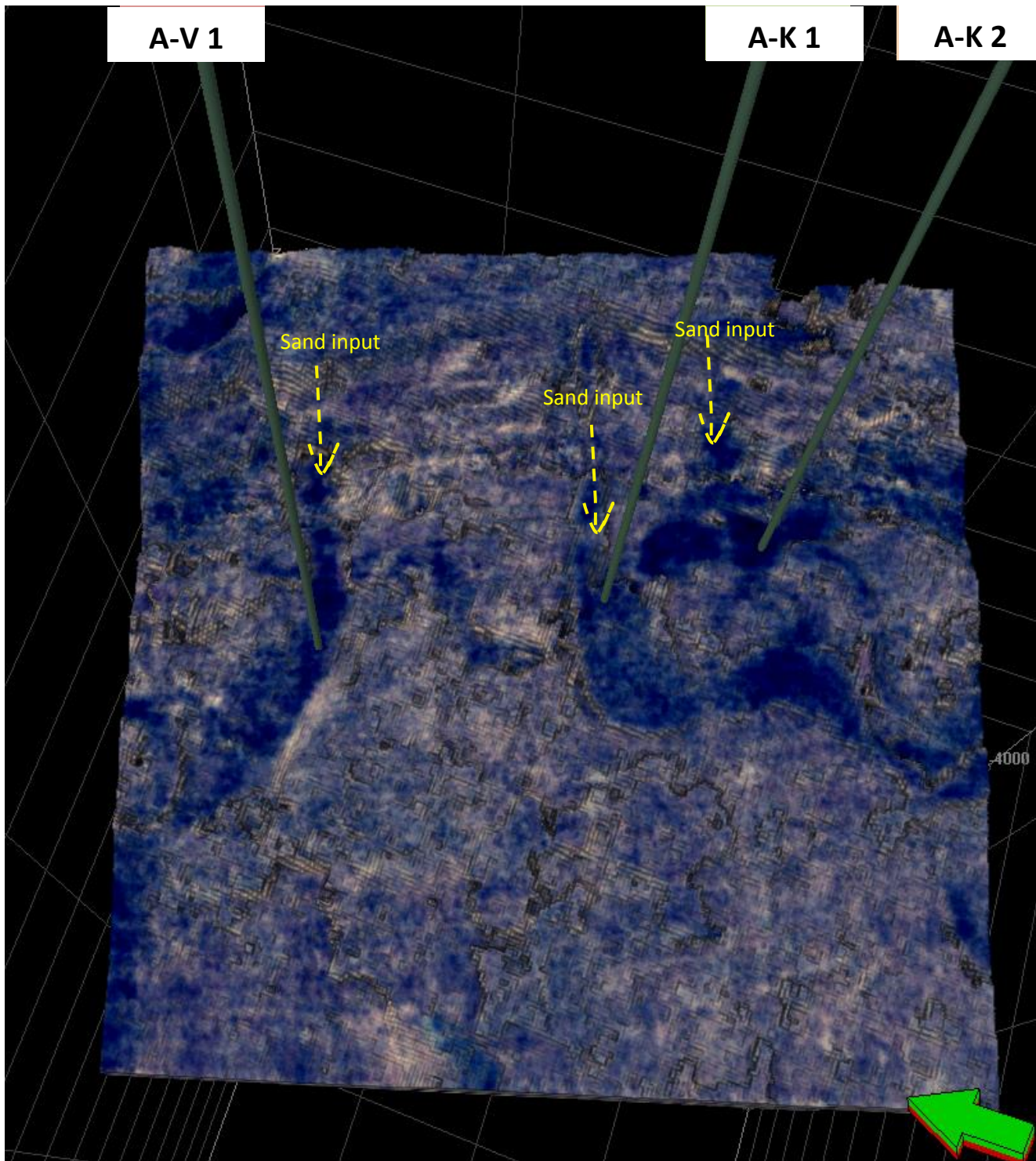


Fig.5.9. Spectral decomposition between top and base of the reservoir. Blending 35hz, 45hz, 50hz ricker frequencies showing the main sand bodies of the distributary channels in the Ibhubesi gas field.

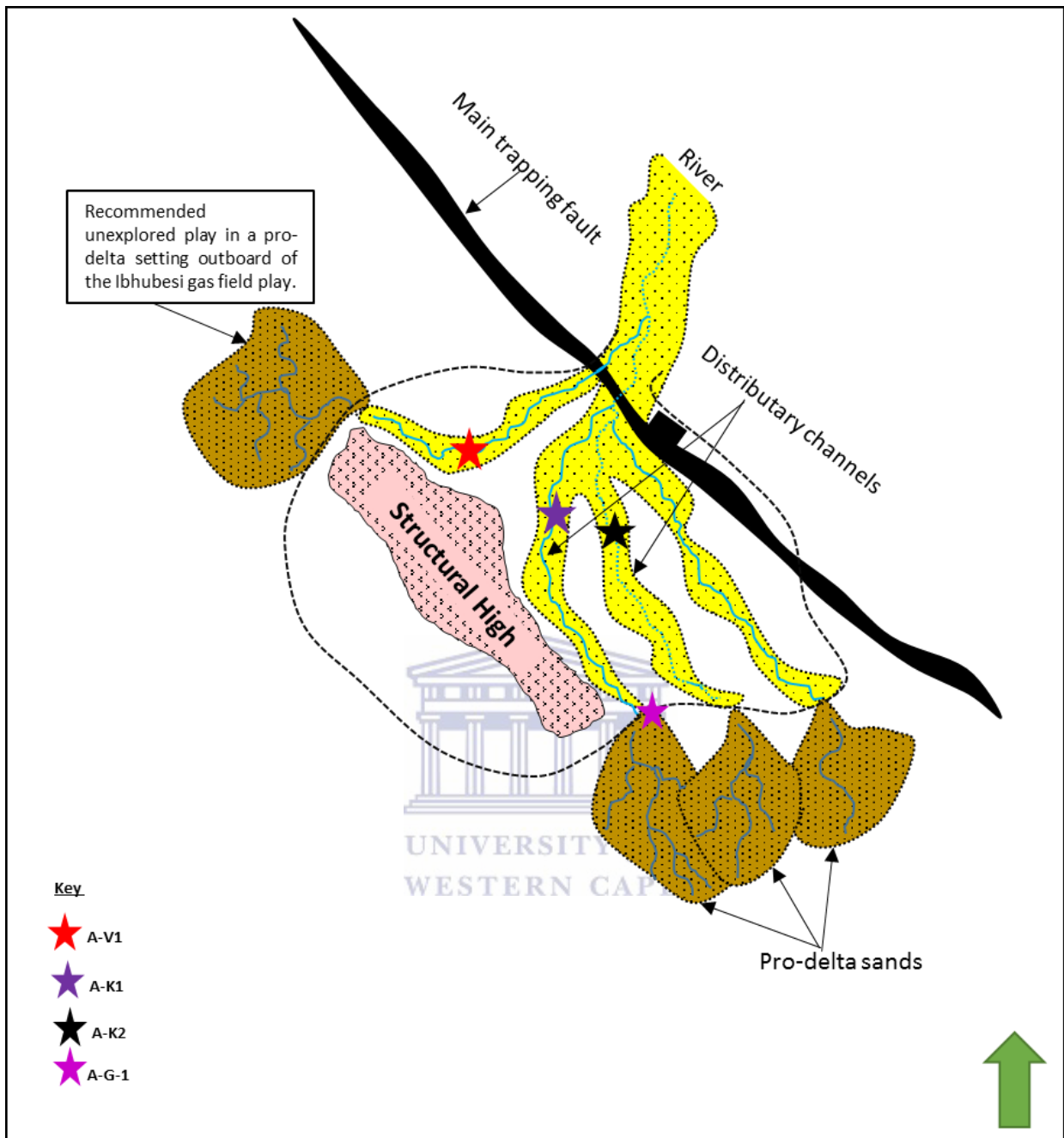


Fig.5.10. Simple cartoon summarizing the fluvial deltaic depositional environment of the Ibhubesi gas field in Albian time.

CHAPTER SIX

6. RESULTS AND INTERPRETATION OF RESERVOIR CHARACTERIZATION FROM CORE LOGS, PETROPHYSICAL EVALUATION, GEOPHYSICAL LOGS AND PETROGRAPHY.

6.1. Core Logging Results and Interpretations

Cores represent the ground truth of the subsurface formations. Therefore, an accurate description of the cores provides a better understanding of the subsurface rock successions of the field or basin of interest. In this section, results from core logging are presented and interpreted. The core samples in this study were evaluated in order to:

- Understand the nature and origin of the depositional environment in Albian;
- Understand the mineralogy of these Albian sands and authigenic clays developed in them;
- To assess poro-perm variations and influence of the authigenic clays on porosities and permeabilities.







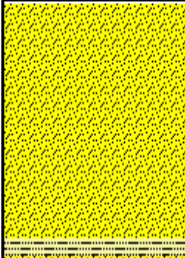







Of the studied four wells, only A-G 1 and A-K 1 had cores. A-G 1 had one core cut from 3370m to 3383m. A-K 1 had two cores cut in the main channel sandstone reservoir. Cores one and two of A-K 1 were cut in reservoir zones four and three respectively. Core one of A-K 1 (see Figure 6.1.1) was cut from 3236m to 3249m and core two (see Figure 6.1.1) was cut from 3283m to 3296m. The cores from both wells were thoroughly investigated at the Petroleum Agency of South Africa (PASA) and subsequently subdivided into three lithofacies. During the examination of the cores, it was apparent that the cores from both wells had three distinct types of lithofacies; hence the subdivision. It was essential to categorize the lithologies in the cores into different facies to help understand the depositional systems in the stratigraphy across the field. The subdivision is based on depositional environment, grain size and the type of lithology. In both A-G 1 and A-K 1 cores, the subdivision of lithofacies is as follows:

Facies one: These are shale units which are frequently coaly and laminated.

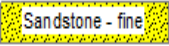
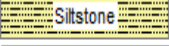
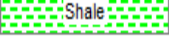
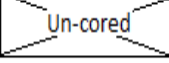
Facies two: Comprises siltstone units which that are often interbedded with lenses of fine grained sands. The silts are occasionally feldspathic and non-glaucconitic.

Facies three: Fine to medium grained massive sandstone. The main framework of this facies is well sorted quartz grains followed by feldspathic grains with authigenic minerals such as chlorite and calcite.

6.1.1 Core Description of A-K 1 (core # 1 and 2) Based on Lithofacies Classification

| Depth in (m) | Lithology | Facies | Description | Depositional Environment | Plate |
|--|---|--------|--|---------------------------|---|
| 3237 |  | 3 | Massive clean sandstone, sub rounded & moderately sorted, coal laminae, Mud drapes. | Fluvial - environment |  |
| 3238 | | | | | |
| 3239 | | | | | |
| 3240 |  | 1 | Dark grey laminated shale. | Shallow marine |  |
| 3241 |  | 2 | Fine grained laminated siltstone, ball & escaping water structures | Fluvial to shallow marine |  |
| 3242 | | | | | |
| 3243 | | | | | |
| 3244 | | | | | |
| 3245 | | | | | |
| Un-cored interval: 3245.53m - 3283.0m (Core #2) | | | | | |
| 3283 |  | 3 | Massive well sorted sandstone with sub angular grains sandstone, soft sediment deformation, mud drapes, spots of oxidation | Fluvial - environment |  |
| 3284 | | | | | |
| 3285 | | | | | |
| 3286 |  | 2 | Siltstone coarsens with depth | Fluvial to shallow marine |  |
| 3287 | | | | | |
| 3288 |  | 3 | Light brown massive sandstone | Fluvial |  |
| 3289 |  | 2 | Siltstone with parallel laminations of coaly shales, ball and flaser bedding structures are present, micaceous minerals | Fluvial to shallow marine |  |
| 3390 | | | | | |
| 3391 | | | | | |
| 3392 | | | | | |
| 3393 | | | | | |

Legend

-  Sandstone - fine
-  Siltstone
-  Shale
-  Un-cored

Facies Description

- 1- Shale
- 2- Siltstone
- 3 - Fine grained sandstone

Fig.6.1.1. Log strip of A-K 1, core 1 and 2.

Lithofacies Three of A-K 1

Both cores of A-K1 have exhibited all the three lithofacies. In core 1, the light brown massive sandstone (facie 3) was noted from 3236.0m to 3239.22m in core 2, the same facies was observed again from 3283.0 m to 3287.33m and between 3287.62m to 3288.7m. In both cores, this facies is predominately made of quartz which is characterized by moderately sorted sub-rounded grains. Authigenic minerals observed from both cores included spots of mica, glauconite and chlorite as the prevailing mineral. Chlorite originates from fragments of volcanic material. The Orange Basin is a volcanic rifted basin with a lot of basaltic/quartzitic basement rocks. The formation of chlorite from the fragments of these volcanics must have been syn-depositional with the reservoir sands for primary porosities to be preserved during diagenesis.

Soft sediment deformation and ripples mark sedimentary structures were observed in both cores. Some coal laminations and mud-drapes were also observed in both cores. Spots of oxidation were observed at m 3237.0 m and 3283.0 m.

Lithofacies Two of A-K 1

Facie two which is a siltstone with lenses of fine grained sands was noted between 3240.14 m and 3245.53 m in core one and it ranged from 3287.33m to 3287.62 m and 3288.7m to 3293.38 m in core two (see Figure 6.1.1.). In all three intervals, this facie is characterized by thin parallel laminations of shale, small scale escaping water structures, flaser bedding and ball structures of sand. The observed mineral components in all three intervals were the micaceous grains. The spots of oxidation were marked in the 3243.12 m and 3289.0 m of core one and two respectively.

Lithofacies One of A-K 1

Facie one which is a shale unit was only noted in core one. This unit ranges between 3239.22m and 3240.14m with an interval of 0.92 m. This black shattered shale unit is dominated by micaceous grains. Few traces of tree leaf fossil were also observed in this interval.

6.1.1.1 A-K 1 Cross-Plots from Core Analysis Results

A number of cross-plots have been created to investigate the relationship between burial depth and reservoir parameters such as porosity, permeability, grain density and fluid saturation. Table 6.1 displays the grain densities of common minerals.

Table 6.1: Grain densities of common minerals (petrowiki.org/Rock_density_and_porosity).

| TABLE 13.3—GRAIN DENSITIES FOR COMMON ROCK-FORMING MINERALS | | | |
|--|---|--------------------------|---|
| <u>Mineral Name</u> | <u>Grain Density (g/cm³)</u> | <u>Mineral Name</u> | <u>Grain Density (g/cm³)</u> |
| Albite (Na Feldspar) | 2.61 | Hornblende | 3.12 |
| Almandine | 4.08 | Kaolinite (Clay 3) | 2.59 |
| Anhydrite | 2.96 | Illite (Clay 4) | 2.66 |
| Anorthite (Ca Feldspar) | 2.75 | Magnesite | 2.97 |
| Apatite | 3.23 | Magnetite | 5.18 |
| Aragonite | 2.99 | Matrolite | 2.25 |
| Augite A | 3.32 | Montmorillonite (Clay 5) | 2.1–2.6 |
| Augite B | 3.42 | Muscovite (Mica 3) | 2.78 |
| Barite A | 4.50 | Olivine A | 3.31 |
| Biotite A (Mica 1) | 3.00 | Olivine C | 3.13 |
| Biotite B (Mica 2) | 3.05 | Orthoclase (K feldspar) | 2.57 |
| Calcite | 2.71 | Phlogophite (Mica 4) | 2.82 |
| Chlorite (Clay 1) | 2.80 | Plagioclase A | 2.64 |
| Clinoperthite A | 2.54 | Plagioclase F | 2.69 |
| Clinoperthite G | 2.57 | Pyrite | 5.02 |
| Coal | 1.2–1.8 | Quartz | 2.65 |
| Diopside | 3.31 | Rhodochrosite | 3.57 |
| Dolomite A | 2.85 | Rutile | 4.2 |
| Dolomite B | 2.87 | Siderite | 3.75 |
| Epidote | 3.40 | Sillikanite | 3.19 |
| Fluorite | 3.18 | Smectite (Clay 5) | 2.1–2.6 |
| Forsterite | 3.22 | Sphalerite | 4.00 |
| Galena | 7.50 | Staurolite | 3.78 |
| Garnet A | 3.60 | Sulfur | 2.07 |
| Garnet I | 4.25 | Sylvite | 1.99 |
| Glaconite (Clay 2) | 2.30 | Topaz | 3.50 |
| Gypsum | 2.31 | Tourmaline | 3.23 |
| Halite | 2.16 | Zircon | 4.70 |
| Hematite | 5.26 | | |

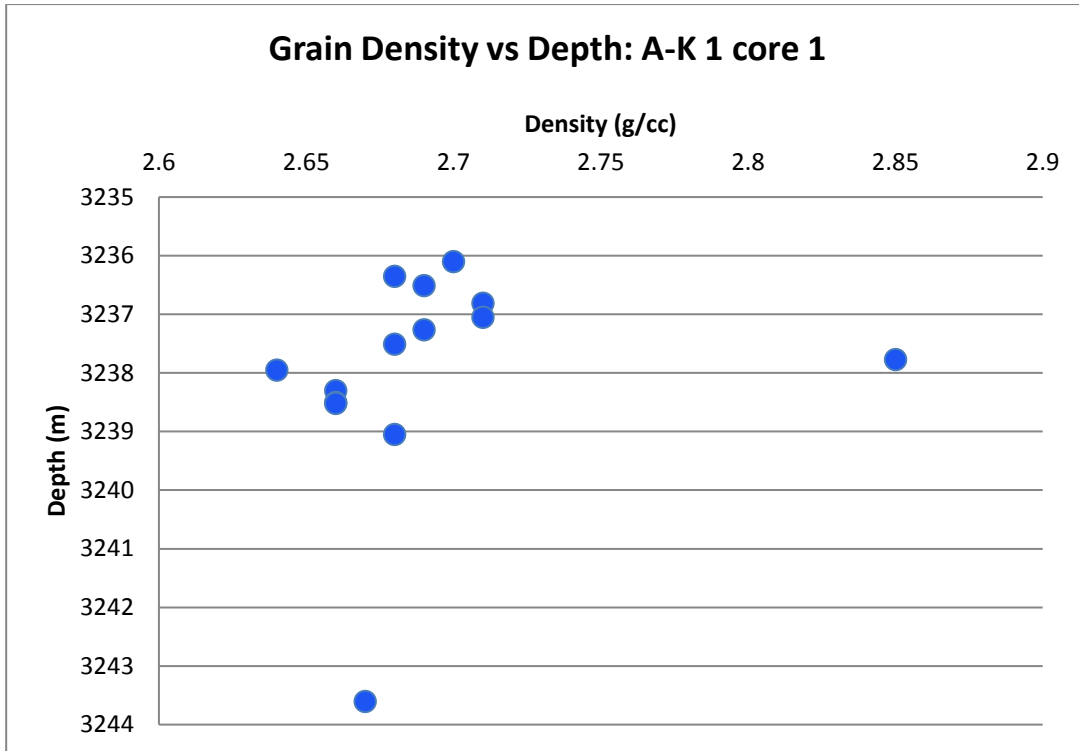


Fig.6.1.2. A-K 1 core 1 grain density vs depth plot.

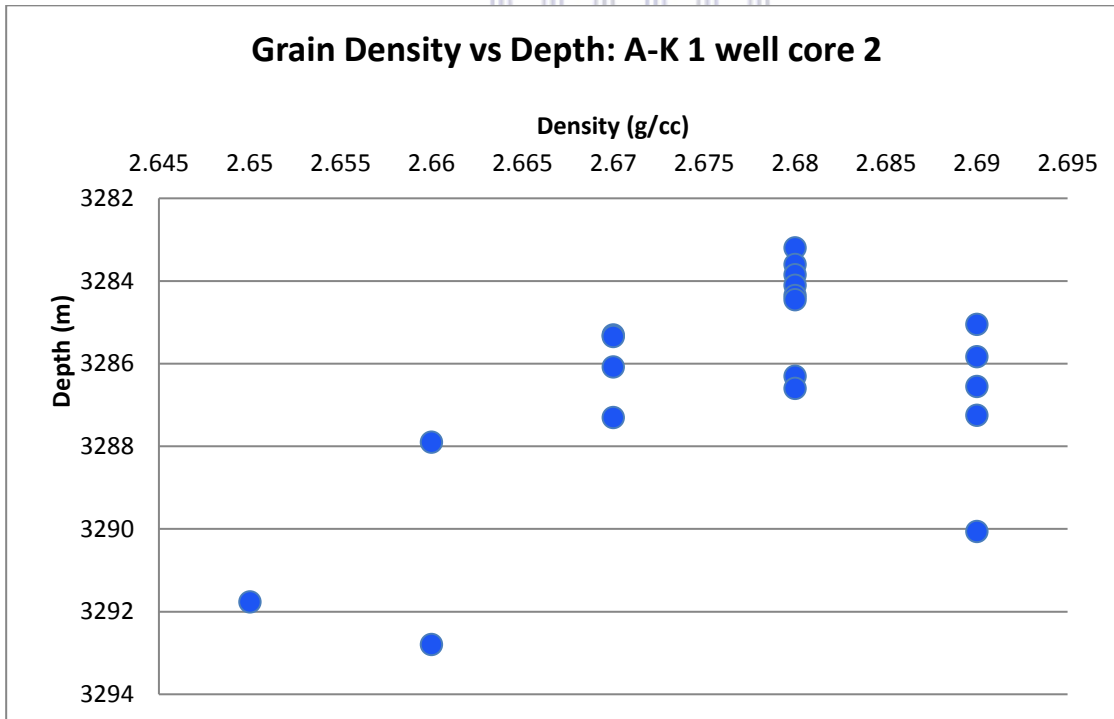


Fig.6.1.3. A-K 1 core 2 grain density vs depth plot.

In core 1 of the A-K 1 well, the reservoir sandstone unit is between 3236m and 3239m. Over this interval grain density ranges between 2.65 g/cc and 2.71 g/cc. The grain densities at 2.65 are attributed to the presence of quartz grains in the core. This was verified during core logging and they are also present on thin sections over this interval. The 2.71 g/cc values are due to the presence of calcite cement. Traces of dolomite are also present in this sandstone unit. This is verified by the 2.85 g/cc value at 3238m.

The reservoir unit of core 2 between 3283m and 3288m has high quantities of feldspathic clay as shown by the 2.66g/cc to 2.69g/cc values. Quartz grains are also present as indicated by the 2.65 g/cc value in Figure 6.1.3.

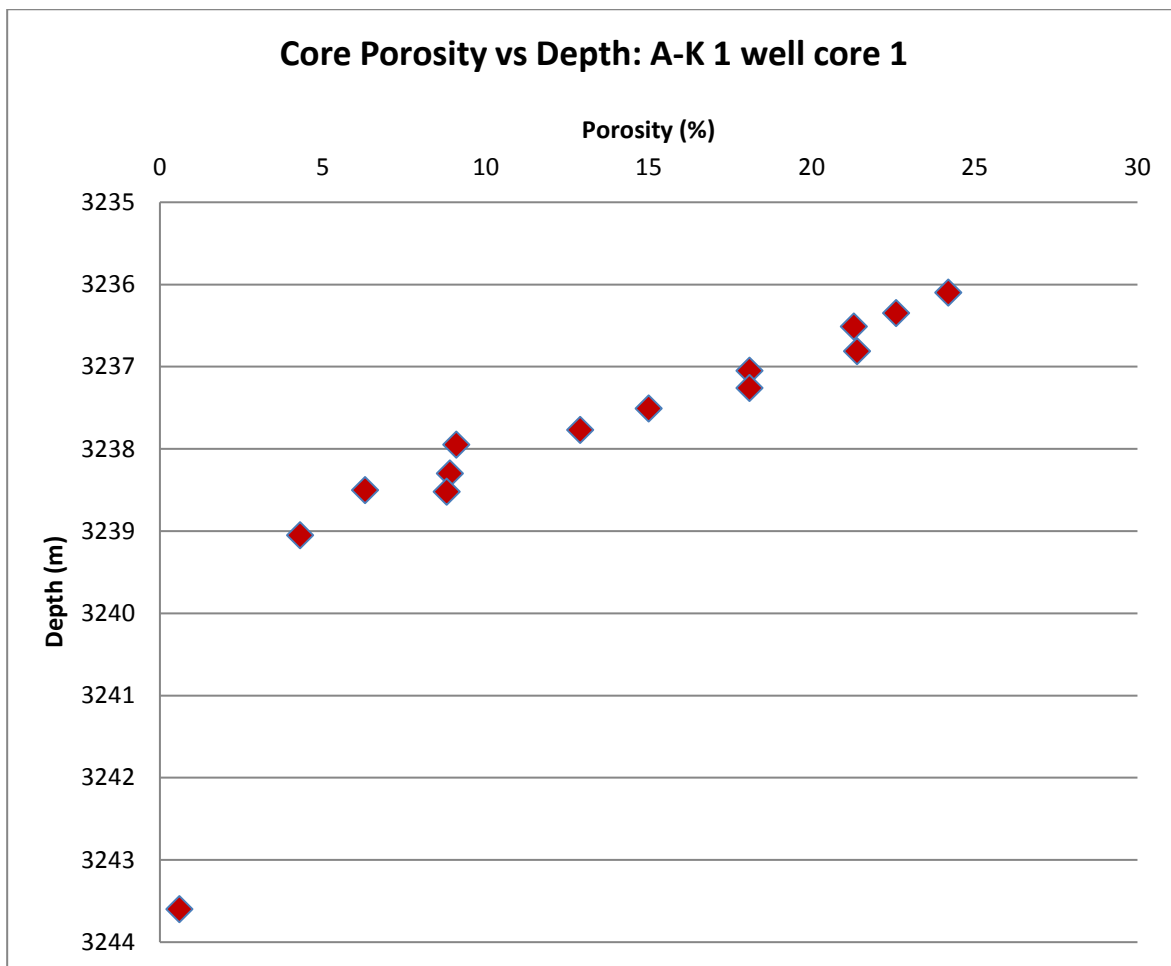


Fig.6.1.4. A-K 1 core 1 core porosity vs depth plot.

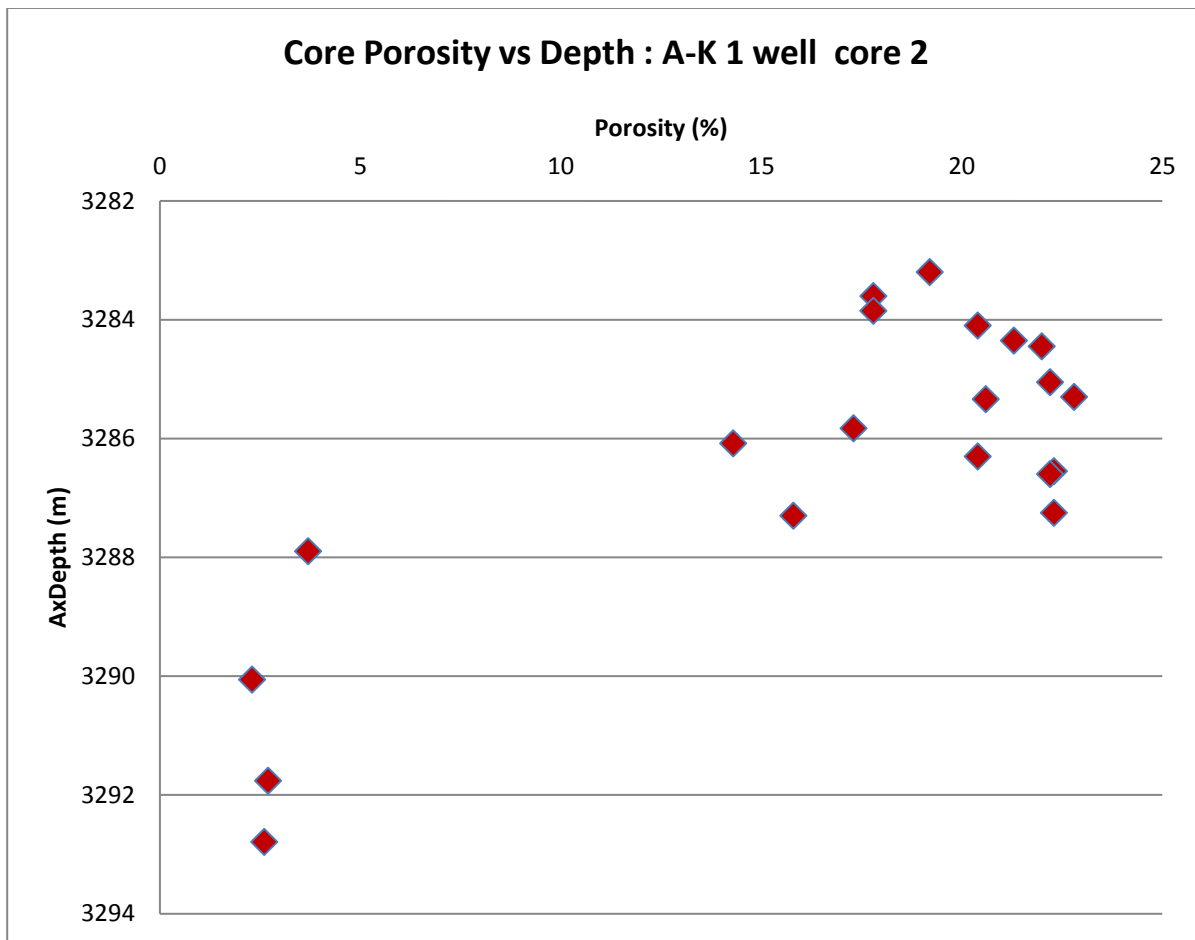


Fig.6.1.5.A-K 1 core 2 core porosity vs depth plot.

The depth-porosity cross plot of A-K 1 well core 1 shows a decline in porosity values with an increase in depth. Towards the top at 3236m porosity reaches a high of 23% and it decreases to a low of 5% at the base of the sand at 3239m. Permeabilities over the aforementioned reservoir unit are also good; indicating that the poro-perm relationship is due to leaching of feldspars and calcite. The top sandstone reservoir unit of core 2 has good quality sands with porosities varying between 24% and 14%. At 3289m to the end of the sand unit at 3393m porosities are very low with values below 5%. This zone is a non-reservoir interval dominated by silt and stringers of shale. The good porosity values in the sand units are associated with the presence of chlorite rims which are coated around quartz grains to prevent quartz-overgrowth but destroy permeability as shown in Figure 6.1.6 and Figure 6.1.7.

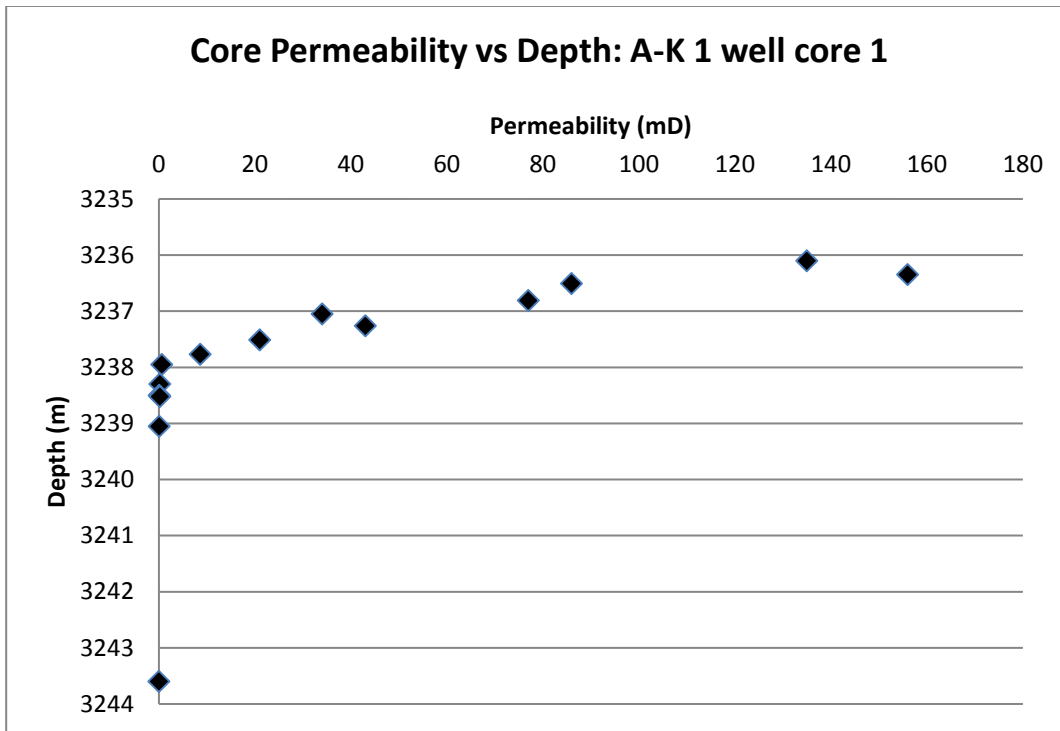


Fig.6.1.6.A-K 1 core 1 core permeability vs depth plot.

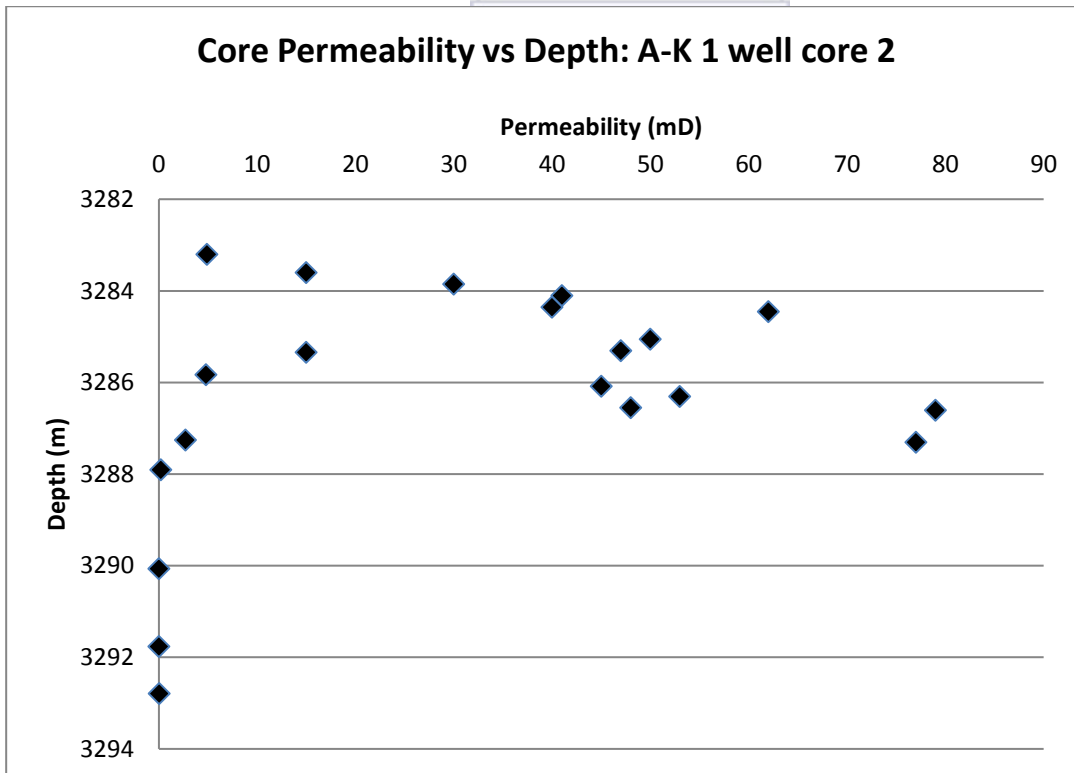


Fig.6.1.7.A-K 1 core 2 core permeability vs depth plot.

Table 6.2: Permeability classification scale (modified after Djebbar, 1999).

| Permeability Values (mD) | Classification |
|--------------------------|----------------|
| Less than 1 | Poor |
| Between 1 and 10 | Fair |
| Between 10 and 50 | Moderate |
| Between 50 and 250 | Good |
| Above 250 | Very Good |

In core 1 of A-K 1 permeability seems to be good at the top of the sandstone reservoir unit to fair towards the base. At the top of the reservoir the permeability values reaches a high of 150 mD. At the base the permeability is just above 1 mD. This permeability trend is consistent with that of the porosity within this reservoir unit. The better poro-perm values at the top of the unit are most likely associated with leaching of calcite cement and feldspar resulting in secondary porosity and improved permeabilities. The poor quality of the reservoir with increasing depth in this interval may be due to high concentrations of calcite and chlorite cements which block the connectivity within the sand preventing the flow of fluids. The interval below the sand which is mainly composed of silt and shale has very low permeability with values below 1mD.

Core 2 of A-K 1 well has poor permeabilities and very good porosities values. This relationship is attributed to the presence of chlorite rims which preserved the primary porosities of this sand unit by inhibiting quartz overgrowths while destroying permeability by cementing the pore connectivity of the reservoir.

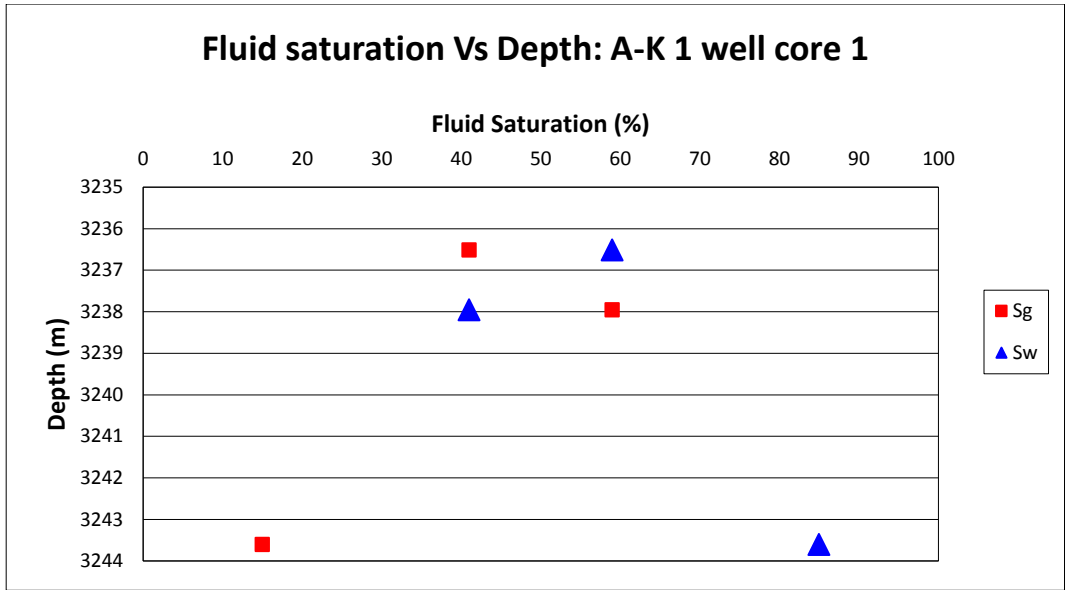


Fig.6.1.8. A-K 1 core 1 fluid saturation vs depth plot.

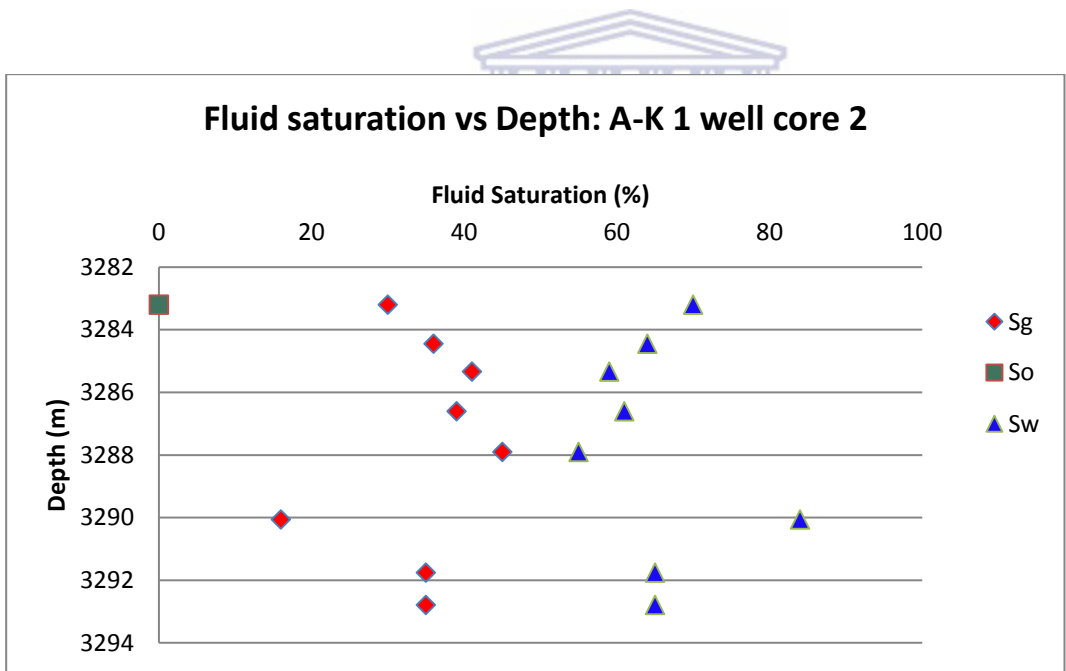
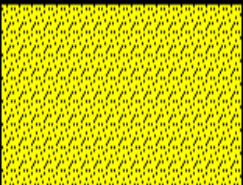
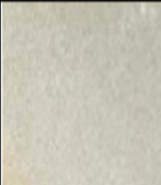




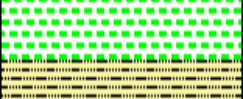

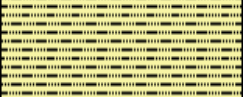
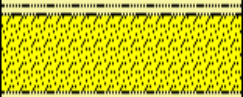

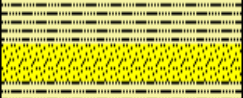

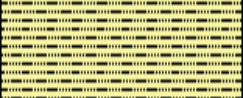





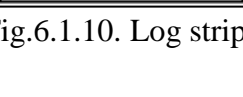

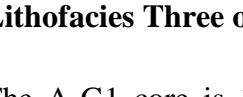
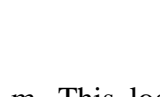


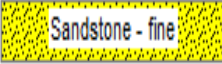
Fig.6.1.9. A-K 1 core 2 fluid saturation vs depth plot.


Core 1 of A-K 1 has sparse data. The plotted values of fluid saturation against depth show an increase gas saturation with increasing depth and a decrease in water saturation with depth. Core 2 of the A-K 1 well has the same trend as core 1. Water saturation seems to decrease with depth while gas saturation appears to increase with depth. Oil saturation is zero in both cores.

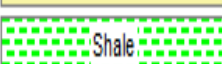
6.1.2. Core Description of A-G 1 (core # 1) based on Lithofacies Classification

| Depth in (m) | Lithology | Facies | Description | Depositional Environment | Plate |
|--------------|---|--------|---|--------------------------|---|
| 3371 |  | 3 | Massive sandstone, well sorted with round to subangular grains. | Fluvial |  |
| 3372 | | | | | |
| 3373 |  | 1 | Very laminated dark grey shale | Shallow marine |  |
| 3374 |  | 2 | Laminated siltstone | Fluvial- marine |  |
| 3375 |  | 3 | Light brown massive sandstone | Fluvial |  |
| 3376 |  | 2 | Laminated Siltstone | Fluvial - marine |  |
| 3377 |  | 1 | Laminated shale | Shallow marine |  |
| 3378 |  | 2 | Siltstone with flaser bedding | Fluvial-marine |  |
| 3379 |  | 3 | Massive sandstone | Fluvial |  |
| 3380 |  | 2 | Siltstone with mud drapes | Fluvial-marine |  |
| 3381 |  | 3 | Laminated Sandstone | Fluvial |  |
| 3382 |  | 2 | Siltstone with ball structures | Fluvial-marine |  |
| 3382 |  | 1 | Shale showing H ₂ O rxn | Shallow marine |  |

Legend

 Sandstone - fine

 Siltstone

 Shale

Facies Description

1- Shale

2- Siltstone

3 - Fine grained sandstone

Fig.6.1.10. Log strip of A-G 1, core 1.

Lithofacies Three of A-G 1

The A-G1 core is 13m long and was cut from 3370m to 3383 m. This logged interval is characterized by all the three lithofacies. Facies 3 which is the fine grained sandstone was encountered at three intervals viz: 3370.0m-3373.71m, 3373.71m-3373.89m and 3378.20m-3378.58m. These massive light brown layers of sandstone are characterized by rounded to sub-rounded grains that are well sorted. Interval 3378.20m-3378.58m exhibited small scale parallel

laminations of shale. Authigenic minerals include chlorite, spots of mica, and glauconite. These were observed in all four sand intervals.

Lithofacies Two of A-G 1

Siltstone (facies two) was encountered in five different intervals (see figure 6.1.10.). All the five intervals are dominated by ball structures and flaser bedding sedimentary structures. The presence of these sedimentary structures reflects deposition of the high density sand (facies 3) on top of the low density silt (facies 2). These siltstone layers were compacted with lenses of fine grained sandstone. The sands in this facies do not appear to have any measurable porosity or permeabilities. They are also hard and siliceous. Silica cement is expected to be high in these sands as compaction of claystones would have realised high quantities of water resulting in an increase in quartz precipitation. Reverse grading was noted from 3373.89m to 3374.15m with a colour change from dark to light brown. Spots of micaceous minerals were also observed in all in five intervals.

Lithofacies One of A-G 1

Facies one which is a shale unit was observed at three intervals that are 3373.29 to 3373.56 m, 3374.15m to 3375.08 m and 3380.18 to 3382.43 m. This black shale unit was found to be highly laminated at all three intervals. This was predominately composed of micaceous grains. At an interval of 2.25m (3380.18 to 3382.43 m), the shattered shale unit exhibited water reaction. The dark black colour of this facies together with its predominant characteristics such as laminations is an indication that this facies deposited in a quiet marine environment.

6.1.2.1 A-G 1 Cross-Plots from Core Analysis Results

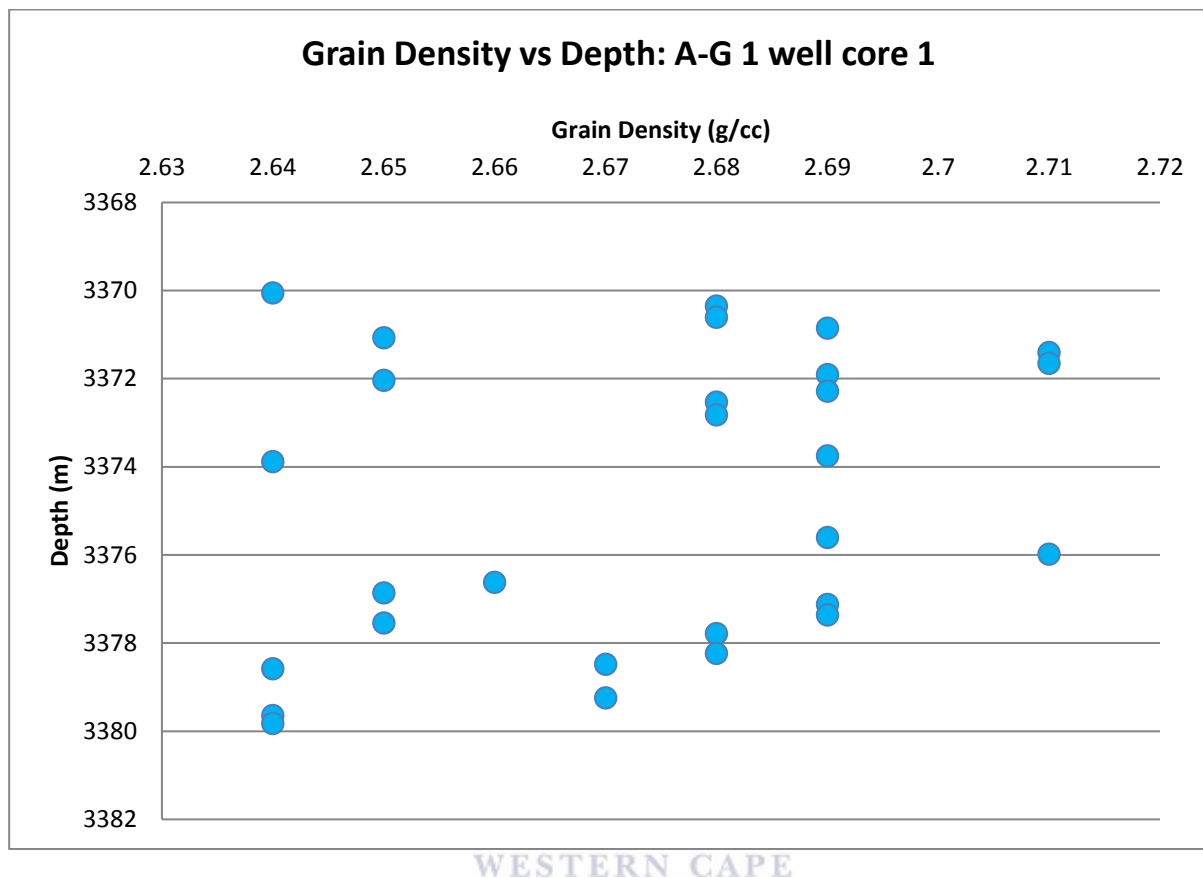


Fig. 6.1.11.A-G 1 core 1 grain density vs depth plot.

The grain density distribution of A-G 1 well over the cored interval from 3370m to 3383m varies between 2.64 to 2.71. The main reservoir unit between 3370m and 3374m has a concentrated cluster at grain densities of 2.64 g/cc, 2.65g/cc, 2.68g/cc and 2.69g/cc and 2.71g/cc. The 2.64g/cc and 2.65g/cc grain density is indicative of the presence of quartz grains derived from a sandstone reservoir. These quartz grains were also noted during the core logging exercise. The grain density of 2.68 g/cc to 2.69 g/cc results from the traces of feldspar present in the sandstone unit. The grain density of 2.71 g/cc indicates the existence of calcite over this reservoir interval. This calcite cement was observed during core logging and it was also picked up clearly by the thin sections of this reservoir interval. Between 3374m and 3376m feldspathic clay and calcite cement seem dominant. On the core this interval is predominately siltstone and shale. The unit between 3376m and 3380 is a sandstone reservoir interval. This unit has a high concentration of quartz grains (2.65 g/cc) and feldspars (2.67 g/cc to 2.68 g/cc).

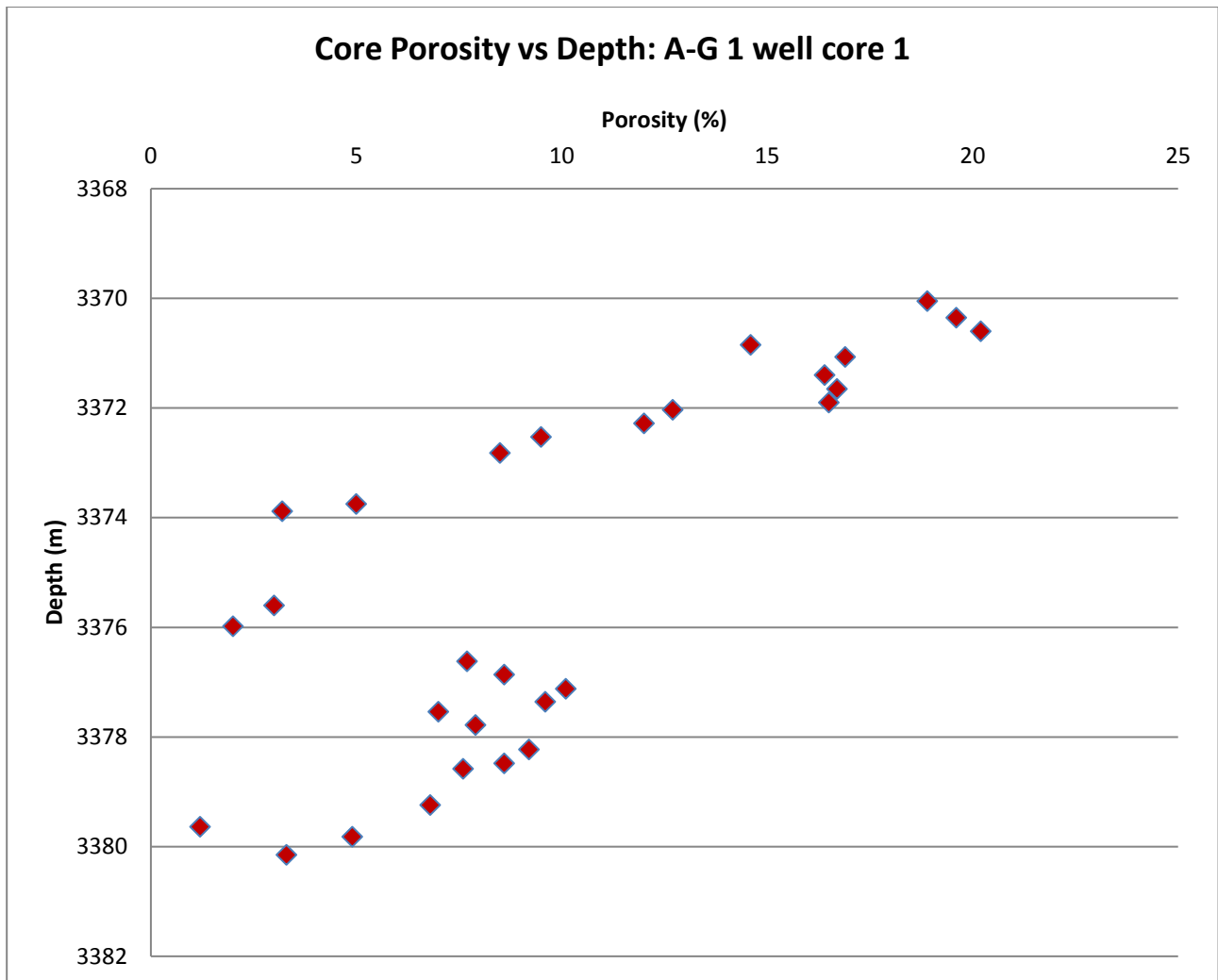


Fig.6.1.12. A-G 1 core 1 core porosity vs depth plot.

The depth-porosity cross plot of the A-G 1 core one shows a decrease in porosity with depth. The top quartzitic sandstone unit between 3370m and 3373m has good porosities ranging between 21% towards the top of the sand body to just below 10% at the base. The silty interval between 3374m and 3376m has low porosity values that are below 5%. The sand unit at the base between 3376m and 3380m has an average of 8-9 %. This basal sandstone interval has poor reservoir qualities compared to the upper sandstone unit. The good porosity values at the top of the cored interval can be attributed to grain coating of chlorite rims. Poor porosities at the lower reservoirs can be caused by a combination of quartz-overgrowth, calcite cement and other authigenic minerals such as kaolinite.

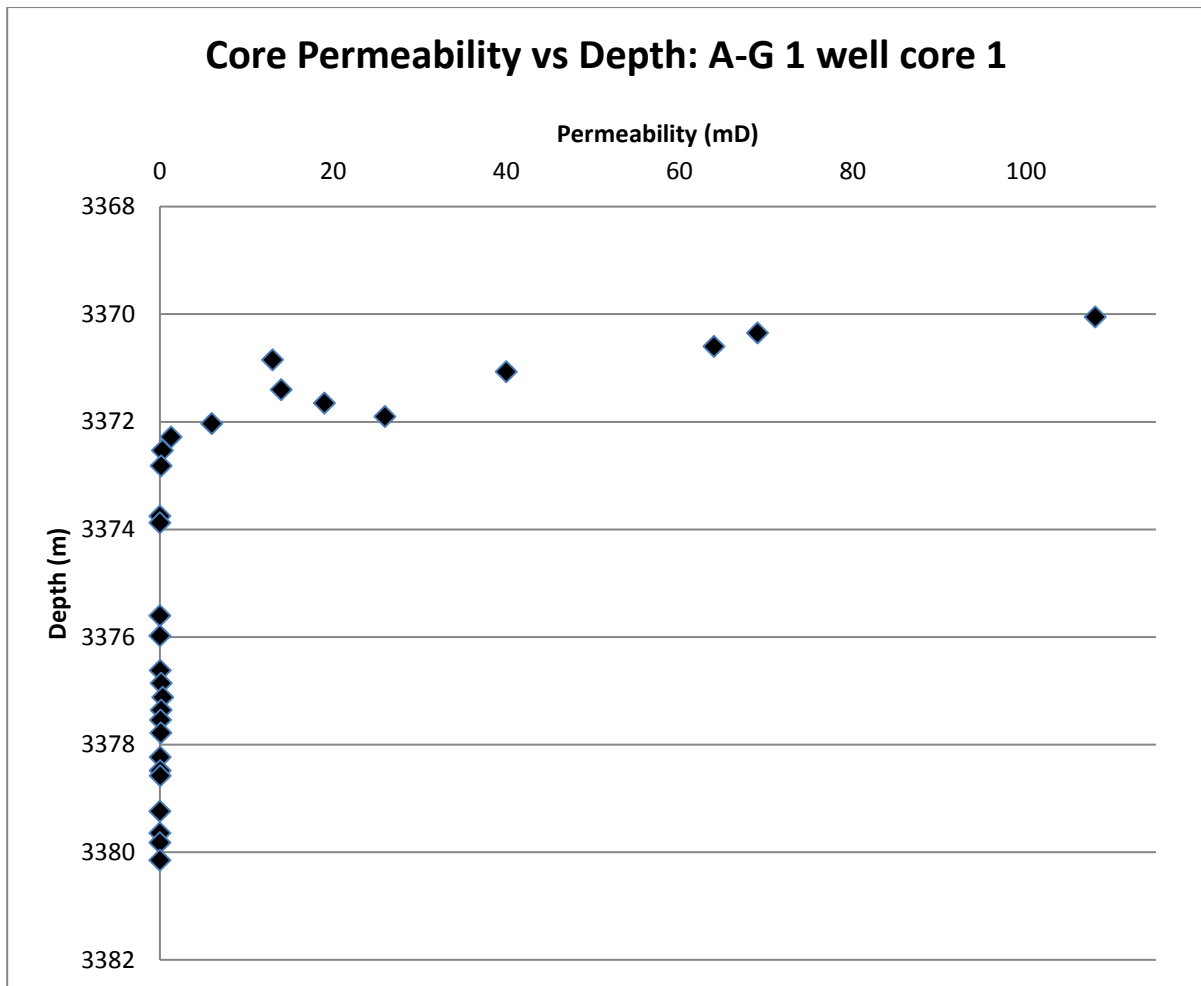


Fig.6.1.13.A-G 1 core 1 core permeability vs depth plot.

Fair permeabilities occur in the upper sandstone unit at between 3372m and 3370m reaching a maximum of 108mD at the top of the reservoir. The low permeability values towards the base could be attributed to the presence of all the authigenic minerals including chlorite, silica, calcite and clay minerals. Below 3372m permeabilities are extremely poor with values below 1mD.

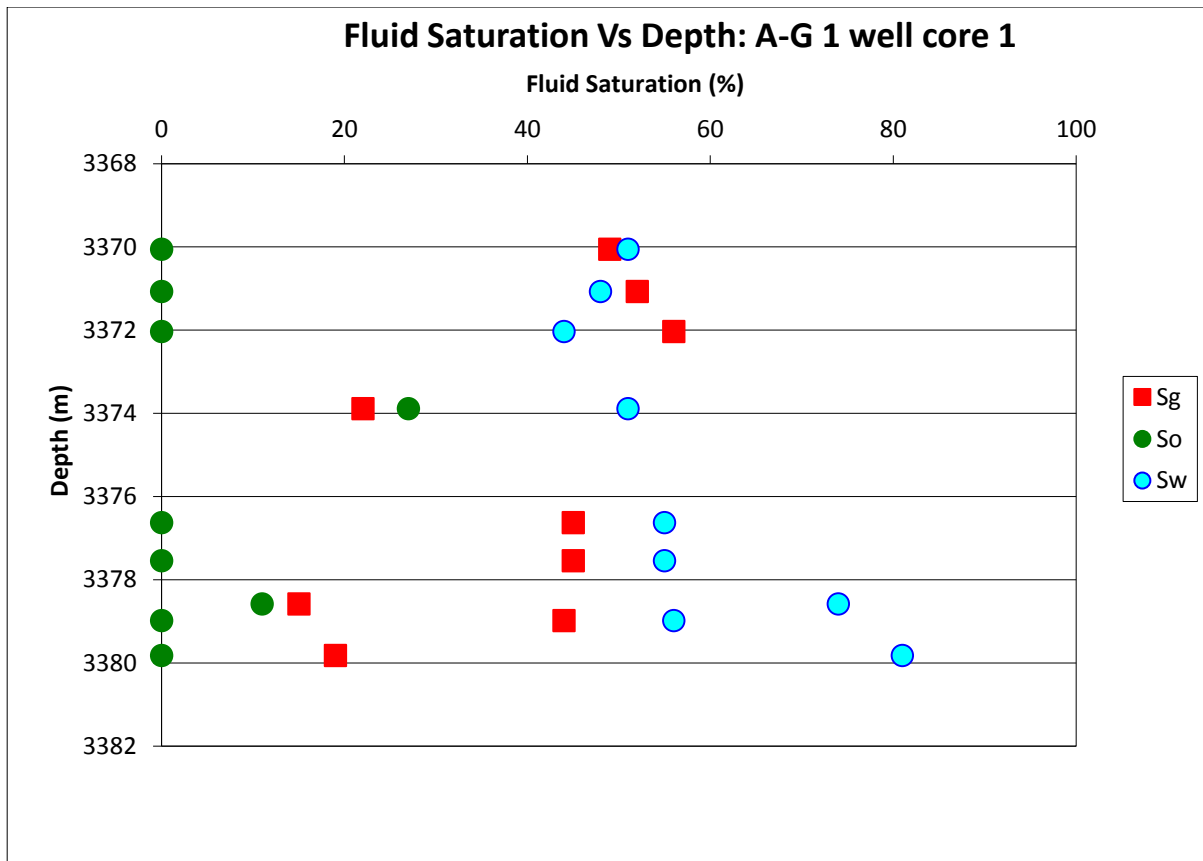


Fig.6.1.14. A-G 1 core 1 fluid saturation vs depth plot.

The depth-fluid saturation cross plot of A-G 1 core 1 shows an increase in gas saturation and a decrease in water saturation with depth between 3370m and 3373m. In the core this interval is within the top massive sandstone unit. The sandstone reservoir between 3377m and 3378m has constant saturations with gas values lower than that of water. Below this zone water saturation increases with depth with gas saturation decreasing with depth. This could be indicating a transition zone from gas to water (gas water contact).

6.2. Results and Interpretations of Petrophysical Evaluation from Geophysical Logs

6.2.1 A-K 2 Well Petrophysical Analysis

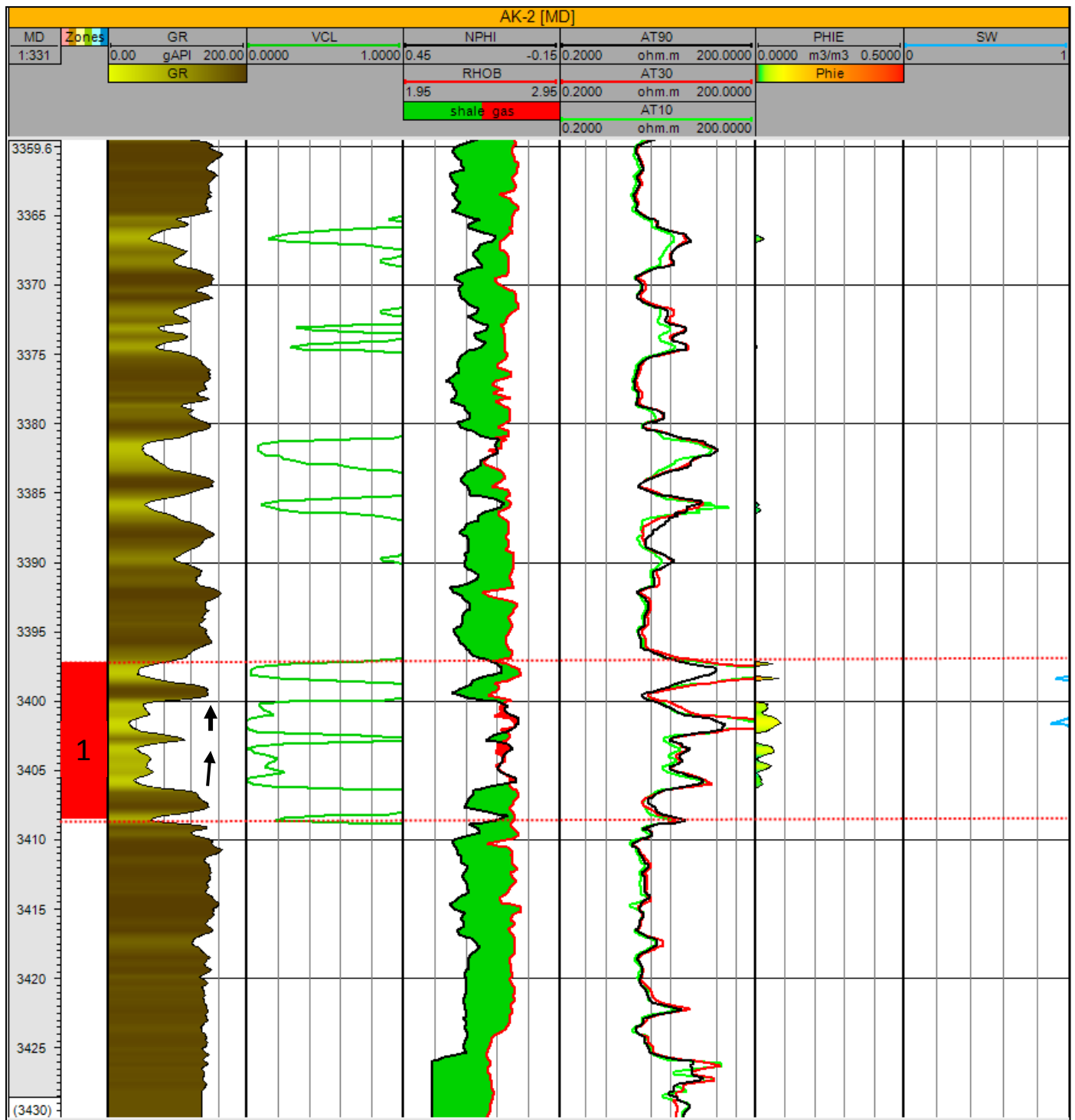


Fig.6.2.1. A-K 2 log template showing petrophysical parameters of zone one.

6.2.1.1 A-K 2 Zone One

Reservoir zone one of the A-K 2 well ranges from 3396.8 m to 3408 m with an average gamma ray response of 60 API. Like in all the reservoirs of A-K 2, the gamma ray log over this zone appears blocky (aggrading) with occasional stringers of high gamma ray values interpreted to be silt/mud. The gamma ray average over the entire zone suggests a dirty sandstone unit. The quality of the sands over this zone is further confirmed by the low porosity values with an average of 5% and 20% volume of shale. Deep resistivity readings reach a maximum of 60 OHMs over the sand units and these high resistivity values correspond with a neutron-density cross-over possible indicating a presence of gas shows within the sandstone stringers. Water saturation is up to 80%.

6.2.1.2 A-K 2 Zone Two

This zone is the main reservoir unit of the A-K 2 well with a top and base of 3237 m and 3261 m respectively. These sands sit below the regional M2K1 unconformity. The unit has a blocky aggrading nature with an average of 40 API. The sands over this unit are interpreted to be channel bar sands. The presence of gas over this zone is validated by very high resistivity reading of up to 128 OHMS and a prominent neutron density separation. The quality of these sands is good with an average porosity of 22% and water saturation of 20%. Porosities are calculated from density log. Good porosities here suggest that chlorite is probably present, preventing quartz-overgrowth. Above and below this sand unit are thick shales acting as both seat and top seals.

6.2.1.3 A-K 2 Zone Three

Reservoir zone three of A K-2 is a coarsening upwards sandstone interval ranging from 3108m to 3124m with a gross thickness of 16m. The average gamma ray response over this zone is 45 API. The quality of this sand is very poor with an average porosity of only 6%. The resistivity values over this interval reach a maximum of 22 OHMS; indicating minimal-none gas accumulation over this zone. It is also safe to say that resistivity logs were not affected by chlorite here as the primary porosities seem to not have been preserved from silicification by chlorite. The neutron-density cross plot is attributed to lithology effect. Judging from a gamma ray nature over this interval, it is possible that these sands are distributary bar sands. Water saturation is 97%.

6.2.1.4 A-K 2 Zone Four

Reservoir zone four is a 13 m thick sand unit represented by a blocky gamma ray log response. The blocky nature of the gamma-ray response is indicative of a fluvial depositional environment. The unit ranges from 2868m to 2881m with an average of 50 API. The density-neutron cross over associated with high resistivities is indicative of small gas accumulations or shows within the reservoir. Resistivities over this zone range between 8-19 OHMS and porosity has an average of 11%. Water saturation has an average of 75%. The poor petrophysical properties of this unit compared to the shallower reservoir below the 14Ht 1 unconformity could be due to intense diagenesis caused by thick overburden.

6.2.1.5 A-K 2 Zone Five

Reservoir five of A K2 ranges from 2700m to 2717m with a gross interval of 17m and an average gamma ray of 50 API. The gamma ray log response at the top of the sand unit has a very sharp top resulting from a period of non-deposition or erosion. This event is the 14Ht1 unconformity which is present in all four wells. The gamma ray log response at the sand unit below the unconformity is generally coarsening upwards from what appears to be very fine grained sediments at the base (silt/clay) to clean coarse sands towards the top of the unit. These sands are interpreted to be channel sands. This interpretation is purely based on wire-line log responses as there were no cores taken at this well. The porosity values which were calculated from a density log for this sand unit range between 12% to 14% and water saturation has an average of 65%. Resistivity logs have an average of 9 OHM; suggesting that the resistivities here could be misleading if chlorite is present. The density neutron cross plot is probably due to gas effect. It must be taken into consideration that resistivity logs in this gas field are not as high as they should be as they are interrupted by chlorite which is a dominant authigenic mineral in the Lower Cretaceous sands of the studied field. Below this sand interval is an approximately 150m thick aggrading unit of fine sediments (silt and clay) with stringers of sands.

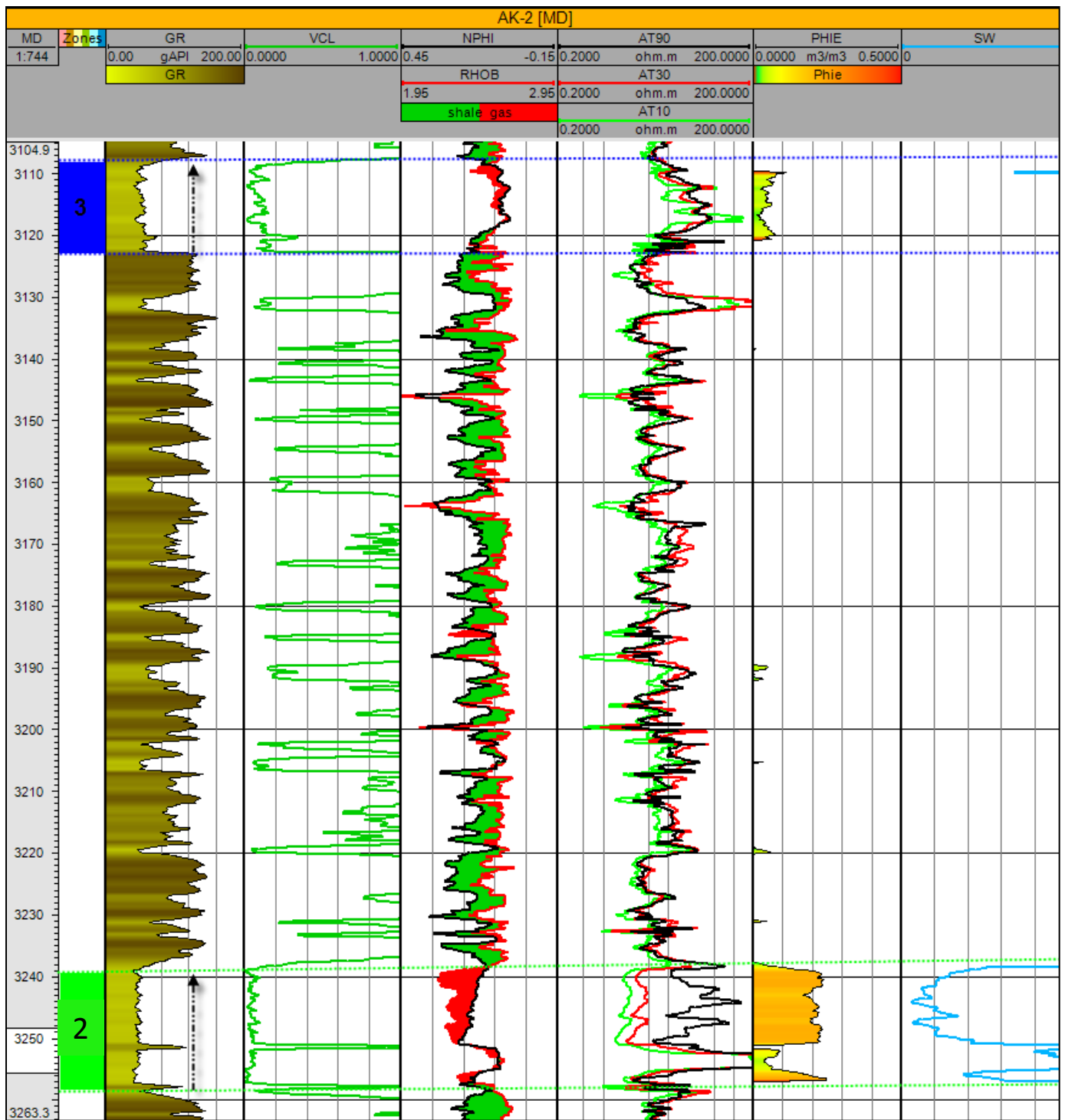


Fig.6.2.2. A-K 2 log template showing petrophysical parameters of zones two and three.

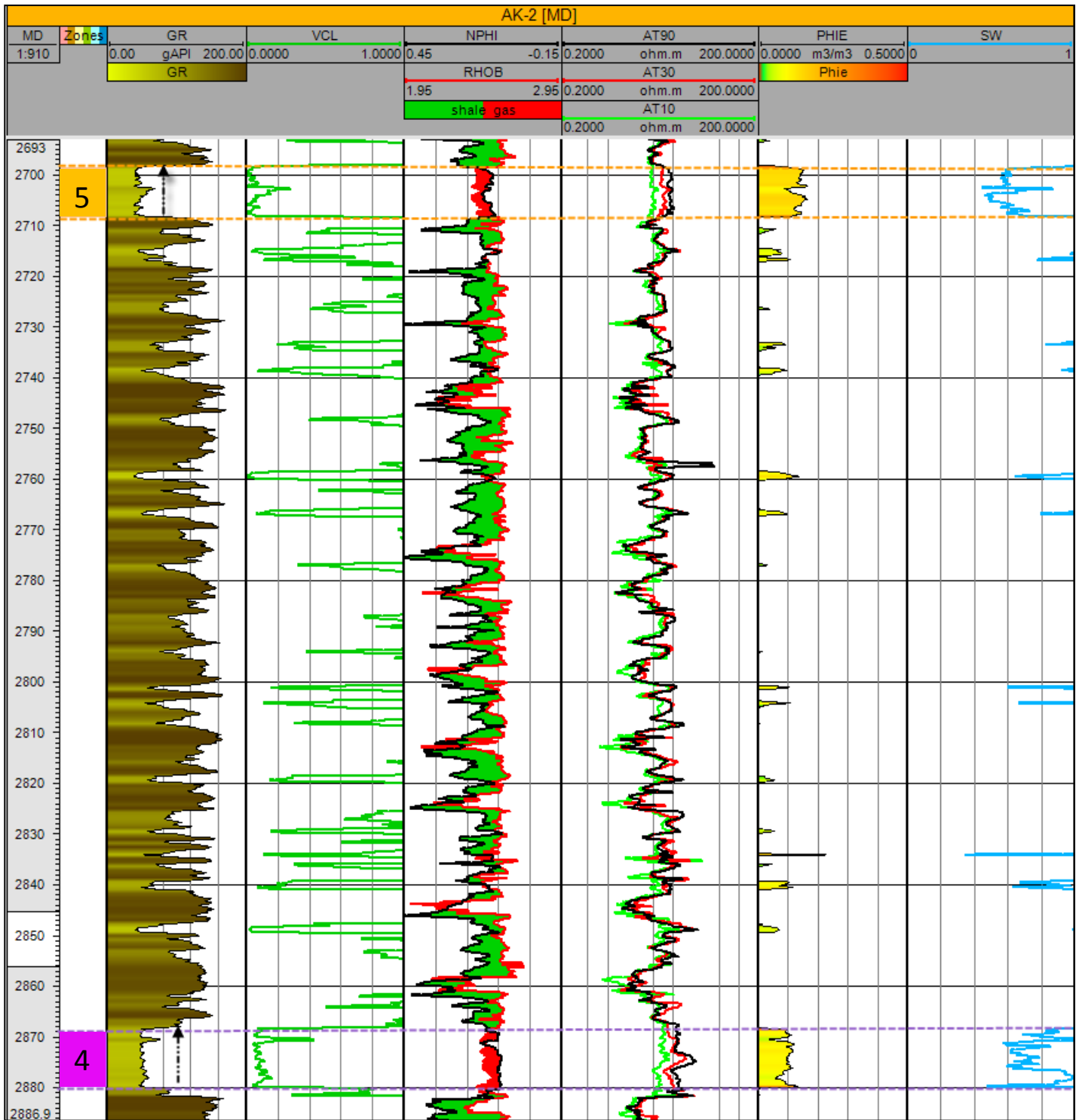


Fig.6.2.3. A-K 2 log template showing petrophysical parameters of zones four and five.

6.2.2 A-K 1 Well Petrophysical Analysis

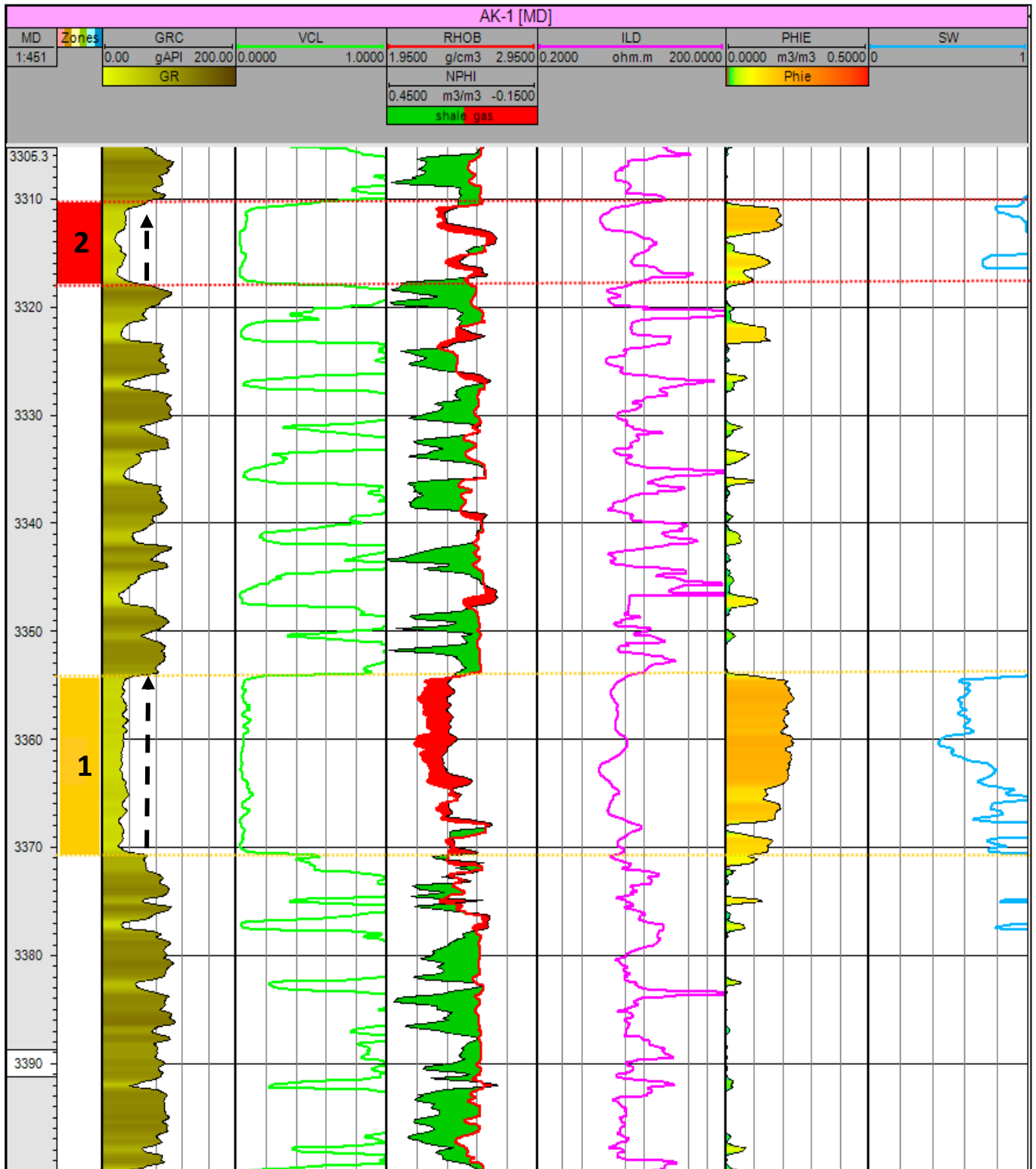


Fig.6.2.4. A-K 1 log template showing petrophysical parameters of zones one and two.

6.2.2.1 A-K 1 Reservoir One

The oldest reservoir unit of the A-K 1 well is a clean aggrading unit with an average gamma-ray response of 30 API. The aggrading nature of the gamma ray log over this interval is indicative of a channel sand. There were no cores taken at this interval; so the interpretation of the lithology is purely based on wireline logs. This interval ranges from 3354.5m to 3370.5m with a gross thickness of 16 m. The unit is characterized by good porosities with an average of 22%, volume of shale with an average of 5% and water saturation with an average of 43%. Good porosities are attributed to the presence of chlorite rims. Resistivities in this zone deep resistivity in particular (ILD) has high reading. This indicates the presence of gas which is further validated by the neutron-density separations.

6.2.2.2 A-K 1 Reservoir Two

Reservoir zone two is a thin interval with a gross thickness of only 7m. The unit ranges from 3310 m to 3317m. The gamma ray response over this unit is generally aggrading with occasional high gamma ray values which are indicative of silts/mud. The aggrading nature of the gamma ray is interpreted to be caused by distributary channel sands. This reservoir zone is considered clean as it has an average gamma ray of 30 API with porosities ranging between 15% and 19%. The deep log resistivity readings reach a high of 60 OHMS; demonstrating a possibility of gas shows trapped within the stringers of sands. Water saturation and volume of shale have an average of 75% and 5% respectively. The neutron-density cross over is representative of a gas effect.

6.2.2.3 A-K 1 Reservoir Three (core two: 3283m-3293m)

This zone has a gross reservoir thickness of 20m ranging from 3270 m to 3290 m. The gamma ray response is indicative of a channel sand. The average gamma ray response is 33 API. This sand unit covers about 50% of core two. In the core this sand reservoir is massive with sub-angular grains, mud drapes and sediment deformation structures. It is also interbedded with thin layers of siltstone. There is also a distinctive gas effect shown by the neutron-density cross-over. The presence of gas here is further validated by very high deep resistivity readings reaching a high of 152 OHMS. Porosities calculated from a density log have an average of 16% and water saturation of 63%. Porosities of this interval are mainly primary porosities which were preserved from quartz-overgrowth by chlorite rims. Secondary porosity is also possible resulting from leaching of calcite cement and feldspar.

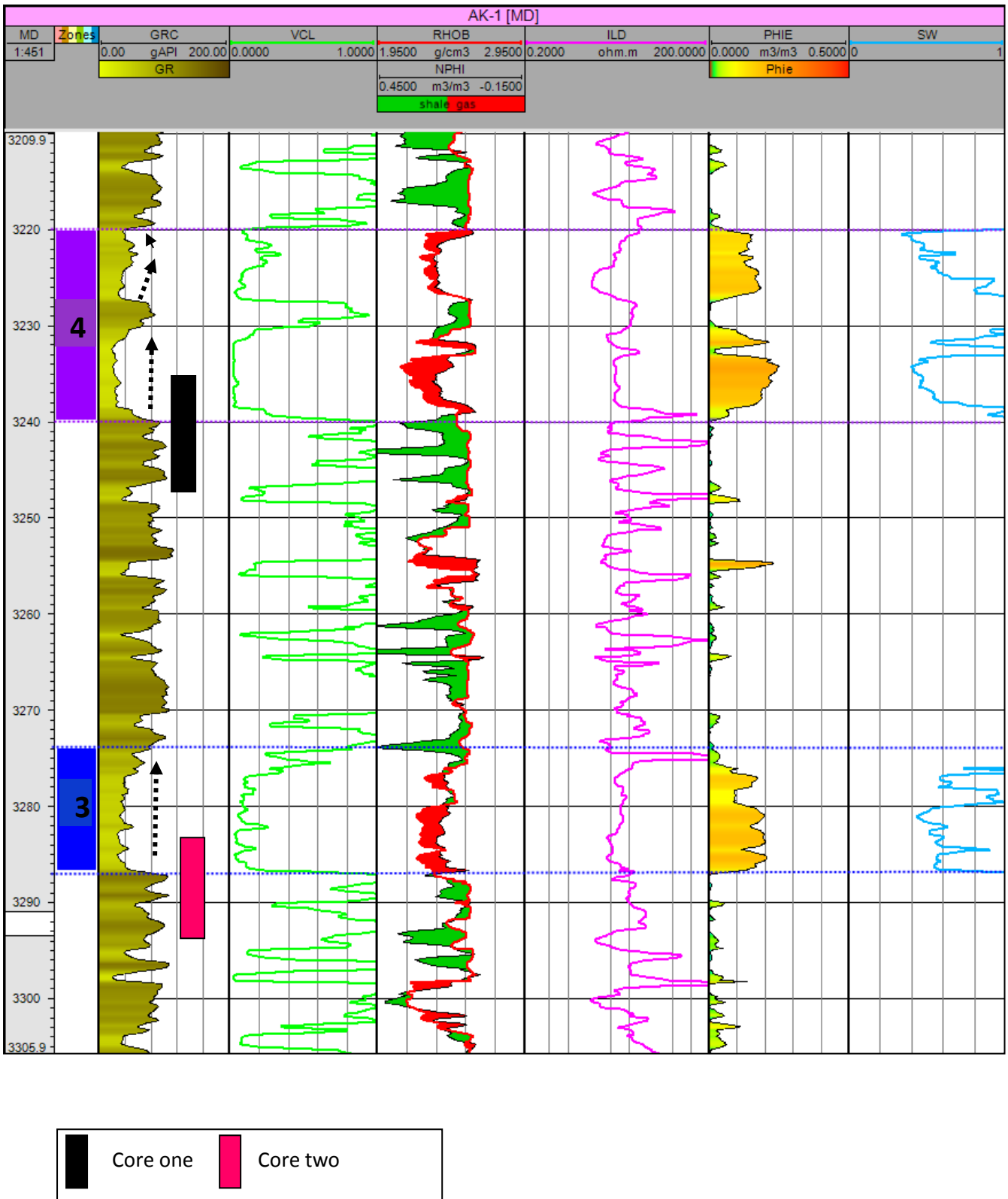
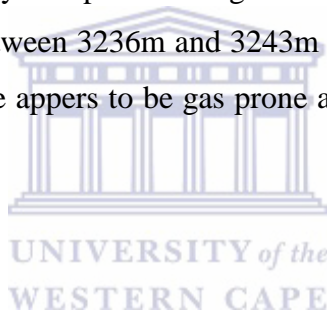


Fig. 6.2.5. A-K 1 log template showing petrophysical parameters of three and four.

6.2.2.4 A-K 1 Reservoir zone Four (Core one: 3237m-3345m)

Zone four is a 20m thick reservoir unit ranging from 3220m to 3240m with a generally aggrading blocky gamma-ray. This type of a gamma ray response over this reservoir interval is indicative of fluvial point bar sands overlain by a crevasse splay. The reservoir is sealed by a thick shale of 40m. The reservoir is part of the cored interval in core one of the well. In the core this unit is a clean massive sand with sub-rounded and moderately sorted grains. The environment of deposition appears to be a deltaic/fluvial environment. The gamma ray average over the sandy interval is 24 API which is indicative of a clean sand. Porosities which were calculated from a density curve reach a maximum of 23 % and water saturation has an average of 43%. The good porosity values at this reservoir are enhanced by chlorite rims as observed from thin sections and core log description. Deep resistivity curve reaches a high of 37 OHMS and does not reflect the presence of hydrocarbons in the zone due to the high content of chlorite in the sands. The presence of gas here is verified by the prominent gas effect shown by the neutron-density crossover. Underlying this sand between 3236m and 3243m is a shale unit which is potentially a source rock. In the core this shale appears to be gas prone as it is coaly and brittle. Beneath this shale is a thick silt interval of 34m.



6.2.3 A-V 1 Well Petrophysical Analysis

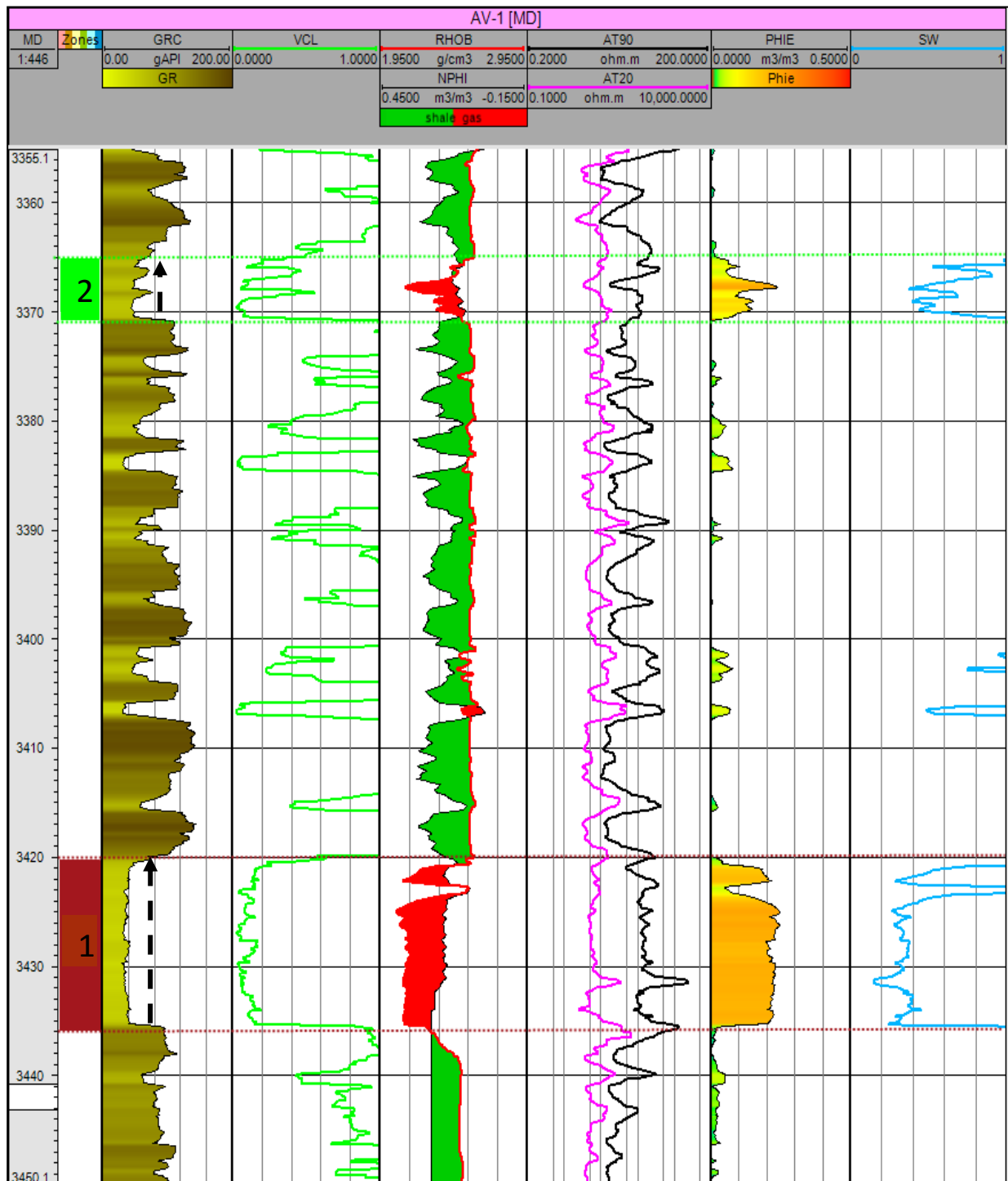


Fig.6.2.6. A-V 1 log template showing petrophysical parameters of zones one and two.

6.2.3.1 A-V 1 Reservoir Zone One

Reservoir zone one is the main reservoir unit in this well with a clear neutron density separation effect and high resistivity values of up to 80 OHM. Gas effect is also shown by the prominent separation of deep and shallow resistivity logs. This unit is a clean channel sand ranging from 3420m to 3435m with a thickness of 15m. Volume of shale is consistent across the entire unit at 5%. Porosity values range between 18% and 22%. Water saturation has an average of 25%. This reservoir interval sits below the M2KI unconformity and correlates well with the main reservoirs of A-K 1 and A-K 2. However, the sands across all the wells are not in communication as they are fed from separate distributary channels.

6.2.3.2 A-V 1 Reservoir Zone Two

Reservoir unit two ranges from 3366m to 3371m with a fining upward sequence. The gamma ray has occasional pikes towards the top of the reservoir which could be the shaly or silty intervals. Shale volume also increases towards the top of the reservoir to up to 40%; indicating that the clean sands are at the base of the unit where the volume of shale is 7%. The clear neutron density separation over this zone with fairly high resistivities of up to 25 OMHS indicates an accumulation of gas. Water saturation has an average of 48%.

6.2.3.3 A-V 1 Reservoir Zone Three

Reservoir zone three of A-V 1 is a 13 m thick reservoir unit with a shaly top and base as seen from the gamma ray log response. The blocky nature of the gamma ray is indicative of a fluvial depositional environment. The unit ranges from 3320m to 3329m with an average of 43 API gamma-ray response. The density-neutron cross-over associated with high resistivities is indicative of gas accumulation within the reservoir. Resistivities over this zone range between 5 to 30 OHMS and porosity has an average of 18%. Water saturation has an average of 40%.

6.2.3.4 A-V 1 Reservoir Zone Four

This is a thin channel sand unit ranging from 3206m to 3212m with a gross thickness of only 6 meters. On a gamma ray log this unit appears to be a clean sand unit with fair porosities of about 15%, shale volume average of 3% and water saturation of 58%. Porosities of this clean sand are presumably killed by quartz-overgrowth as there is no indication of high shale volume. However, resistivity logs and neutron density cross plot do not show any indication of significant hydrocarbon accumulation.

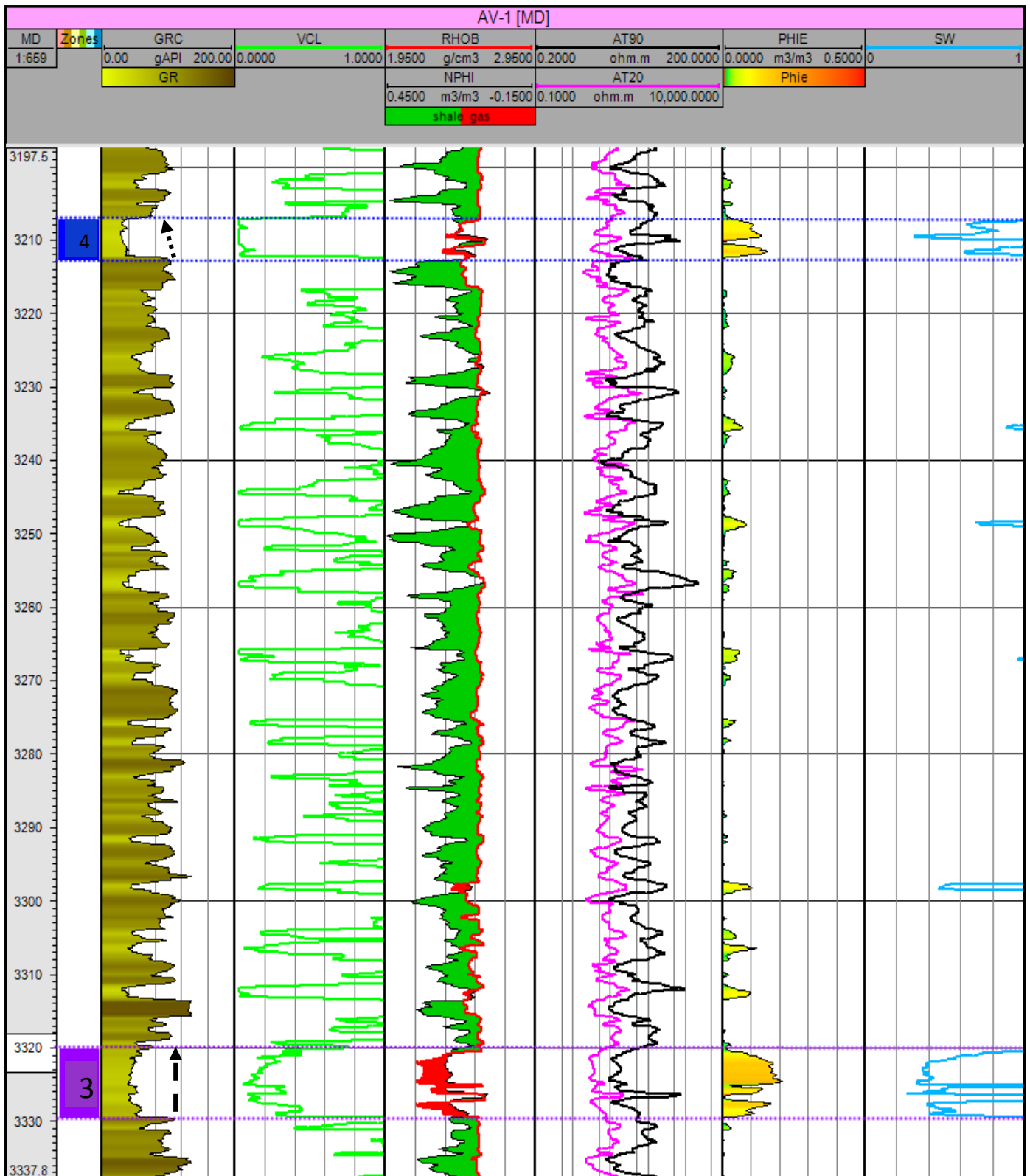


Fig.6.2.7. A-V 1 log template showing petrophysical parameters of zones three and four.

6.2.5 A-G 1 Well Petrophysical Analysis

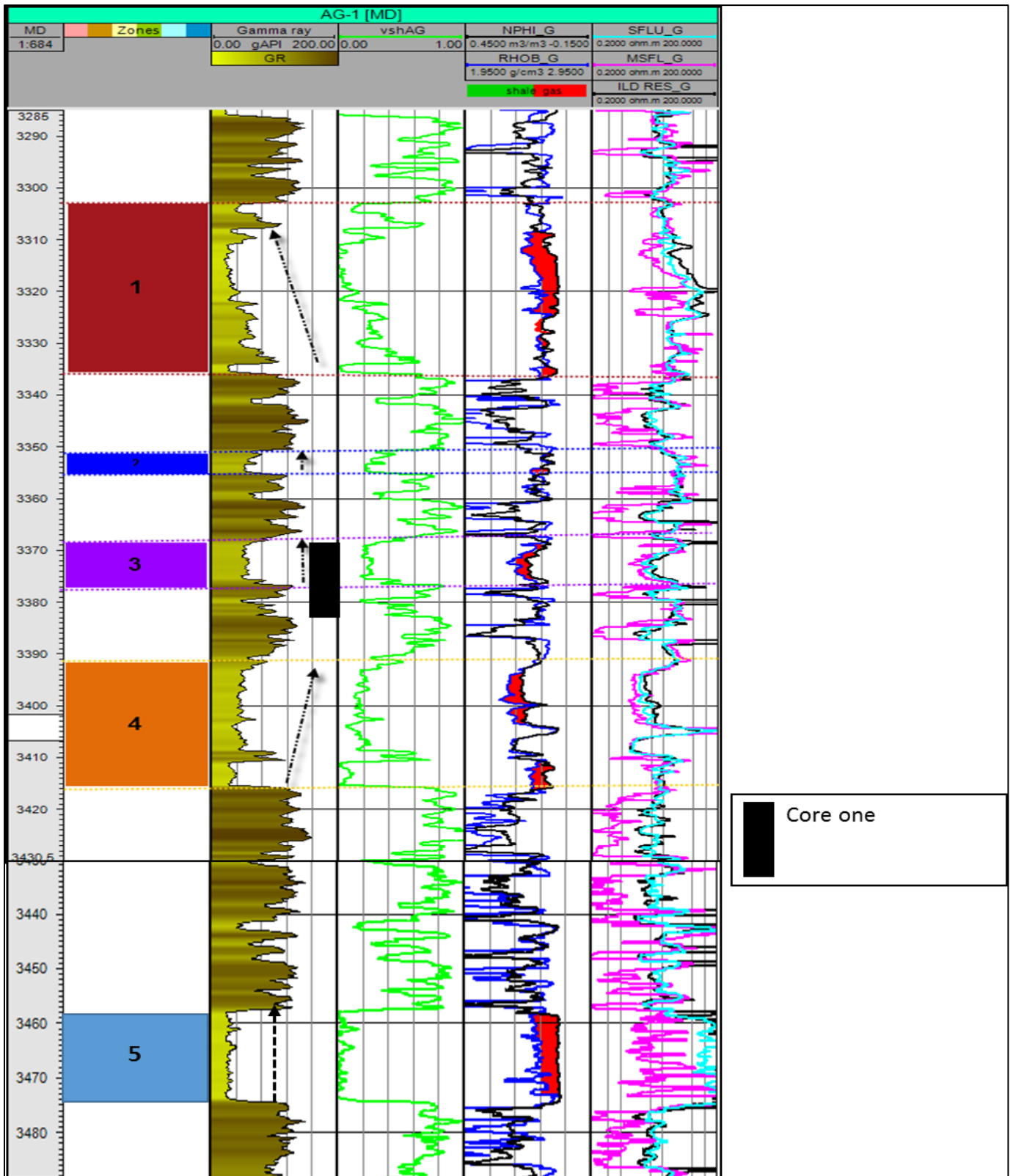


Fig.6.2.8. A-G 1 log template showing petrophysical parameters of all five zones.

6.2.4.1 A-G 1 Reservoir Zone One

The A-G 1 well is a distal well near the Albian shoreline away from the distributary channels. Zone one of the A-G 1 well is a clean shoreline bar sand unit with an average gamma ray and shale volume of 30 API and 1% respectively. This unit ranges from 3457m to 3474 with a thickness of 17m. There is a clear separation of resistivity curves with deep resistivity reading of up to 375 OHMS. The presence of gas over this zone which has been interpreted as the main reservoir unit of A-G1 is further validated by the clear gas effect on density-neutron curves.

6.2.4.2 A-G 1 Reservoir Zone Two

This zone has a reservoir thickness of 24m ranging from 3391 m to 3415 m. The gamma ray response fines upwards with an average of 40 API. Like in the other reservoir zones (with an exception of reservoir zone three) the lithology interpretation is based on a gamma ray response as there were no cores taken at this interval. This zone has a distinctive gas effect shown by the neutron-density cross-over. The presence of gas in this reservoir is further validated by very high deep resistivity readings of up to 85 OHMS. The volume of shale over this interval is 25%.

6.2.4.3 A-G 1 Reservoir Zone Three (core one: 3370m-3383m)

Reservoir zone three ranges between 3368 m to 3376 m and it incorporates the sand unit of the A-G 1 core. This reservoir interval is characterized by an aggrading gamma-ray response (blocky) with a sharp top and base. The average gamma ray and volume of clay responses have an average of 50 API and 23 % respectively. High gamma ray readings reaching 120 API below the reservoir unit correspond to the shale unit observed in the core. The gross thickness over this is 8 m. porosities over this zone reach a maximum of 21%. These are primary porosities preserved from quartz overgrowth by chlorite rims. This is validated by the poro-perm relationship in this zone. Permeabilities are good at the top with an average of 60mD and less than 1mD between 3372 and 3376m. Water saturation has an average of 50%. Resistivity logs are not really helpful over this zone as they are distracted by chlorite. Neutron –density cross plot has a clear gas effect which indicates a presence of gas in the reservoir unit. Hydrocarbon accumulation over this zone was also verified by fluid studies conducted on the core.

6.2.4.4 A-G 1 Reservoir Zone Four

Zone four of AG-1 well ranges from 3351 m to 3355m with a gross thickness of only 4 meter. The overall gamma-ray trend over this interval is aggrading. This response is interpreted to be a

channel sand. Like in all the other reservoir units of A-G 1 with an exception of reservoir three, there were no cores taken at this interval so the interpretations of the lithology is based purely on a gamma ray log. This is a dirty unit with an average gamma ray of 50 API and shale volume of 25%. Resistivity curves (SFLU, MSFL and ILD) do not indicate any presence of hydrocarbons. The lower resistivities might also be caused by an effect of chlorite if present. Below this sand unit is a 36 m shale interval acting as the top intra-formational seal for reservoir unit three.

6.2.4.4 A-G 1 Reservoir Zone Five

Zone five ranges from 3303m to 3336m with a sharp gamma ray base and a generally retrograding gamma ray response between 3100 m and 3175 m. From 3334m to 3308m the gamma ray response coarsens upwards to a very sharp top at 3030m. This type of a gamma ray response is indicative of a shoreline sands. No cores were taken at this interval; therefore the lithology and depositional environment predictions are purely based on a gamma ray log response. The gamma ray over the sandy interval has an average of 45 at the base to 20 API towards the top. The reservoir has a gross interval of 33m. The clear neutron-density cross over with clear separation of resistivity curves is indicative of gas accumulation in the cleaner sand at the top of the unit. This reservoir zone is directly underlain by a 110 m thick erratic high gamma ray formation interpreted to be floodplain muds/silts.

6.2.5. Mineralogy Predictions from Well Logs

In the absence of cores or core plugs grain density from a density log can be used to infer the types of minerals present in the reservoir zones of interest. In this section a number of density-neutron cross plots have been constructed for all the four wells to help identify minerals present in the reservoir zones. It is important to note that this method of mineralogy prediction could be misleading at times as it is inaccurate. In this research study this technique is used only as a high level indicator of mineralogy identifier particularly for wells with no cores and thin sections (A-K 2 and A-V 1). Detailed petrology is achieved by conducting studies such as thin section evaluation and SEM.

Table 6.3: Densities of common clay minerals. (petrowiki.org/Rock_density_and_porosity).

| TABLE 13.3—GRAIN DENSITIES FOR COMMON ROCK-FORMING MINERALS | | | |
|---|---------------------------------------|--------------------------|---------------------------------------|
| Mineral Name | Grain Density (g/cm ³) | Mineral Name | Grain Density (g/cm ³) |
| Albite (Na Feldspar) | 2.61 | Hornblende | 3.12 |
| Almandine | 4.08 | Kaolinite (Clay 3) | 2.59 |
| Anhydrite | 2.96 | Illite (Clay 4) | 2.66 |
| Anorthite (Ca Feldspar) | 2.75 | Magnesite | 2.97 |
| Apatite | 3.23 | Magnetite | 5.18 |
| Aragonite | 2.99 | Matrolite | 2.25 |
| Augite A | 3.32 | Montmorillonite (Clay 5) | 2.1–2.6 |
| Augite B | 3.42 | Muscovite (Mica 3) | 2.78 |
| Barite A | 4.50 | Olivine A | 3.31 |
| Biotite A (Mica 1) | 3.00 | Olivine C | 3.13 |
| Biotite B (Mica 2) | 3.05 | Orthoclase (K feldspar) | 2.57 |
| Calcite | 2.71 | Phlogophite (Mica 4) | 2.82 |
| Chlorite (Clay 1) | 2.80 | Plagioclase A | 2.64 |
| Clinoperthite A | 2.54 | Plagioclase F | 2.69 |
| Clinoperthite G | 2.57 | Pyrite | 5.02 |
| Coal | 1.2–1.8 | Quartz | 2.65 |
| Diopside | 3.31 | Rhodochrosite | 3.57 |
| Dolomite A | 2.85 | Rutile | 4.2 |
| Dolomite B | 2.87 | Siderite | 3.75 |
| Epidote | 3.40 | Sillikanite | 3.19 |
| Fluorite | 3.18 | Smectite (Clay 5) | 2.1–2.6 |
| Forsterite | 3.22 | Sphalerite | 4.00 |
| Galena | 7.50 | Staurolite | 3.78 |
| Garnet A | 3.60 | Sulfur | 2.07 |
| Garnet I | 4.25 | Sylvite | 1.99 |
| Glaconite (Clay 2) | 2.30 | Topaz | 3.50 |
| Gypsum | 2.31 | Tourmaline | 3.23 |
| Halite | 2.16 | Zircon | 4.70 |
| Hematite | 5.26 | | |

6.2.6.1 A-K 2

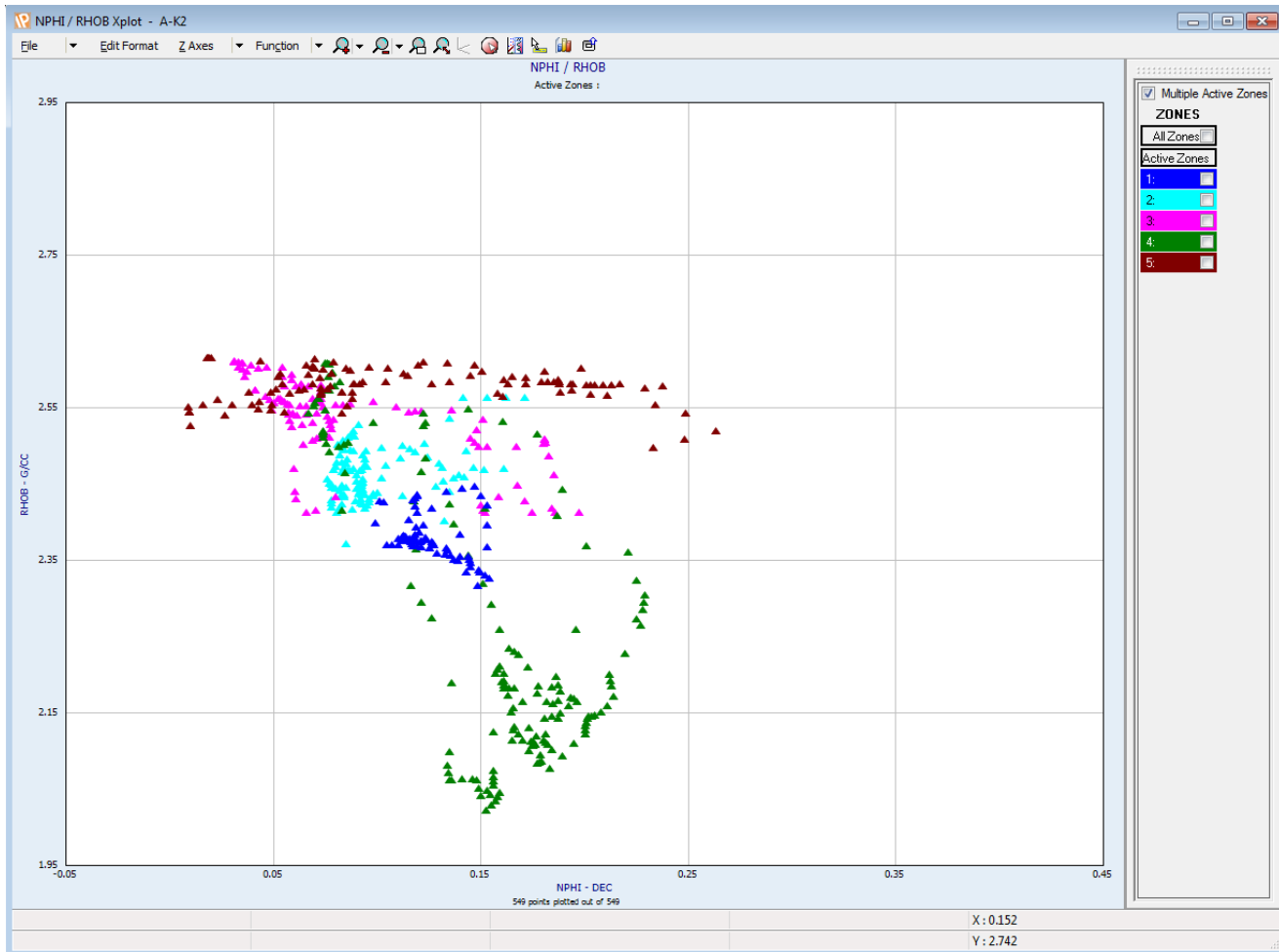


Fig.6.2.9. Neutron-density plot for mineralogy prediction for zones of A-K 2 well.

The depth density cross-plot of the A-K 2 reservoirs shows a density distribution varying between 2.61 g/cc and 2 g/cc. Sandstone reservoir unit 5 is largely distributed between 2.55g/c and 2.65 g/cc. This reservoir unit appears to be a clean sand interval made of primarily quartz grains with traces of kaolinite and montmorillonite. Sandstone reservoir 4 of the A-K 2 well has a dense concentration of density values between 2.1 g/cc and 2.3 g/cc. These densities value are indicative of high concentration of glauconite and montmorilloite. Another cluster of points for this reservoir unit is around 2.59 g/cc. These low density values could be attributed to the presence of kaolinite. This interpretation is solely based on the density log response. Reservoir zone 3 has density distribution between 2.61 g/cc and 2.4 g/cc with a dense distribution at 2.55 g/cc. This shows high quantities of kaolinite in the matrix of the sandstone reservoir 3. Reservoir zones 1 and 2 have density distributions between 2.3 g/cc and 2.57 g/cc. Density values of 2.3 g/cc which are mainly present at reservoir one are caused by the presence of glauconite. This mineral is

present in the basin as it was observed in the cores of A-G 1 and A-K 1. The presence of glauconite in reservoir one unit is indicative of a continental shelf depositional environment. The density values of 2.57 g/cc which are present in both reservoirs 1 and 2 suggest a presence of orthoclase potassium feldspar. The dense distribution of points at 2.45 g/cc in sand reservoir 2 could be indicative of the presence of montmorillonite.

6.2.6.2 A-K 1

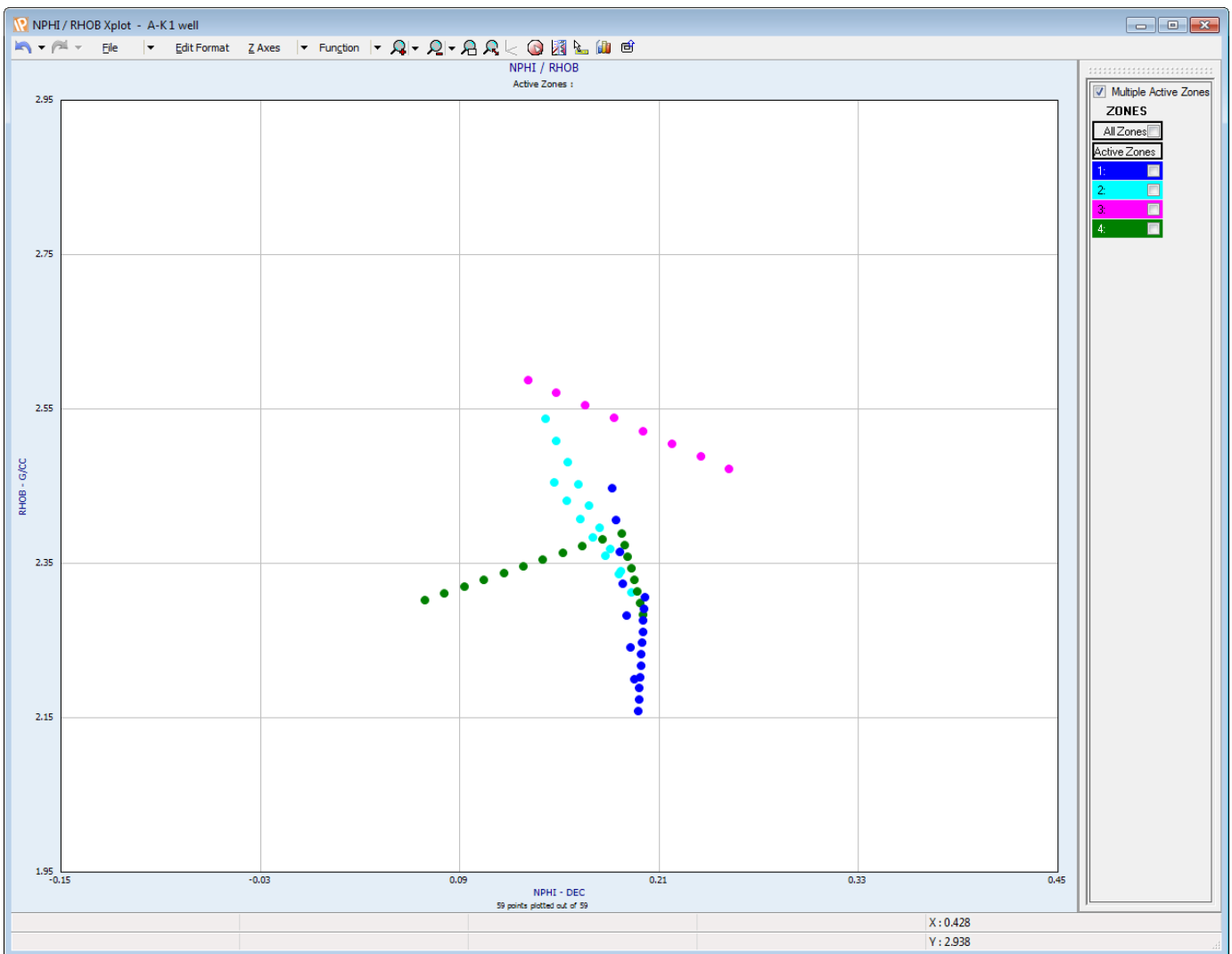


Fig.6.2.10. Neutron-density plot for mineralogy prediction for zones of A-K 1 well.

The density-neutron cross plot of the reservoir zones at A-K 1 have a distribution of grain density between 2.57 g/cc and 2.15 g/cc. Reservoir zone four (green dots) has a high concentration of density values between 2.65 g/cc and 2.55 g/cc. These density values are indicative of a quartz

rich sandstone with kaolinite as a dominant clay mineral. Kaolinite commonly forms when feldspar is altered during diagenesis to form pore filling cement which reduces porosity.

Zone three has a sparse distribution with grain density values of 2.3 g/cc, 2.2 g/cc and 2.5 g/cc. These densities could be attributed to the presence of plagioclase. Both reservoir zones one and two seem to be dominated by kaolinite and plagioclase minerals.

6.2.6.3 A-V 1

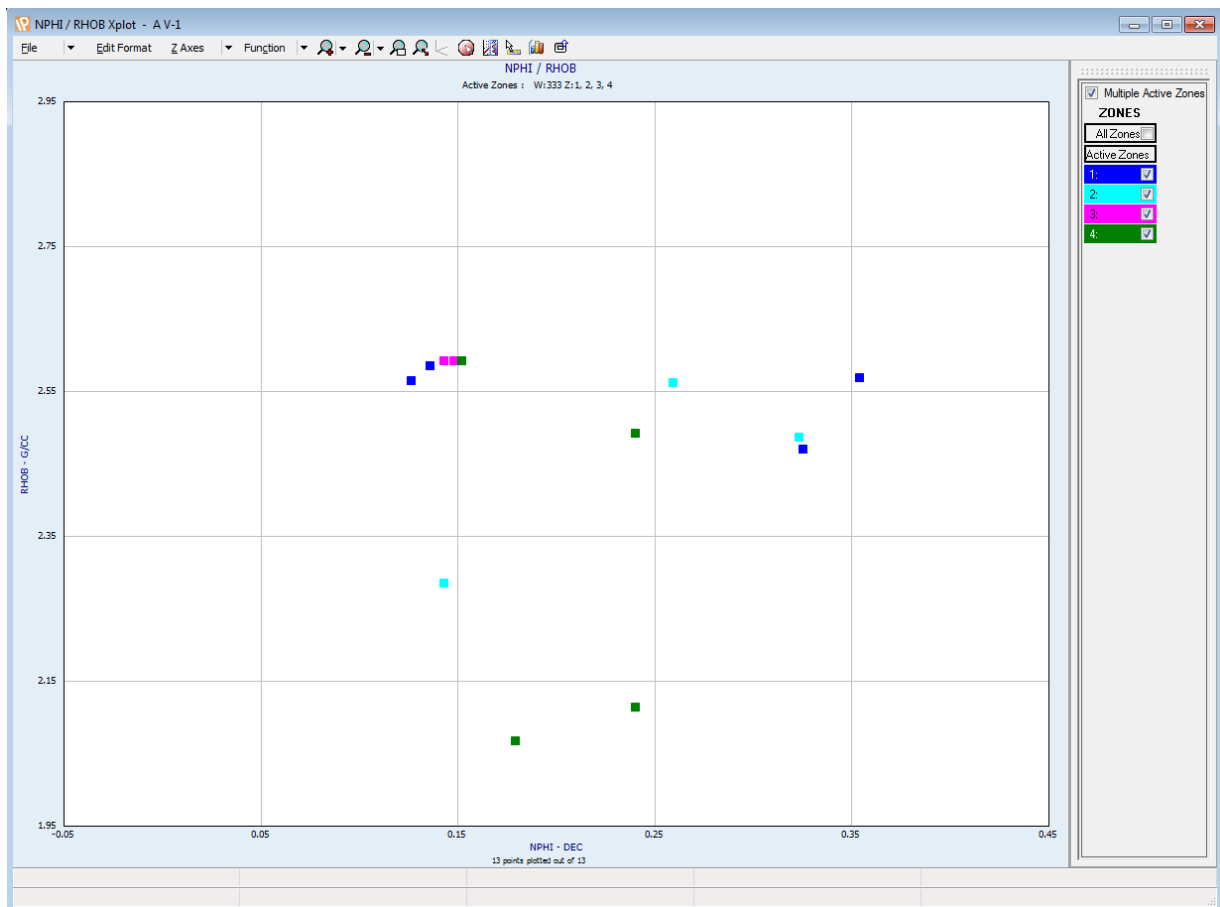


Fig.6.2.11. Neutron-density plot for mineralogy prediction for zones of A-V 1 well.

The four reservoir zones of A-V 1 have density values ranging between 2.57 g/cc and 2.07 g/cc. Reservoirs three and four are sparsely distributed between the aforementioned ranges. This distribution is indicative of the presence of montmorilliite as the dominant clay mineral in these reservoirs. Reservoir units one and three have points concentrated at 2.57 g/cc; which are attributed to the presence of potassium feldspar.

6.2.6.4 A-G 1

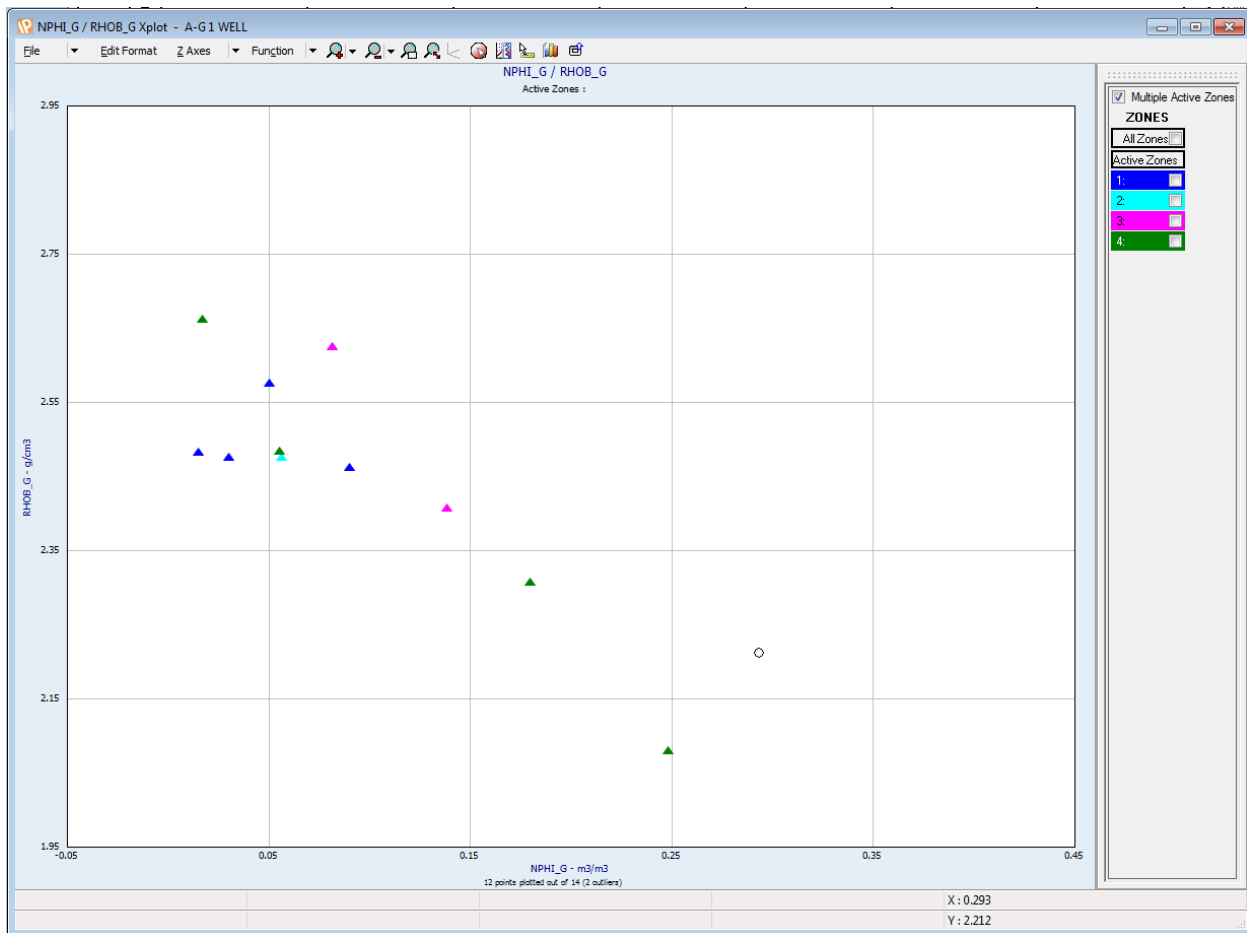


Fig.6.2.12. Neutron-density plot for mineralogy prediction for zones of A-G 1 well.

The neutron-density cross-plot of the A-G 1 reservoir intervals shows a density distribution varying between 2.65 g/cc and 2g/cc. Reservoir zone one has a distribution of density values between 2.45 and 2.55. Reservoir zone four has a sparse distribution of density points with the highest grain density value of 2.65g/cc and lowest value of 2 g/cc. The cross-plot indicates the presence of calcite cement predominantly in reservoir unit 4. Kaolinite and feldspar are also present.

6.2.6. Results and Interpretation of Petrography

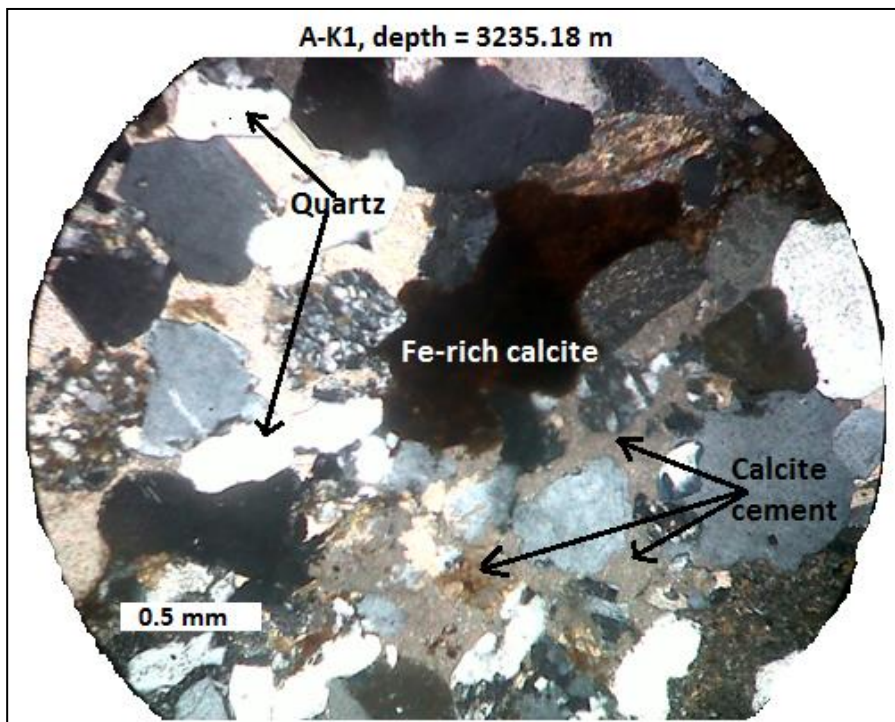
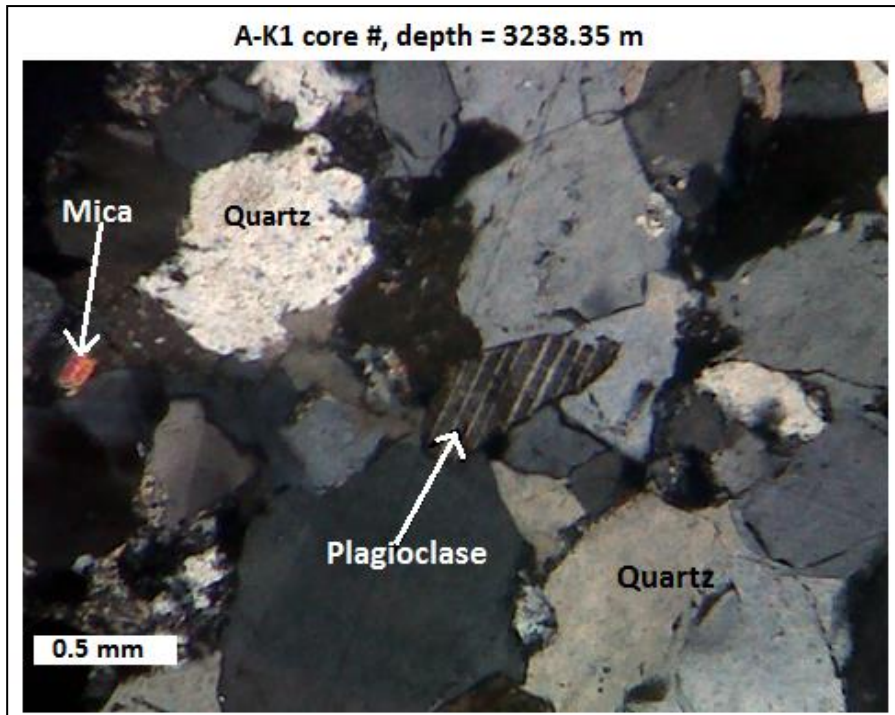
For a proper analysis of a sandstone reservoir it is important to understand not only the types of clay minerals present in a reservoir unit, but also to understand their distribution and origin. This section focuses on petrography analysis of the selected studied wells. The analysis was conducted for the wells with cores namely A-G 1 and A-K 1 wells. This was carried out to further investigate various factors affecting reservoir quality such as types of clay minerals present in the cored reservoir units, texture of these clay minerals and that of the sand grains, connectivity of the pore spaces. The aforementioned reservoir properties are easily studied under a microscope on thin sections as it is impossible to see them with a human eye. Thin sections were prepared for selected depths from the three studies conventional core cores of Cretaceous age. These are mainly in the sandstone reservoir units (facies 3).

6.2.7.1. A-K 1

Numerous thin sections taken from the sand intervals of the A-K 1 well cores were examined under the microscope. Only four of the examined thin sections have been analysed in detail due to their excellent resolution. The four analysed thin sections were taken at the following depths: 3238.35 m, 3235.18 m, 3236.96 m and 3236.27m.

Thin sections of A-K1 have quartz grains as the main framework with traces of feldspathic grains and chert fragments. These moderately packed quartz grains are characterized by a sub-rounded shape and they seem to be the major cementing material in the reservoir zones of A-K1. Calcite is also a dominant cement (depths, 3235.18m, 3236.96m and 3236.27 m) resulting in reduction of primary porosity. This calcite cement appears to be rich in iron; indicating that the processes of oxidation occurred with or after the formation of calcite. The abundant calcite cement as observed from all the studied thin sections of A-K1 reflects dissolution from shelly materials and precipitation of calcium carbonate from fluid sediment interface (Fadipe, 2009). The quartz cement occurs as quartz overgrowth cement around the quartz grains. This silica cement was possibly formed around Mid Albian during diagenesis resulting to silification of what was probably good clean sand. It is also possible that dewatering of clays during compaction resulted in high silica saturation which increased quartz overgrowths. The highly deformed accessory minerals such as mica are indicative of compaction effects during burial. These deformed accessory minerals, mica in particular seem be squeezed in between quartz grains; thus reducing the primary porosity of the sands.

Chlorite is another dominant mineral in these Lower Cretaceous reservoirs of A-K 1 as it was also observed in the cores during core logging. Chlorite is often a good primary porosity preserver, doing so by coating itself around quartz grains to prevent quartz overgrowth. Grain coating cementation is mostly associated with syn-depositional processes (Hurst & Archer, 1986). The best porosities in the AK-1 core logs occur in sands with high quantities of chlorite. Figure 6.2.13 shows thin section photographs of A-K 1 well.



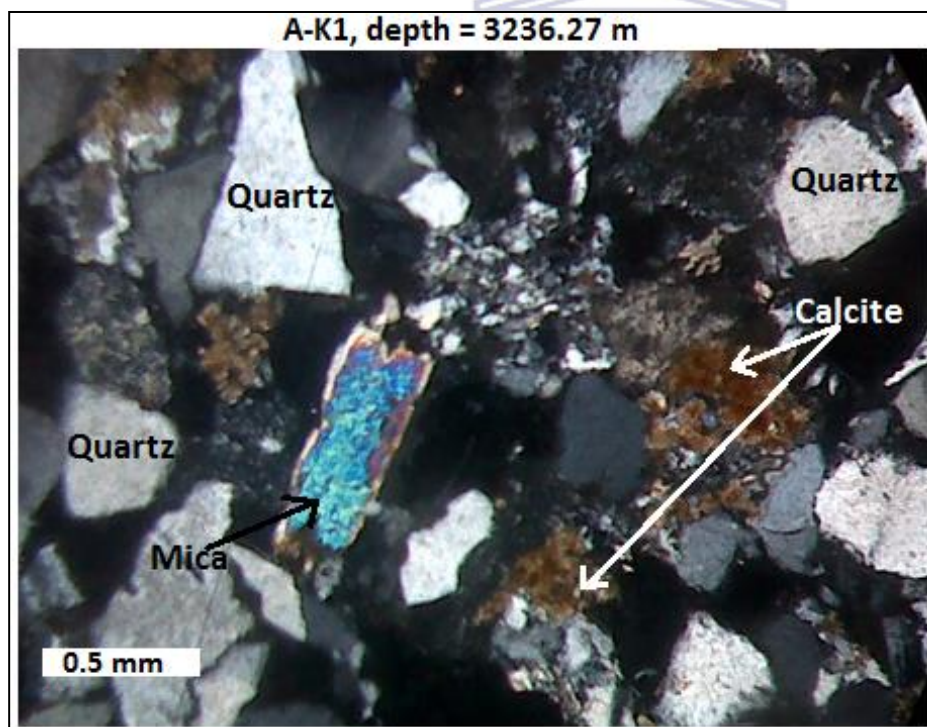
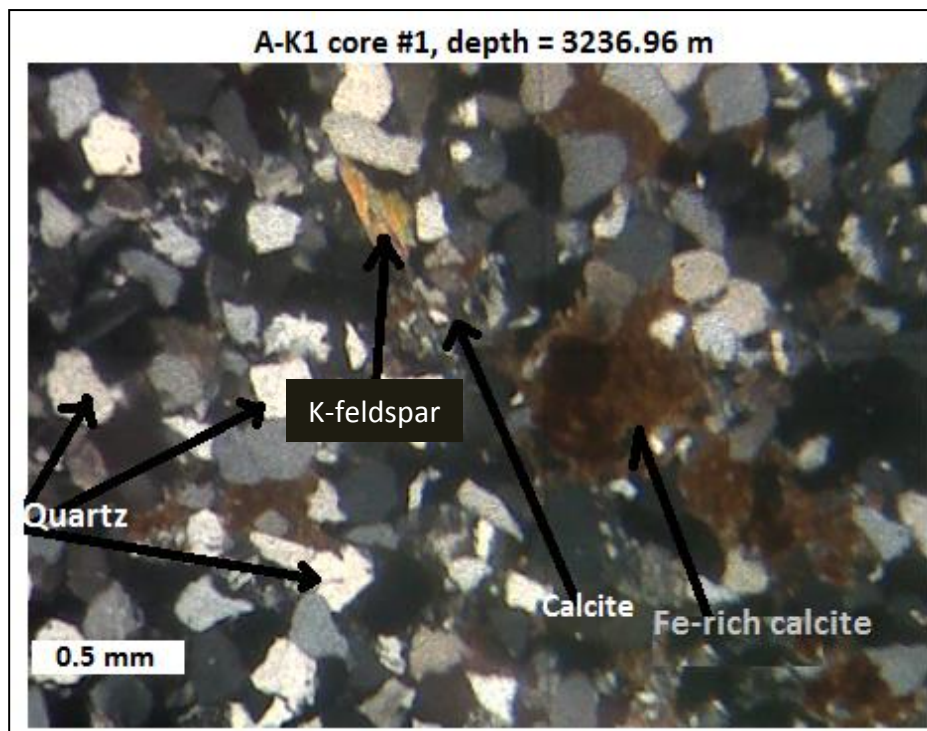


Fig.6.2.13.Thin section photographs of A-K 1 well.

6.2.6.2. A-G 1

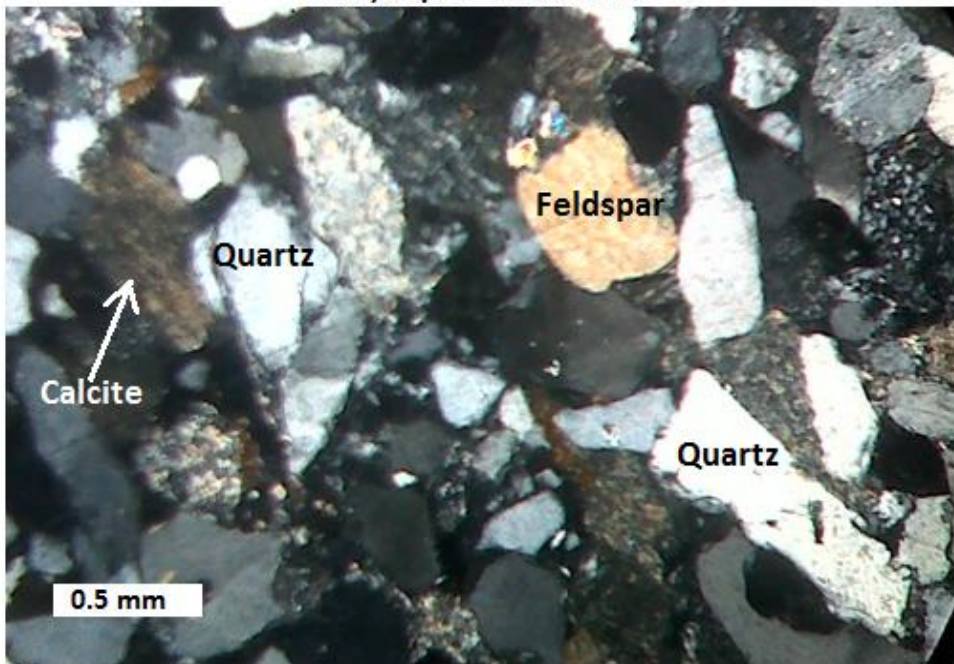
The rock forming minerals of the well A-G1 do not differ much from those of A-K 1. Quartz is a dominant mineral as observed in the thin sections in Figure 6.2.14 below. Quartz grains appear well sorted and sub-rounded at 3371.28m and 3372.70m. Thin section at 3370.24 has elongated quartz grains and well-rounded feldspar grains.

The grains of A-G 1 cores are mainly quartzitic with high concentration of feldspathic grains (e.g at depth 3370.24m). The main cementing material are quartz overgrowths formed by quartz precipitation during diagenesis under high temperatures. Quartz overgrowths as seen from the thin sections are the primary cause of low poro-perm values in the reservoir units of this cored reservoir interval. Feldspar on the other hand, is unstable and often dissolves during diagenesis to form secondary porosity. The improved porosities between 3370m and 3372m (refer to figure 6.1.4) are probably caused by a combination of feldspar leaching and chlorite rims. Other abundant cements at A-G 1 are calcite, kaolinite and chlorite. At the depth of 3372.70 m, the mineral mica has an elongated shape indicating that it underwent deformation under ductile conditions. Deformation of this mineral might have been due to compaction, a process which occurs as a result of overburden pressure during the process of sedimentation. Compaction during burial also causes dewatering of silts and clays. This water circulates around quartz grains and enhances quartz-overgrowth.

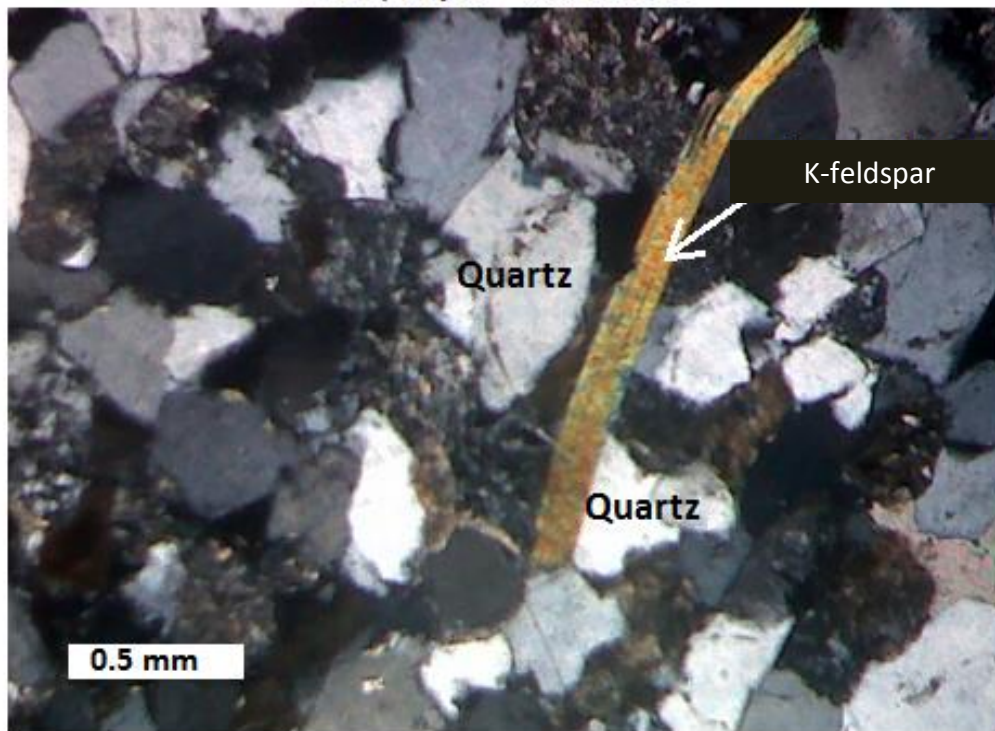
Kaolinite forms pore-filling cements which may vary in pore sizes but are distributed across the pores of a sand reservoir to reduce porosity (Hurst & Archer, 1986). According to Selley (1976), Kaolinites and traces of illite are often formed when feldspar is altered either by hydrothermal process or superficial processes.

The presence of chlorite on the other hand is good news for preserving primary porosity of the reservoir by preventing quartz overgrowth. However, chlorite also heavily destroys permeability by cementing pore connectivity. As rifted volcanic margin, the Orange basin has abundant volcanic material which is the source of chlorite. The formation of chlorite rims around the quartz grain from the volcanic fragments must have occurred early before diagenesis to prevent quartz-overgrowth as seen in Figure 6.2.14.

A-G1, depth = 3370.24 m



A-G1, depth = 3372.70 m



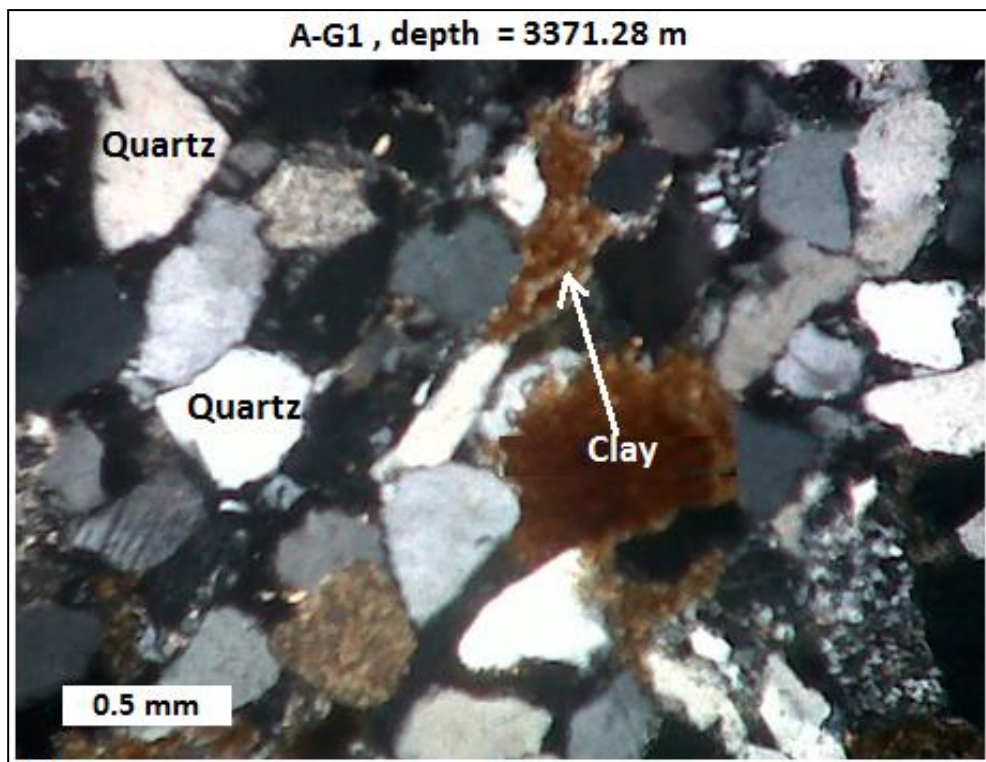
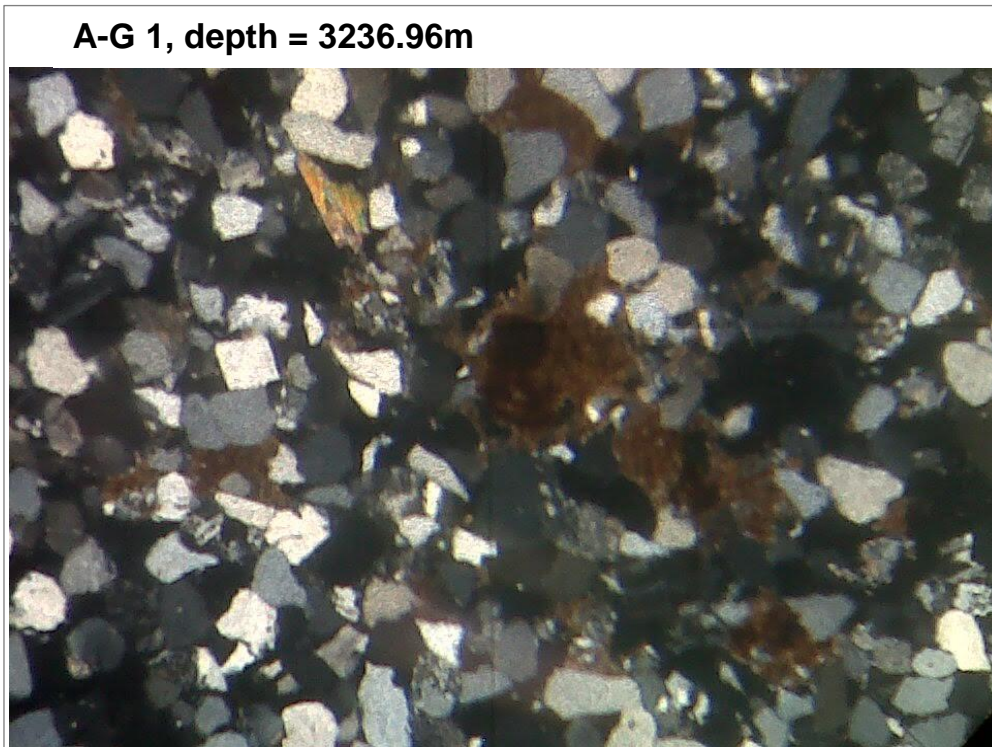


Fig. 6.2.14. Thin section photographs of A-G 1 well.

Section Three

Chapter Seven

- Conclusions and Recommendations

UNIVERSITY of the
WESTERN CAPE

CHAPTER SEVEN

7.1 Conclusions

The key objectives of this research study were to characterize and map the lateral extent of the Albian reservoirs in the Ibhubesi gas field by integrating seismic data, core logs and well logs. Four key wells (A-K 2, A-K 1, A-V 1 and A-G 1) which were drilled to test the potential of the Albian reservoirs of the Ibhubesi gas field were studied.

The mapping of the Albian reservoirs on a 3D seismic data covering the Ibhubesi field indicated that during Albian, block 2A was in a fluvial deltaic environment. Seismic attributes such as spectral deposition, RMS and maximum amplitudes revealed that all three wells covered by the 3D seismic data were drilled on sweet spots of the channel axis where better sands are expected to develop in this depositional setting. Down dip of the well locations, the A-V 1 and A-K 1 channels divert south west and south east respectively possibly following incised valleys and or due to a syn-rift horst block which exists between A-V 1 and A-K 1. Brighter amplitudes on seismic attributes are present in the southwestern corner of the mapped 3D survey. These amplitudes could be sheet sands/splay of the A-V 1 channel. More of these fluvial deltaic sands are expected to occur across the Albian shelf in the southern Orange Basin where the Orange and Olifants Rivers were active in Albian. This proven play at Ibhubesi gas field is structural as the sands are trapped against a northwest-southeast trending fault. Any sands of this nature in this basin may require structural trapping as a stratigraphic trap may leak and fail if the sands are not shalying out up dip.

Core log interpretation was carried on wells with cores namely, A-K 1 and A-G 1. Two cores from A-K 1 were evaluated and only one from A-G 1. The A-K 1 cores one and two were cut from reservoir units four and three respectively. A-G 1 core was cut from reservoir unit three. The core logging exercise was carried out to fully examine and understand the origin and nature of the depositional environment of the Albian sandstone reservoirs and also to evaluate the types of minerals present in these sands and their influence on reservoir quality. All three cores were subdivided into three facies based on lithology and depositional environment. The three facies are:

- Facies one: shale
- Facies two: siltstone
- Facies three: sandstone

Facies three are the main reservoir units with generally fine to medium grained sands which are dominantly made of quartz grains. These are fluvial deltaic sandstones. The main authigenic minerals in these sands were chlorite and calcite. Facies two are mainly silts with lenses of fine grained sands which showed no significant amount of chlorite. Facies one were friable coaly shales with high content of organic matter.

Petrophysical analysis of the Albian sands encountered in the studied four wells shows poor to fairly good porosities and generally poor permeability values. Porosities in these sands are a combination of primary and secondary porosity. It is clear that the Albian deltaic sands were generally good sands at the time of deposition but quality was later destroyed by silica cementation from quartz-overgrowth during diagenesis. Although quartz-overgrowth may have destroyed most of the porosities in these sands it is also apparent that some reservoir intervals still have primary porosities which were preserved from silica cement by chlorite rims. Reservoir unit four of A-K 1 where core one was cut from had good porosities of up to 23%. These good porosities values are attributed to the presence of chlorite as seen from core descriptions and thin sections of reservoir unit four. Permeabilities were also better in this sand unit; indicating that potassium feldspar and or calcite cement dissolution occurred resulting to improved pore connectivity and secondary porosity. Resistivity values over most of the reservoir units were generally low even in hydrocarbon bearing zones. These low values are caused by the effect of chlorite on resistivity logs.

Other additional authigenic clays which contributed to the reduction of poro-perm are calcite, illite and kaolinite. The latter result from dissolution of potassium feldspar during diagenesis. Thin sections from A-G 1 and A-K 1 wells show feldspar as the secondary dominant mineral after quartz. As an unstable mineral, dissolution of feldspar under high temperatures during diagenesis resulted to secondary porosities. The downside of having these porosity preservers, chlorite in particular is that they heavily disconnect pore connectivity resulting in very poor permeability values. As a rifted volcanic margin, the Orange Basin would have had volcanic material deposited in Albian during the deposition of clastic material. These volcanic rocks are the source of chlorite. For preservation of primary porosity to be effective, the formation of chlorite would have had to be pre-diagenesis of the Albian sands.

7.2. Recommendations

- ❖ Follow the play ponding against the syn-rift structural high along the incised valleys.
- ❖ An extension of 3D seismic outboard of block 2A is recommended which will assist in capturing splays of the deltaic channels if present.
- ❖ A series of rock physics studies and modelling such as the AVO may need to be conducted to predict the presence of hydrocarbons in these sands.
- ❖ It is recommended to follow mapping the fluvial/deltaic anomalies outside of the studied 3D volume (northwest and southeast).
- ❖ Regional mapping of the trapping fault maybe required as the field does not appear to be purely stratigraphic. This may help to unlock a new field north and south of the current Ibhubesi gas field.
- ❖ Well stimulation by hydraulic fracking would be recommended if the field will ever be developed to enhance productivity (this has also been recommended on final well reports).
- ❖ Hydraulic fluids for well stimulation should contain minimal hydrochloric acid since the main cementing clay is chlorite which is highly reactive to acid.
- ❖ Spectral gamma ray should be considered in the next exploration or appraisal wells to help quantify clay minerals.
- ❖ Resistivity logs are recommended to be corrected for the effect of chlorite in future wells which will target this play type in Orange Basin.

REFERENCES

- American Petroleum Institute, 1998.** Recommended practices for Core Analysis. Exploration and Production Department, API, pp. 14-188.
- Adekola, S. A., 2010.** Integrated approach to solving reservoir problems and evaluations using Sequence Stratigraphy, Geological Structures and Diagenesis in Orange Basin, South Africa. P.h.D. Thesis (unpublished) University of the Western Cape, Bellville, pp. 21-172.
- Bahorich, M., and Farmer, S., 1995.** 3-D seismic discontinuity for faults and stratigraphic features: The coherence cube. In The leading edge, published by Society of Exploration Geophysicists, vol.14, issue 10, pp. 1054.
- Broad, D. S., Jungslager, E.H.A, McLachlan, I.R., and Roux, J., 2006.** Offshore Mesozoic Basin. In: Johnson, M.R., Anhaeusser, C.R. and Thomas, R.J. (editors), The Geology of South Africa. Geological Society of South Africa, Council for Geoscience, Pretoria, pp. 553-571.
- Brown, L.F., Benson, J.M., Brink, G.L., Doherty, S., Jollands, A., Jungslager, E.H.A., Keenan, J.H.G., Muntingh, A., and van Wyk, N.J.S., 1995.** Sequence stratigraphy in offshore South African Divergent Basins: An atlas on exploration for Cretaceous lowstand traps by Soekor (Pty) Ltd. AAPG, Tulsa, Oklahoma 74101 United states, vol.41, pp. 127-182.
- Campher, C., 2009.** Geological modelling of the offshore Orange Basin, west coast of South Africa. M.Sc. Thesis (unpublished), University of the Western Cape, Bellville, pp. 185-187.
- Catuneanu, O., 2005.** Principles of Sequence Stratigraphy. University of Alberta Edmonton, Elsevier science, first edition, pp. 1-300.
- Chidsey, T. C., 2002.** Geological and Petrophysical Characterization of the Ferron Sandstone for 3D Simulation of a Fluvial-Deltaic Reservoir. Utah Geological Survey publication, pp. 6-32.

- Chopra, S., and Marfurt, K.J., 2007.** Seismic Attributes for Prospect Identification and Reservoir Characterization. Society of Exploration Geophysics, Tulsa U.S.A. pp. 45-115.
- Chopra, S., and Marfurt, K.J., 2005.** Seismic attributes -A historical perspective, Society of Exploration Geophysics, Tulsa U.S.A. pp. 70.
- Clark, J., and Khan, T., 2010.** South African investment opportunity Block 5/6. PetroSA brochure, pp. 1-4.
- Clemson, J., Cartwright, J., and Swart, R., 1999.** The Namib Rift: a rift system of possible Karoo age, offshore Namibia. In: Cameron, N.R., Bate, R.H., Clure, V.S. (Eds.), The Oil and Gas Habitats of the South Atlantic. Geological Society, London, Special Publications, vol. 153, pp. 381–402.
- Das Ujjal, Kr., Pant,D.C., Parida, G., Rakesh,R., and Ashutosh, B., 2013.** Application of Multi-Attributes and Spectral Decomposition with RGB blending for understanding the strati-structural features: A Case study. 10th Biennial International Conference & Exposition, pp. 2-7.
- Djebbar, T., Donaldson, E.C., 1999.** Theory and practice of measuring reservoir rock and fluid transport properties. Butterworth-Heimann, USA, first edition, pp.87-150.
- De Vera, J., Granado, P., McClay, K., 2009.** Structural Evolution of the Orange Basin gravity driven system, Offshore, Namibia. Journal of Marine and Petroleum Geology, vol.27, pp. 223-237.
- Derder, O., 2003.** Limitations to conventional wire-line logging tools in defining and evaluation thin bedded clastic succession in the Upper Cretaceous Orange Basin, South Africa. Garyounis University, Benghazi, Libya, Special Publication, pp. 201–216.
- Donald, H., 2011.** First steps in seismic interpretation. Published by Society of exploration geophysicists, Tulsa, Oklahoma, series no 16, pp. 1-30.
- Doveton, J. H., 1999.** Basics of Oil and gas log analysis. Published by Kansas Geological Survey, pp. 1-24.

- Emery, K.O., Uchupi, E., Brown, C.O. Phillips, J., and Simpson, E.S.W., 1975.** Continental margin off western Africa: Cape St. Francis (South Africa) to Walvis Ridge (South-West Africa). AAPG Bulletin 59 (1), pp. 3-59.
- Emery, D. and K. J. Myers. 1996.** Sequence Stratigraphy. Oxford Blackwell Science. Geological Magazine Publications, United Kingdom, vol. 134, Issue 4, pp. 575-582.
- Evennick, J. C., 2008.** Introduction to well logs and subsurface maps. Published by PennWell Corporation 1421, South Sheridan Road Tulsa, Oklahoma 74112-6600 USA. pp. 18-23
- Fadipe, O. A., 2009.** Facies, Depositional Environments and Reservoir Properties of the Albian Age Gas bearing Sandstone of the Ibhubesi Oil Field, Orange Basin, South Africa. M.Sc. Thesis (unpublished), University of the Western Cape, Bellville, pp. 2-178.
- Gerrard, I., and Smith, G. C., 1983.** Post-Paleozoic succession and structure of the southwestern African continental margin. In: Studies in continental margin geology, AAPG Memoir 34 (ed. Watkins, J.S. and C.L. Drake), American Association of Petroleum Geologists, pp. 49-74.
- Granado, P., De vera, J., and Mcclay, K. R., 2009.** Tectonostratigraphic evolution of the Orange Basin, SW Africa. Department of Earth Sciences, Royal Holloway, University of London, Egham, Surrey, TW20 0EX, UK, pp 1-8.
- Hartwig, A., 2014.** Hydrocarbon Migration and Leakage Dynamics of the Orange Basin, South Africa. Thesis (unpublished), University Berlin, pp. 55-123.
- Hartwig, A., di Primio, R., Anka, Z., and Horsfield, B., 2012.** Source rock characteristics and compositional kinetic models of Cretaceous organic rich black shales offshore southwestern Africa. Thesis (unpublished), University Berlin, pp. 51, 17-34.
- Hartwig, A., Anka, Z., and di Primio, R., 2012.** Evidence of a widespread paleo-pockmarked field in the Orange Basin: An indication of an early Eocene massive fluid escape event offshore South Africa. Thesis (unpublished), University Berlin, pp. 332-334, 222-234.
- Herron, D.A., and Latimer, R.B., 2011.** First steps in seismic interpretation. Society of Exploration Geophysicists, P.O. Box 702740, Tulsa, OK 74170-2740, pp. 28.

Horsfall, O. I., Uko, E. D., and Tamunobereton-ari, I., 2013. Comparative analysis of sonic and neutron-density logs for porosity determination in the South-eastern Niger Delta Basin, Nigeria. Department of Physics, Rivers State University of Science and Technology, PMB 5080, Port Harcourt Nigeria. American Journal of Scientific and Industrial Research, pp. 1-11.

Hurst, A., and Archer, J. S., 1986. Some applications of clay mineralogy to reservoir description. Department of reservoir evaluation, Statoil, forus, postboks 300, n-4001 Stavanger, Norway and ERC Energy Resource Consultants ltd., 15 Welbeck st., London w1m 7pf, pp. 1-16.

Jahn, F., Cook, M., and Graham, M., 1998. Hydrocarbon exploration and developments. Published by Elsevier Science B.V. Amsterdam, The Netherlands, first edition, pp. 9-26.

Jikelo, A.N. (2000). Petroleum Prospectivity of deep water orange Basin, South Africa
Petroleum Agency S.A Parow South Africa.

Jungslager, E.H.A., 1999. Petroleum habitats of the Atlantic margin South Africa. Geological Society, London, special publications 1999, v.153, pp. 153-168.

Kennedy, M., 2015. Practical Petrophysics, Developments in Petroleum Science. Published by Elsevier science B.V. Amsterdam, The Netherlands, vol. 62 pp. 34-36.

Konecki, M.C., Duff, P.G., and Mckay, B.A., 1963. Core analysis in Australia (methods employed and facilities available) by department of national development bureau of mineral resources geology and geophysics, pp. 2-50.

Li, M., Zhao, Y., 2014. Geophysical exploration technology: applications in lithological and stratigraphic reservoirs. Published by Elsevier science B.V. Amsterdam, The Netherlands, first edition, pp. 63-102.

Light, M.P.R., Maslanyj, M.P., Greenwood, R.J., and Banks, N.L., 1993. Seismic sequence stratigraphy and tectonics offshore Namibia. In: Williams, G.D., Dobb, A. (Eds),

Tectonics and Seismic Sequence Stratigraphy. Geological Society Special Publications, London, vol. 71, pp. 163–191.

McPhee, C., Reed, J., and Zubizarreta, I 2015. Core Analysis: A best practice guide.

Published by Elsevier science B.V. Amsterdam, The Netherlands Developments in petroleum science first edition, vol. 64, pp. 40-171.

Menzies, M.A., Klemperer, S.L., Ebinger, C.J., and Baker, J., 2002. Volcanic Rifted Margins. Boulder, Colorado. Geological Society of America Special Paper 362, pp. 81-90.

Muntingh, A., and Brown, Jr, L. F., 1993. Sequence Stratigraphy of Petroleum Plays, Post-Rift Cretaceous Rocks (Lower Aptian to Upper Maastrichtian), Orange Basin, Western Offshore, South Africa. In Weimer, P., Posamentier, H., eds., Siliciclastic sequence stratigraphy-recent developments and publications: AAPG memoir 58, pp. 71-98.

Onajite, E., 2013. Seismic data analysis techniques in hydrocarbon exploration. Published by Elsevier Science, Amsterdam, The Netherlands, first edition, pp. 1-190.

Opuwari, M., 2010. Petrophysical Evaluation of the Albian Age Bearing Sandstone Reservoirs of the O-M Field, Orange Basin, South Africa. PhD Thesis (unpublished), University of the Western Cape, Bellville, pp. 50-160.

Paton, D.A., di Primio, R., Kuhlmann, G., Van der Spuy, D., Horsfield, B., 2007. Insights into the Petroleum System Evolution of the Southern Orange Basin, South Africa. South African Journal of Geology, 110: pp. 261-274.

Paton, D. A.; van der Spuy, D.; Di Primio, R. and Horsfield, B., 2008. Tectonically induced adjustment of passive margin accommodation space; influence on the hydrocarbon potential of the Orange Basin, South Africa. AAPG Bulletin 92(5): pp. 589-609.

Petroleum Agency of South Africa, 2008. Petroleum Exploration Information and Opportunities. <http://www.petroleumagencysa.com>.

Petroleum Agency of South Africa, 2011. Petroleum Exploration Information and Opportunities. PASA brochure, pp. 1-3.

Petroleum Agency of South Africa, 2014. Petroleum Exploration Potential of the Orange Basin. PASA brochure, pp. 1-8.

Ray, F. M., Pinnock, S. J., Katamish, H. and Turnbull, J. B. 2010. The Buzzard Field: anatomy of the reservoir from appraisal to production Geological Society, London, Petroleum Geology Conference series 2010, vol. 7, pp. 369-386.

Rider, M., and Kennedy, M., 2013. The geological interpretation of well logs. Rider-French Consulting limited, Scotland, third edition, pp. 47-408.

Roberts, D. G., and Bally, A. W., 2012. Regional geology and tectonics: Phanerozoic passive margins, cratonic basis and global tectonic maps. Published by Elsevier science B.V. Amsterdam, The Netherlands, pp. 559.

Salomo, J., 2011. Seismic Stratigraphy of the Deep-Water Area in the Northern Orange Basin, Offshore South Africa. AAPG International Conference and Exhibition, Milan, Italy, article #10389, pp. 1-31.

Slatt, R.M., 2013. Stratigraphic reservoir characterization for petroleum geologists, geophysicists and engineers, second edition. Elsevier Amsterdam, Developments in petroleum science, vol. 61, pp. 140-158.

Schlumberger, (1982). Log interpretation principles and applications. Schlumberger Education Services, Houston Texas, pp 1-179.

Schmidt, S., 2004. The Petroleum Potential of the Passive Continental Margin of South-Western Africa: Basin Modelling Study. P.h.D. Thesis (unpublished), Rheinisch-Westfälische Technische Hochschule Aachen, German, pp 21 172.

Selley, R.C., 1976. An Introduction to Sedimentology. Academic Press, London, vol. 113, pp. 40-94.

Selley, R.C., and Sonnenberg, S. A., 2014. Elements of petroleum geology: Published by Elsevier San Diego Californian USA, Third edition, pp. 377-427.

- Stevenson, I. R., and McMillan, I.K., 2004.** Incised valley fill stratigraphy of the Upper Cretaceous succession, proximal Orange Basin, Atlantic margin of southern Africa. *Journal of the Geological Society*, De Beers Marine, Geological Society Publishing House, vol. 161, pp. 1-18.
- Telford, W.M., Geldart, L.P., and Sheriff, R.E., 2004.** *Applied Geophysics*. Cambridge University Press, pp 1-70.
- Thompson, D. M., and Woods, A. M., 1993.** *Development Geology Reference Manual: AAPG Methods in Exploration Series, No.10*. Published by the American Association of Petroleum Geologists, Tulsa, Oklahoma, U.S.A. 74101, pp. 183-184.
- Ubani, C. E., Adeboye, Y. B., Oriji, A. B., 2012.** Advances in coring and core analysis for reservoir formation evaluation. Department of petroleum and gas engineering, University of Port-Harcourt, P/H, Nigeria. Published in *Petroleum & Coal*, vol.54, pp. 1-10.
- Ulusay, R., Aydan, O., Gercek, H., Hindistan, M.A., Tuncay, E., 2016.** Rock mechanics and rock engineering: From the past to the future. Proceedings of the 2016 ISRM international symposium, Eurock 2016 Cappadocia Turkey, vol. 1, pp107.
- Van der Spuy, D., 2003.** Aptian source rocks in some South African Cretaceous basins. Geological Society, London, Special Publications 207(1), pp. 185-202.
- Worthington, P.F., 1991.** Effective integration of core and log data. BP-research, Sunbury on Thames United Kingdom. Published on 1991 SCA conference, paper No. 9102, pp. 1-9.
- Zimmerle, W., 1995.** *Petroleum Sedimentology*. Published by Kluwer Academic Publishers, The Netherlands, pp. 71-79.

Related Websites:

<http://www.scihub.org/AJSIR> ISSN: 2153-649X, doi:10.5251/ajsir.2013.4.3.261.271

(Accessed: 15 May 2015)

http://petrowiki.org/Rock_density_and_porosity (Accessed: 17 June 2015)

<http://www.geostud.dk/deltas-and-estuaries.html> (Accessed: 20 September 2016)

http://www.cgg.com/data/1/rec_docs/883_shale_volume_calculation.pdf

(Accessed: 21 August 2016)

http://petrowiki.org/Rock_density_and_porosity (Accessed: 12 May 2015)

http://homepages.see.leeds.ac.uk/~earpwjg/PG_EN/CD%20Contents/GGL-66565%20Petrophysics%20English/Chapter%2016.PDF (Accessed: 02 October 2016)

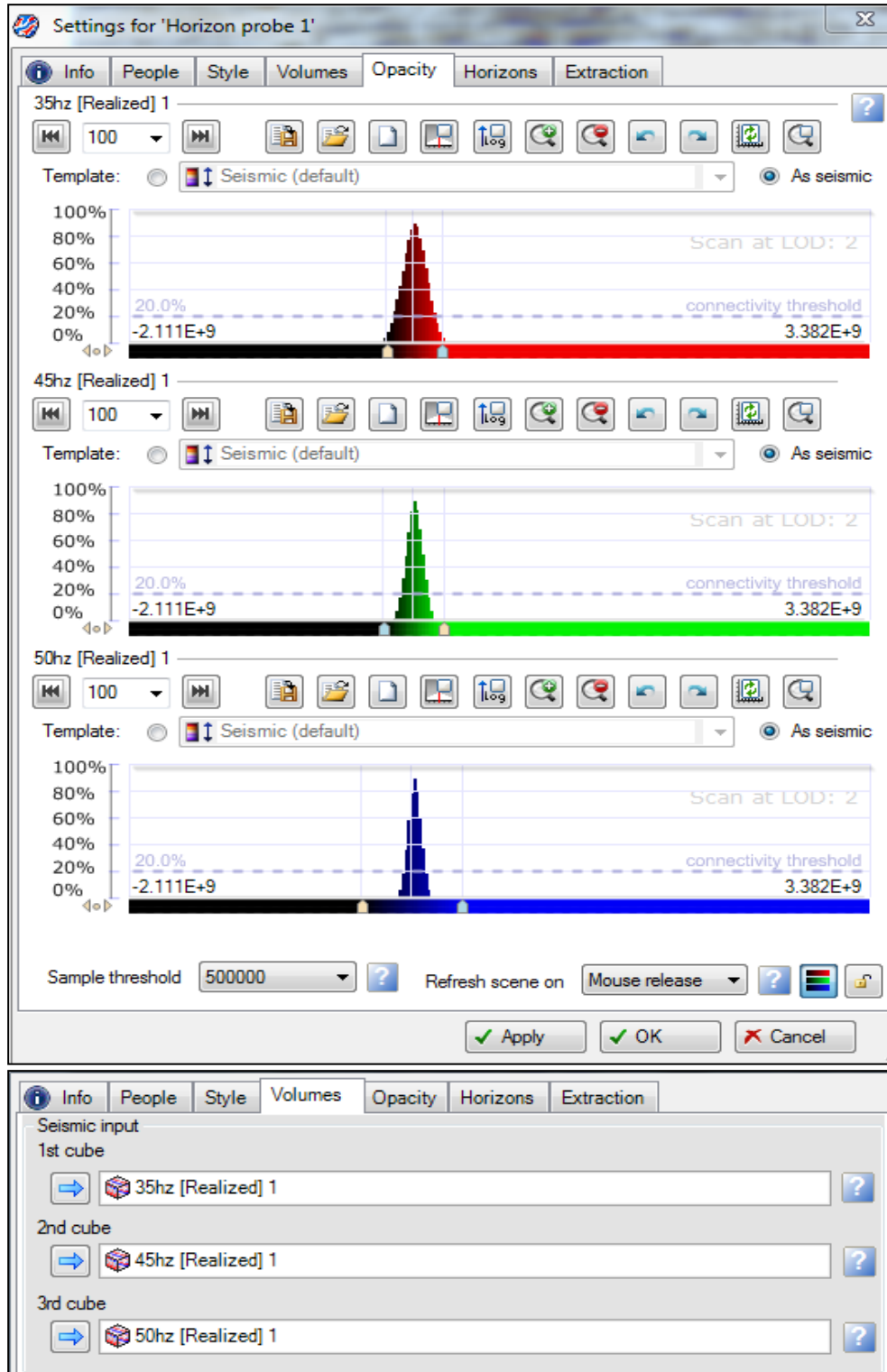
<http://www.software.slb.com/products/petrel/petrel-geophysics/seismic-interpretation#>
(Accessed: 25 May 2016).



APPENDICES

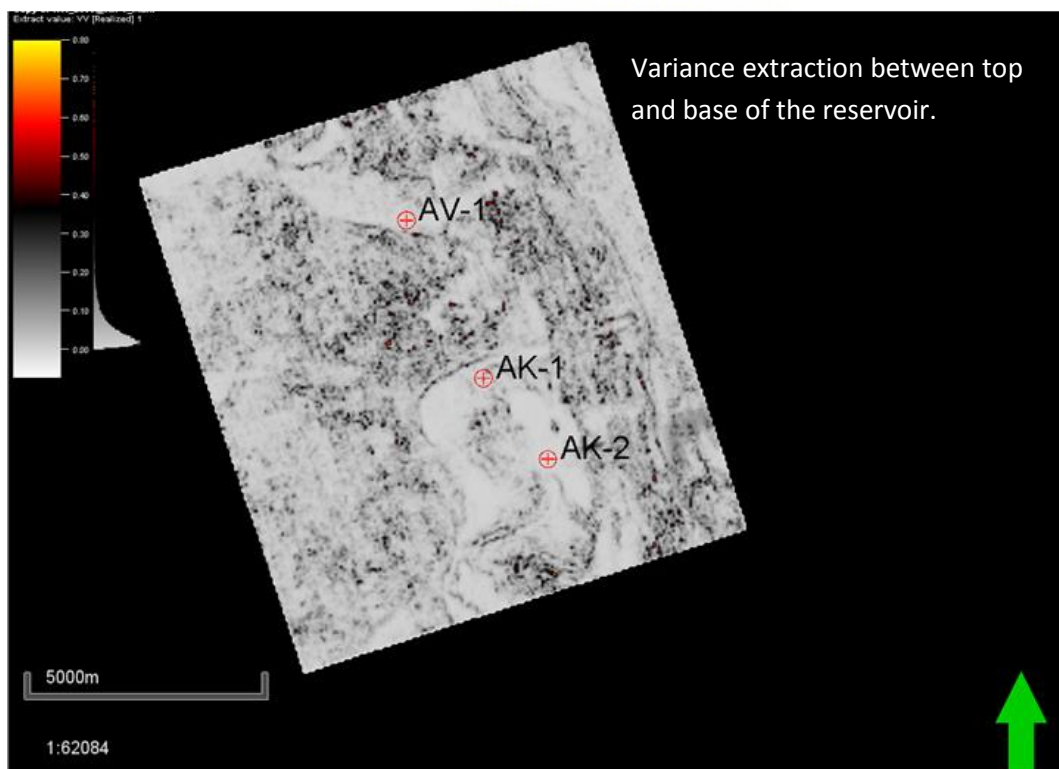
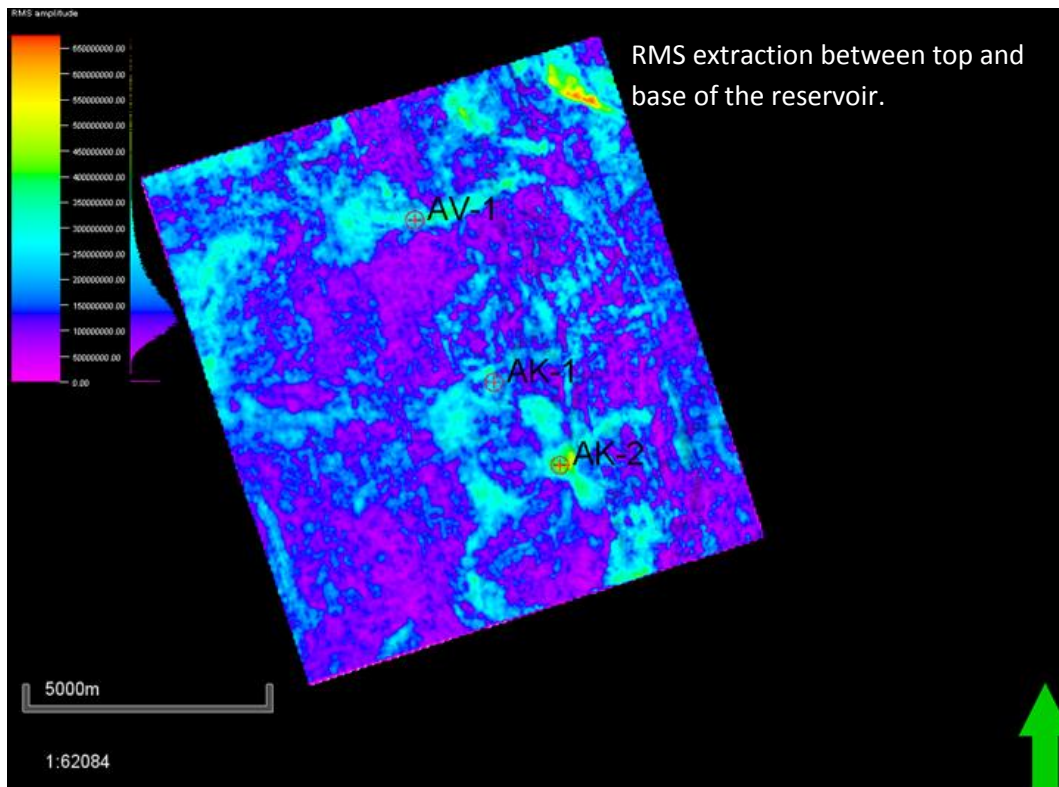
Appendix A

Spectral decomposition settings.



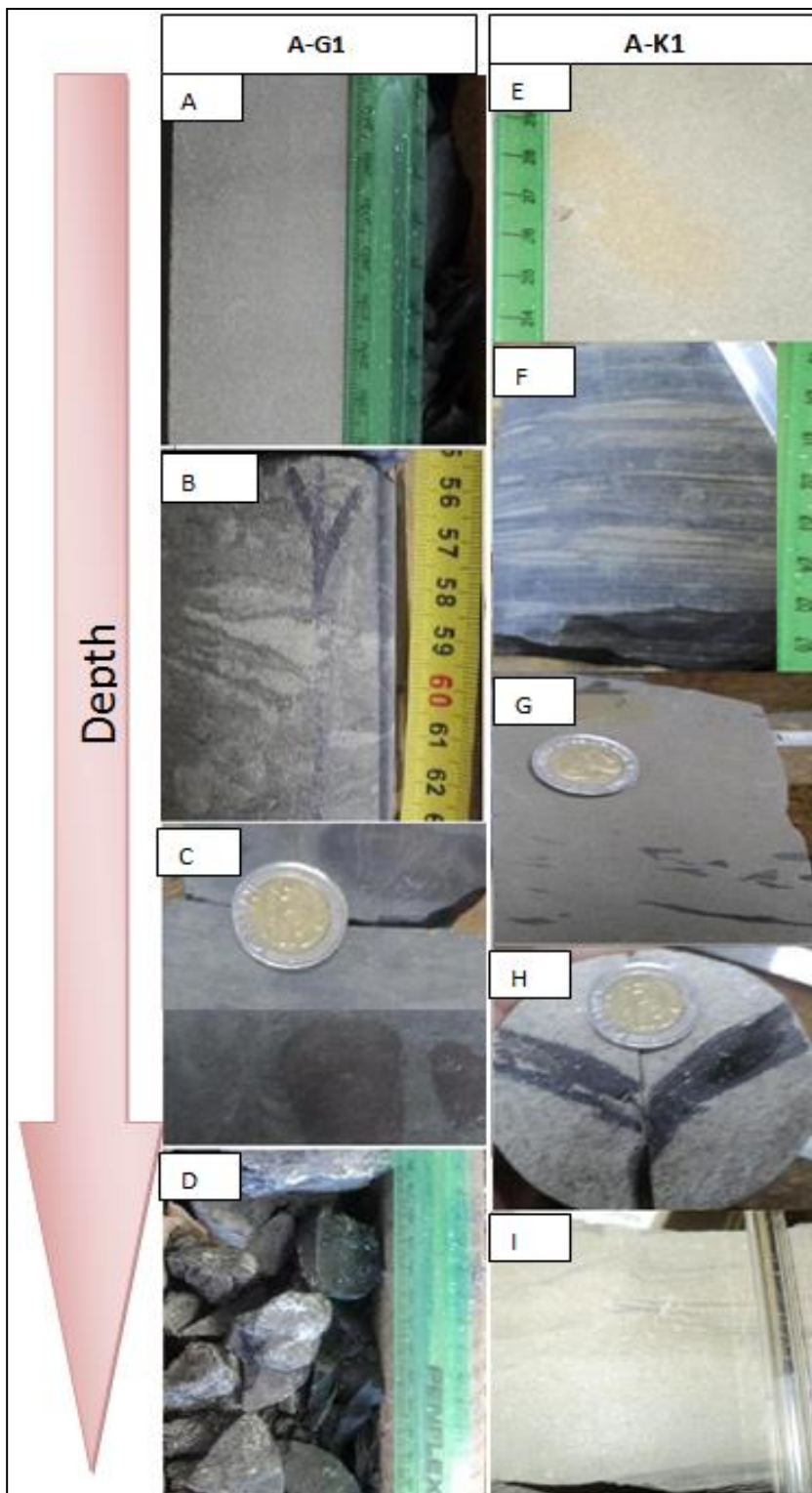
Appendix B

Seismic attribute extractions between top and base of the reservoirs.



Appendix C

Selected plates from A-G 1 and A-K 1 cores.



(A) Massive sandstone. (B) Sand lenses in a siltstone. (C) Shale with oxidation spots. (D) Shattered shale showing water reaction. (E) Massive sandstone. (F) Silt with sandstone lenses. (G) mud-drapes in a sandstone unit. (H) Layer of coal within a massive sandstone. (I) Water escaping Structures.

Appendix D

Core analysis results of A-G 1 well Core.

| Depth (m) | Porosity (%) | Kair (mD) | Sg(%) | So(%) | Sw(%) | Calc | Dol | Grain Density (g/cc) |
|-----------|--------------|-----------|-------|-------|-------|------|-----|----------------------|
| 3370.05 | 18.9 | 108 | 49 | 0 | 51 | 0.5 | 5 | 2.64 |
| 3370.35 | 19.6 | 69 | | | | | | 2.68 |
| 3370.6 | 20.2 | 64 | | | | | | 2.68 |
| 3370.85 | 14.6 | 13 | | | | | | 2.69 |
| 3371.07 | 16.9 | 40 | 52 | 0 | 48 | 0.5 | 0.5 | 2.65 |
| 3371.4 | 16.4 | 14 | | | | | | 2.71 |
| 3371.65 | 16.7 | 19 | | | | | | 2.71 |
| 3371.9 | 16.5 | 26 | | | | | | 2.69 |
| 3372.03 | 12.7 | 6 | 56 | 0 | 44 | 0.5 | 0 | 2.65 |
| 3372.28 | 12 | 1.3 | | | | | | 2.69 |
| 3372.53 | 9.5 | 0.32 | | | | | | 2.68 |
| 3372.82 | 8.5 | 0.149 | | | | | | 2.68 |
| 3373.75 | 5 | 0.018 | | | | | | 2.69 |
| 3373.88 | 3.2 | 0.01 | 22 | 27 | 51 | 1 | 0 | 2.64 |
| 3375.6 | 3 | 0.017 | | | | | | 2.69 |
| 3375.98 | 2 | 0.016 | | | | | | 2.71 |
| 3376.62 | 7.7 | 0.03 | 45 | 0 | 55 | 0.5 | 0 | 2.66 |
| 3376.86 | 8.6 | 0.151 | | | | | | 2.65 |
| 3377.12 | 10.1 | 0.33 | | | | | | 2.69 |
| 3377.36 | 9.6 | 0.151 | | | | | | 2.69 |
| 3377.54 | 7 | 0.079 | 45 | 0 | 55 | 0.5 | 0 | 2.65 |
| 3377.78 | 7.9 | 0.104 | | | | | | 2.68 |
| 3378.23 | 9.2 | 0.028 | | | | | | 2.68 |
| 3378.48 | 8.6 | 0.025 | | | | | | 2.67 |
| 3378.58 | 7.6 | 0.025 | 15 | 11 | 74 | 0.5 | 0 | 2.64 |
| 3379.24 | 6.8 | 0.018 | | | | | | 2.67 |
| 3379.64 | 1.2 | 0.013 | | | | | | 2.64 |
| 3379.82 | 4.9 | 0.01 | 19 | 0 | 81 | 1 | 1 | 2.64 |
| 3380.15 | 3.3 | 0.015 | | | | | | 2.67 |

Appendix E

Core analysis results of A-K 1 well Core 1.

| Depth | Porosity (%) | Kair (P1) | Sg | So | Sw | Density |
|---------|--------------|-----------|----|----|----|---------|
| 3236.1 | 24.2 | 135 | | | | 2.7 |
| 3236.35 | 22.6 | 156 | | | | 2.68 |
| 3236.51 | 21.3 | 86 | 41 | 0 | 59 | 2.69 |
| 3236.81 | 21.4 | 77 | | | | 2.71 |
| 3237.05 | 18.1 | 34 | | | | 2.71 |
| 3237.26 | 18.1 | 43 | | | | 2.69 |
| 3237.51 | 15 | 21 | | | | 2.68 |
| 3237.77 | 12.9 | 8.6 | | | | 2.85 |
| 3237.95 | 9.1 | 0.63 | 59 | 0 | 41 | 2.64 |
| 3238.3 | 8.9 | 0.22 | | | | 2.66 |
| 3238.5 | 6.3 | 0.074 | | | | 2.66 |
| 3238.52 | 8.8 | 0.23 | | | | 2.66 |
| 3239.05 | 4.3 | 0.06 | | | | 2.68 |
| 3243.6 | 0.6 | 0.04 | 15 | 0 | 85 | 2.67 |

Appendix F

Core analysis results of A-K 1 well Core 2.

| Depth | Porosity | Kair (mD) | Density | Sg | So | Sw |
|---------|----------|-----------|---------|----|----|------|
| 3283.2 | 19.2 | 4.9 | 2.68 | | 30 | 0 70 |
| 3283.6 | 17.8 | 15 | 2.68 | | | |
| 3283.85 | 17.8 | 30 | 2.68 | | | |
| 3284.1 | 20.4 | 41 | 2.68 | | | |
| 3284.35 | 21.3 | 40 | 2.68 | | | |
| 3284.45 | 22 | 62 | 2.68 | | 36 | 64 |
| 3285.05 | 22.2 | 50 | 2.69 | | | |
| 3285.3 | 22.8 | 47 | 2.67 | | | |
| 3285.34 | 20.6 | 15 | 2.67 | | 41 | 59 |
| 3285.83 | 17.3 | 4.8 | 2.69 | | | |
| 3286.08 | 14.3 | 45 | 2.67 | | | |
| 3286.3 | 20.4 | 53 | 2.68 | | | |
| 3286.55 | 22.3 | 48 | 2.69 | | | |
| 3286.6 | 22.2 | 79 | 2.68 | | 39 | 61 |
| 3287.25 | 22.3 | 2.7 | 2.69 | | | |
| 3287.3 | 15.8 | 77 | 2.67 | | | |
| 3287.9 | 3.7 | 0.194 | 2.66 | | 45 | 55 |
| 3290.06 | 2.3 | 0.013 | 2.69 | | 16 | 84 |
| 3291.76 | 2.7 | 0.016 | 2.65 | | 35 | 65 |
| 3292.79 | 2.6 | 0.023 | 2.66 | | 35 | 65 |